THE RESISTIVITY OF THIN POTASSIUM FILMS AT 0.1 TO 4.2 K

By

Yao-Jin Qian

A DISSERTATION

Submitted to
Michigan State University
in partial fulfillment of the requirements
for the degree

DOCTOR OF PHILOSOPHY

Department of Physics

1989

ABSTRACT

THE RESISTIVITY OF THIN POTASSIUM FILMS
AT 0.1 TO 4.2 K

By

Yao-Jin Qian

We have investigated electrical resistivity $\rho(T)$ of potassium thin films over the range of 2.7 to 77 μm on amorphous microslide glass, high purity crystal Si and crystal KF ((100) cleaved) substrates from 0.1 to 4.2 K with the precision of 1-0.1 ppm.

The potassium films were made first by thermal evaporation inside a high vacuum chamber which was surrounded by a Glove-Box filled with Ar at one atmosphere pressure. A sample can containing a copper sheet coated with K film as a gas absorber, was used to transfer samples to the dilution refrigerator where the measurements were made.

K films on glass and Si substrates have predominantly (110) planes parallel to the surface in contrast to K on KF substrates, which has predominantly (100) planes parallel to the surface. We found that there was no appreciable difference in the residual resistivity of the K films as for these two orientations. This contradicts to the prediction of Charge Density Wave theory. Unlike previous measurements on K thin wires $(d\rho/dT)$ always increased monotonically with T over the whole range of the measurement. For K films on all three substrates, we found evidence for the existence of an additional T^5 term in $\rho(T)$, which would be anticipated if the phonon-drag was quenched in the thin films. Various factors including thickness, annealing days at room temperature and substrates affect the magnitude of the coefficient of the T^5 term. For the glass and Si substrates the T^5 term is roughly proportional to the

inverse of film thickness but little change with thickness was observed for films on KF substrates.

The coefficients of T^2 term which we associated with electron-electron scattering show a similar dependence on the same factors seen for the T^5 term.

We observed a very large Kondo-like effect in $\rho(T)$ of K films on glass substrates over the range of 0.5 K down to the lowest temperature reached. But the magnitude varies widely with film thickness. However for K films on Si and KF substrates the Kondo-like effect is small and shows little change with sample thickness.

TO MY WIFE

ACKNOWLEDGMENTS

I am very grateful to Dr. Peter A. Schroeder for his kindness, patient guidance, encouragement and suggestions throughout the completion of this thesis, making it a very enjoyable learning process.

I would also like to express my gratitude to Dr. william P. Pratt, Jr. who through the years gave me invaluable aid and suggestions to the laboratory works and measurements. A special thanks is owed to Dr. Zhaozhi Yu for his help and advice in the operation of dilution refrigerator. I am also very grateful to Dr. Jing Zhao for his help in the collection of some experimental data. I wish to thank Dr. Yiyun Huang and Mr. Ping Zhou for their help to determine the crystal structure of K films. I would also like to extend my thanks to Machine Shop for their help in the construction of the apparatus. I thank the NSF for the financial support for the completion of this work.

TABLE OF CONTENTS

LIST OF FIGURES

LIST OF TABLES

Chapter 1 Introduction

1.1 General Background of Resistivity

1.1.1 Simple theory

Electrical resistivity has long been recognized as a very important property of materials. Understanding the physical process that determines the electrical resistivity of simple metals is a fundamental test of our knowledge of solid state physics. The macroscopic equations for the transport properties of an isotropic metal in zero magnetic field can be written as

$$\vec{E} = \rho\vec{j} + S\vec{\nabla}T \qquad (1.1.1.1)$$

$$\vec{Q} = \frac{TS}{\rho}\vec{E} - \kappa\vec{\nabla}T \qquad (1.1.1.2)$$

where $\vec{E}$ is electrical field and $\vec{j}$ and $\vec{Q}$ are the electrical and heat current density respectively, and S is the thermoelectric power, κ is the thermal conductivity [1]. From the above equations one can see that the electrical resistivity is defined as

$$\rho = \left.\frac{E}{j}\right|_{\vec{\nabla}T=0} \qquad (1.1.1.3)$$

The beginning of the understanding of electrical conduction can be traced back to the beginning of this century, when Drude[2] first constructed a very successful theory based on the model of kinetic gases. He treated electrons as a gas of solid spheres with uniform charge -e and and found that the electrical current density could be written as

$$\vec{j} = -ne\vec{v} \qquad (1.1.1.4)$$

where n is the density of the electron gas, and $\vec{v}$ is drift velocity of electron gas. If the relaxation time between two successive collision events is τ, then the v could be replaced by

$$\vec{v}_{avg} = - \frac{e\vec{E}\tau}{m} \qquad (1.1.1.5)$$

and from equation 1.1.1.3, 1.1.1.4 and 1.1.1.5 one obtained the Drude expression for the electrical resistivity

$$\rho = \frac{m}{ne^2\tau} \qquad (1.1.1.6)$$

or

$$\rho = \frac{mv}{ne^2 l} \qquad (1.1.1.7)$$

where $l=\tau v$ is the mean free path, the length traveled by the electrons between successive collisions. From equation 1.1.1.7 one obtains

$$\rho l = \frac{mv}{ne^2} = \text{constant} \qquad (1.1.1.8)$$

But the classical treatment of the electron gas also resulted in a specific heat of $(3/2)k_B$ per electron that was never observed. Shortly after the discovery of the quantum nature of the electron gas, Sommerfield applied Fermi-Dirac statistics of the free electron gas to the problem of electrical conduction. The Fermi distribution of electrons in equilibrium is

$$f(\vec{v}) = 2(m/h) \frac{1}{\exp[((1/2)mv^2-\mu)/k_B T]+1} \qquad (1.1.1.9)$$

Upon the reexamination of the Drude model one concludes that if the velocity in equation 1.1.1.7 is replaced by the electron velocity at the Fermi surface, then the general form of the Drude expression should still be correct.

To a first approximation, the temperature dependent part of the resistivity is independent of the residual resistivity caused by elastic scattering of electrons by impurities and point imperfections in metals; that is the resistivity can be written as

$$\rho = \rho_0 + \rho(T) \qquad (1.1.1.10)$$

This is known as Matthiessen's rule. If equations 1.1.1.7 and 1.1.1.10 are true, then the mean free path can also be written as

$$l_{eff}^{-1} = l_0^{-1} + l^{-1}(T) \qquad (1.1.1.11)$$

In the same approximation $\rho(T)$ can be written as the sum of the contributions from different scattering mechanisms. Thus the resistivity of bulk metals could be expressed as

$$\rho = \rho_0 + \rho_{el\text{-}el}(T) + \rho^N_{el\text{-}ph}(T) + \rho^U_{el\text{-}ph}(T) \qquad (1.1.1.12)$$

where $\rho_{el\text{-}el}(T)$ is the resistivity contribution due to electron-electron scattering, $\rho^N_{el\text{-}ph}(T)$ is the contribution due to the normal process electron-phonon scattering and $\rho^U_{el\text{-}ph}(T)$ is due to umklapp process electron-phonon scattering. Correspondingly to Eq. 1.1.1.12 we also have

$$l^{-1}(T) = (l_{el\text{-}el}(T))^{-1} + (l^N_{el\text{-}ph}(T))^{-1} + (l^U_{el\text{-}ph}(T)) \qquad (1.1.1.13)$$

We will discuss the detail temperature dependence of each term in the following sections.

1.1.2 Theory of Electron-Phonon Scattering

The distribution function of electrons in metal is determined by the famous Boltzmann equation[1],[3]

$$\frac{\partial f}{\partial t} + \vec{v}\cdot\vec{\nabla}_r f + \vec{E}\cdot\vec{\nabla}_k f = \left.\frac{\partial f}{\partial t}\right|_{coll} \qquad (1.1.2.1)$$

Usually the integrodifferential nature of the Boltzmann equation makes it very difficult to solve, but frequently it is appropriate to replace the collision term in the equation by a relaxation-time approximation, that is

$$\left.\frac{\partial f}{\partial t}\right|_{coll} = -\frac{f_1}{\tau} \qquad (1.1.2.2)$$

and

$$f = f_0 + f_1 \qquad (1.1.2.3)$$

where f_0 is the equilibrium electron distribution function which does not contribute to the electrical conduction. Under dc current

conditions the first term on the left side of equation 1.1.2.1 is zero, and for bulk materials there is no spatial dependence of the distribution function, thus the second term on the left side of Boltzmannn equation is also zero, and the resistivity of isotropic metals can be formally written as

$$\rho = \vec{E}/\{-\frac{2}{(2\pi)^3}\int e\vec{v}f_1 d\vec{k}\} \qquad (1.1.2.4)$$

It is clear from equations 1.1.2.1 and 1.1.2.2 that the temperature dependence of resistivity can only be obtained by the quantum mechanical calculation of relaxation time τ and correspondingly, the mean free path of $l=v_F\tau$.

For normal electron-phonon processes, the quasi-momentum $\vec{k}$ of electrons plus the quasi momentum $\vec{q}$ of phonons is conserved during the scattering process. That is $\vec{k}\pm\vec{q}=\vec{k}'$, where a +(-) sign refers to an electron absorbing (emitting) a phonon as in figure 1.1.2.1. The Bloch-Gruneisen[3] expression for $\rho_{el\text{-}ph}(T)$ is derived from the following assumptions; (1) the Fermi surface of metal is a perfect sphere, and it does not touch the first Brillouin zone; (2) the phonon gas is always in an equilibrium state; (3) the phonon spectrum of metals follows the Debye phonon spectrum; (4) only the contribution from normal electron-phonon processes are considered. For a temperature T less than ten percent of the Debye Temperature the Bloch-Gruneisen expression for the resistivity of a metal simplifies to the simple power law

$$\rho^N_{el\text{-}ph}(T) = CT^5 \qquad (1.1.2.5)$$

This so called Bloch T^5 power law can be understood in terms of the following physical picture. From figure 1.1.2.2 one can see that at low temperatures ($T<<\Theta_D$) the crystal momentum $q=k_BT/\hbar c$, and the number of phonons that can scatter an electron is proportional to T^2. Furthermore electron-phonon scattering strength at this low temperature increases linearly with T, so that the net effect of electron-phonon scattering is

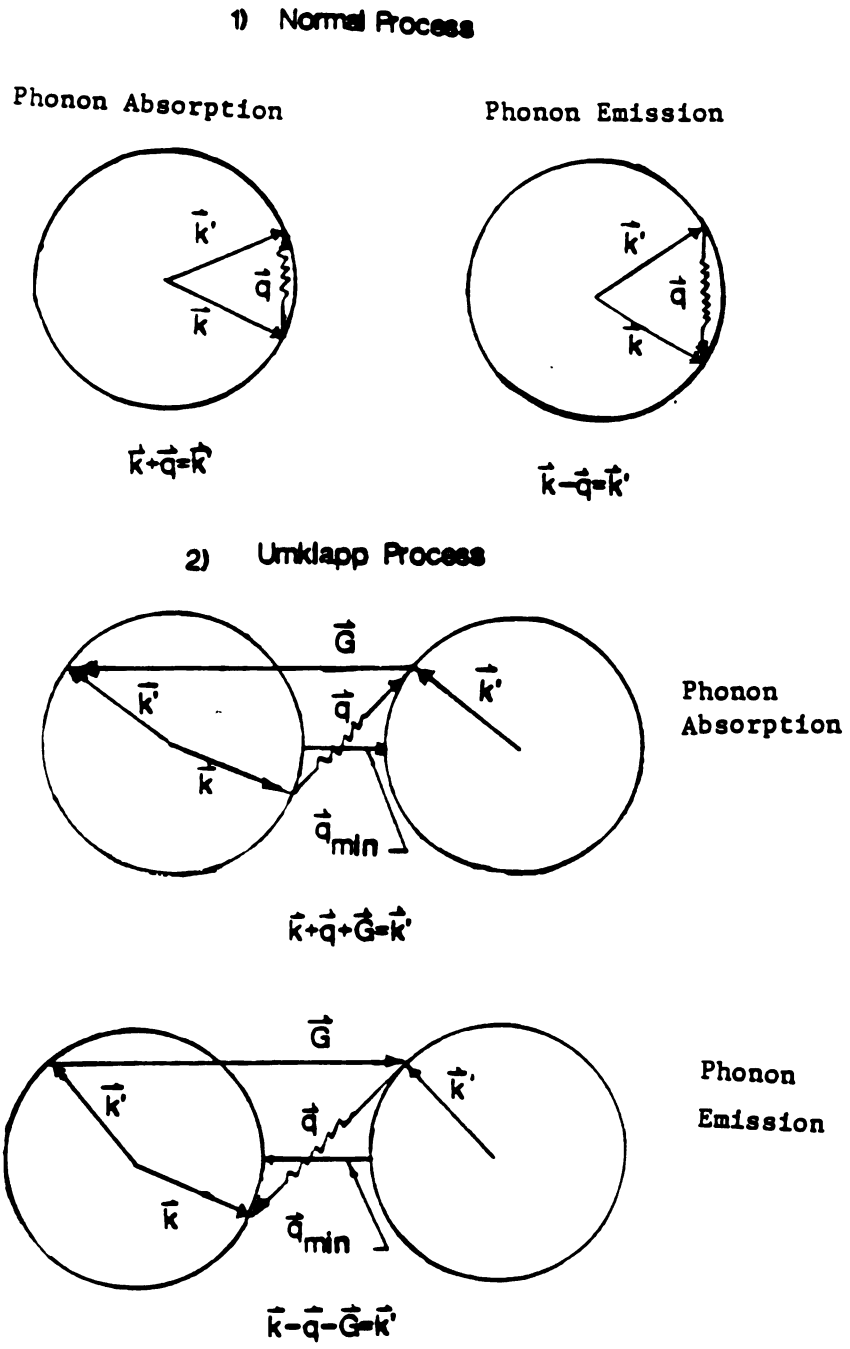

Fig. 1.1.2.1 Normal and umklapp electron-phonon scattering

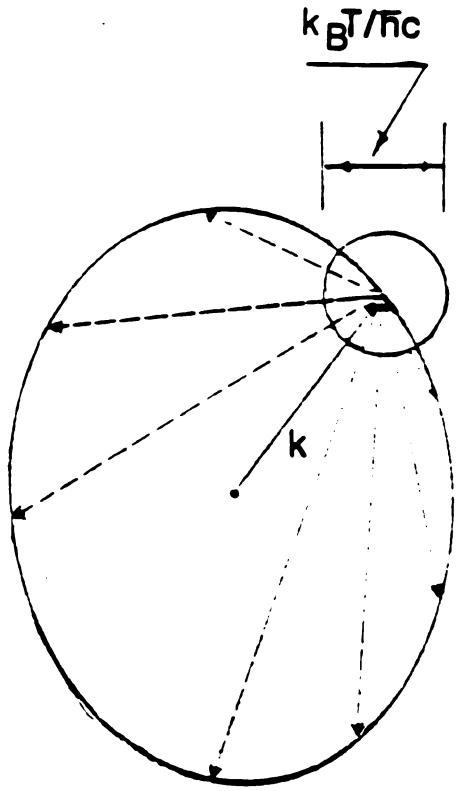

Fig. 1.1.2.2 Construction of the wave vectors of those phonons allowed by the conservation laws to participate in a one-phonon scattering process. At temperature well below θ_D the only phonons that can actully participate in scattering events have wave vectors within small sphere of size $k_BT/\hbar c$.

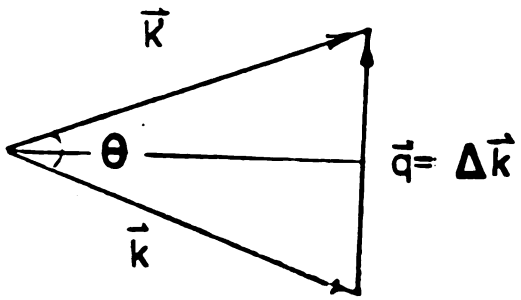

$$|\vec{q}|=|\Delta\vec{k}|=|\vec{k}-\vec{k}'|\simeq k\sin(\theta/2)$$

Fig. 1.1.2.3

proportional to T^3. However well below the Debye temperature Θ_D each electron-phonon scattering event only changes the electron wave vector by small amount, as shown in figure 1.1.2.3. From the figure

$$\Delta k = |\vec{k}' - \vec{k}| = k(1-\cos\theta)$$
$$\approx k\theta^2/2 \qquad (1.1.2.6)$$

but $\theta \approx q/k$ from figure 1.1.2.3 and $q \approx k_B T/\hbar c$, so we have

$$\frac{\theta^2}{2} \propto T^2 \qquad (1.1.2.7)$$

From equations 1.1.2.6 and 1.1.2.7 one can see that $\Delta k \propto T^2$, and this introduces another factor of T^2 to the resistivity, and the combined final results is the $T^3 \cdot T^2 = T^5$ Law.

However the above result ignores the contribution to the resistivity from umklapp processes. One should also include the umklapp term $\rho^U_{el\text{-}ph}(T)$ in the calculation from the Boltzmann equation 1.1.2.1 and quantum mechanics. Peierls[4] pointed out that under these circumstance the result is very different from the T^5 Law predicted for normal electron-phonon scattering process. For an umklapp process the conservation of momentum becomes

$$\vec{k} \pm \vec{q} + \vec{G} = \vec{k}' \qquad (1.1.2.8.5)$$

where G is a reciprocal lattice vector, and +(-) sign indicates phonon absorption (emission) by the electron during the scattering process. Figure 1.1.2.1 illustrates the situation for Umklapp scattering. Since the Fermi surface of the system does not touch the first Brillouin zone, one can clearly see from the illustration, that for an umklapp electron-phonon scattering to happen the crystal momentum q of phonons should be equal or larger than q_{min}. Since $\hbar\omega_{min} = \hbar c q_{min}$, there is minimum requirement of energy for a phonon to participate in umklapp process electron-phonon scattering. The number of phonons participating in umklapp processes is

$$n \propto \exp(-\hbar\omega_{min}/k_B T)$$
$$\propto \exp(-\Theta/T) \qquad (1.1.2.8)$$

Since the resistivity is proportional to the number of participating phonons, one can see that $\rho^U_{el-ph}(T)$ will decrease exponentially with temperature. The detailed calculation[5],[6] confirms this conclusion from the above simple physical picture and gives the result

$$\rho^U_{el-ph}(T) = BT^n \exp(-\Theta/T) \qquad (1.1.2.9)$$

Where Θ is a characteristic temperature and B is a constant.

All the above calculations are based on the assumption that the phonon system is always in equilibrium, and is not disturbed by the electrical conduction current passing through the metal. This is certainly not always true. If the scattering mechanism tending to restore the phonon system to equilibrium is not large enough at very low temperatures, the phonon system will drift with the momentum obtained from scattering by the electron gas that carries the electrical current. Since the phonon system is dragged by the electron system, this phenomenon is called the "Phonon Drag" effect, and it can effect the low temperature behavior of resistivity in Alkali metals profoundly.[5],[6]

Let a phonon system be in the equilibrium state with phonon distribution function G_0. When it is disturbed by the passing of a electrical current, the new distribution function is displaced along the direction of current density $\vec{j}$, and can be written in the form[5]

$$G = G_0 - \Phi(\vec{q}) \frac{\partial G_0}{\partial E(q)}$$
$$= G_0 - \vec{q}\cdot\vec{u} \frac{\partial G_0}{\partial E(q)} \qquad (1.1.2.10)$$

where $\vec{u}$ is the unit vector along the direction of electrical current density $\vec{j}$. When one solves the Boltzmann equation with the non-equilibrium state phonon distribution function, one obtains the following result

$$\rho = \rho_0 + \rho_{el\text{-}ph}\left(1 - \frac{P_{1L}^2}{P_{11}P_{LL}}\right) \qquad (1.1.2.11)$$

where ρ_0 is the residual resistivity and P_{1L}, P_{11} and P_{LL} are variational integrals[5] arising from scattering processes. $\rho_{el\text{-}ph}$ is the electron-phonon resistivity without any phonon drag effect. P_{11} and P_{LL} are positive definite, and thus the resistivity due to electron-phonon scattering is reduced by the factor of $(1-P_{1L}^2/P_{11}P_{LL})$. For a pure, perfect, monovalent metal with a spherical Fermi Surface the normal process of electron-phonon scattering obeys the conservation of total quasi momentum $\vec{k}+\vec{q}=\vec{k}'$, and one obtains the following relation

$$P_{11} = P_{LL} = -P_{1L} \qquad (1.1.2.12)$$

thus the resistivity arising from normal electron-phonon scattering is completely canceled by the "phonon-drag" effect, the vanishing of this resistivity under ideal conditions can be understood from the following physical picture. At the very low temperatures there are so few phonon-phonon, or phonon-imperfection scattering events that whatever crystal momentum is gained by the phonons from electron-phonon scattering can not be redistributed quickly. Thus the whole process could be reversed and the gained crystal momentum will return to the electron gas, and there is no electrical resistivity for the electron-phonon system. However for umklapp processes things are more complicated. Ziman[5] argued that the integral P_{1L} contains a cross term proportional to $\vec{K}\cdot\vec{q}$, where $\vec{K}=\vec{k}_1-\vec{k}_2$, which is usually negative for umklapp processes where $\vec{K}$ and $\vec{q}$ tend to be in opposite directions. This negative term makes P_{1L} smaller than P_{11} and consequently P_{LL}, and the phonon drag effect will not be zero for umklapp processes. Kaveh and Wiser[6] in their calculation of electrical resistivity of potassium metal at low temperatures analysed in detail the "phonon-drag effect" factor for both the normal and umklapp process of electron-phonon scattering with the

assumption of 1.1.2.10, where $\Phi(\vec{q})=\vec{q}\cdot\vec{u}$, and due to the difference of these two effects they derived the following result,

$$\rho_{el\text{-}Ph}(T) = (1+2\alpha_{11}(T)+\alpha_{LL}(T))\rho^{U}_{el\text{-}ph}(T)$$
$$= \gamma(T)\rho^{U}_{el\text{-}ph}(T) \qquad (1.1.2.13)$$

where $\gamma(T)$ is about 1.4 and only weakly dependent on the temperature, and $\rho^{U}_{el\text{-}ph}(T)$ is the resistivity contribution from umklapp processes with an equilibrium phonon system. It is clear from their calculation that the net result of "phonon drag" in K metal at low temperature is the domination of electron-phonon scattering by umklapp processes, and there is no component of the T^5 Law arising from normal electron-phonon scattering.

Later on Kaveh and Wiser[26], Leavens and Laubitz[27] at the same time independently investigated the effects of a different phonon trial function $\Phi(\vec{q})$ obtained from the phonon Boltzmann equation, where

$$\Phi(\vec{q})=\vec{q}\cdot\vec{u} + \text{extra term} \qquad (1.1.2.14)$$

They found that the result of this modification is that it introduces one more factor $(1-\Delta(T))$ in the equation of 1.1.2.13. So we have

$$\rho_{el\text{-}ph}(T)=(1-\Delta(T))\gamma(T)\rho^{U}_{el\text{-}ph}(T) \qquad (1.1.2.15)$$

where $\Delta(T)$ is nearly constant and about 0.54. From the above equation one can see that this additional factor does not change the temperature dependence of $\rho_{el\text{-}ph}(T)$, but only reduces it by a factor of 2 as compared with the result in eq. 1.1.2.13.

Taylor et al.[28] and Danino et al.[29] pointed out that if a very high density of dislocation lines existed in K samples (greater than approximately 10^{10} dislocations per cm^2), the phonon drag would be partially quenched by the phonon-dislocation scattering. The physical idea behind this proposal was that at very high dislocation density, the phonon-dislocation scattering would bring back the phonon system back to a near equilibrium state, thus partially quenching the phonon drag.

However Gugan[30] pointed out that in the above picture the dislocation density was too high to explain the experimental data. Hence it could not be used to account for the experimental observations[31] of the effect of the strain on the sample. Engquist[32] and Danino et al.[33] proposed another mechanism based on the anisotropy of electron-dislocation scattering to explain the partial quenching of phonon-drag in a strained sample. Since dislocations are highly anisotropic, the relaxation time $\tau_{dis}(\vec{K})$ time for the electron-dislocation scattering depends on the direction of $\vec{K}=\vec{k}-\vec{k}_2$, where $\vec{k}_1$ and $\vec{k}_2$ are the wave vectors of electrons beforeand after electron-dislocation scattering. The $\tau_{dis}(\vec{K})$ in turn affects the distribution functions of both the electron and phonon systems, since these two systems are coupled by the corresponding Boltzmann equations. In order to explain the experimental observation of the resistivity of strained potassium the dislocation density required in this model was about 2×10^9dislocations/cm^2, which was far smaller than the Taylor & Danino's[28,29] model required. According to Kaveh and Wiser the $\tau_{dis}(\vec{K})$ would not only partially quench the phonon drag, but also enhance the $\rho^N(T)$ and reduce the $\rho^U(T)$ at the same time.

1.1.3 Theory of Electron-Electron Scattering

The standard theory[5] of resistivity due to electron-electron scattering is based on the Landau theory of Fermi liquids. It was first suggested by Landau and Pomeranchuk[7] and Baber[8] that for a three dimensional pure, free-electron gas like metal there should exist a T^2 contribution to the resistivity arising from electron-electron scattering[5]. This simple power law behavior can easily be understood from phase-space arguments.

There are two kinds of electron-electron scattering processes, namely normal electron-electron scattering and umklapp electron-electron scattering. In figure 1.1.3.1 we illustrate these two very different process. For a simple free-electron like metal with spherical Fermi surface the total quasi electron momentum is conserved during normal electron-electron scattering,

$$\vec{k}_1 + \vec{k}_2 = \vec{k}_3 + \vec{k}_4 \qquad (1.1.3.1)$$

where $\hbar\vec{k}_1$ and $\hbar\vec{k}_2$ are electron quasi momentums before the scattering, $\hbar\vec{k}_3$ and $\hbar\vec{k}_4$ after the scattering. Thus there is no resistivity contribution due to normal electron-electron scattering since no net change of total electron momentum happened during the scattering event. The only way the electron-electron scattering contributes to the resistivity is through umklapp processes in which

$$\vec{k}_1 + \vec{k}_2 = \vec{k}_3 + \vec{k}_4 + \vec{G} \qquad (1.1.3.2)$$

where $\vec{G}$ is a reciprocal lattice vector. Also during the scattering process the total energy of electron system is conserved

$$E(\vec{k}_1) + E(\vec{k}_2) = E(\vec{k}_3) + E(\vec{k}_4) \qquad (1.1.3.3)$$

The scattering rate for electron-electron scattering could be written as

$$\tau^{-1}_{el\text{-}el}(\vec{k}_1) = \sum_{k_1 k_2 k_3} P(\vec{k}_1,\vec{k}_2,\vec{k}_3,\vec{k}_4) \qquad (1.1.3.4)$$

where P is the probability that two electrons initially in occupied states $\vec{k}_1$ and $\vec{k}_2$ will be scattered into $\vec{k}_3$ and $\vec{k}_4$. Since $\vec{k}_1$ and $E(\vec{k}_1)$ are fixed we only have three vectors to determine, but there are the conservation laws of equation 1.1.3.2 for quasi momentums and equation 1.1.3.3 for energies. In three dimension there are only five independent variables and we can replace equation 1.1.3.4 with

$$\tau^{-1}_{el\text{-}e}(k_1) = \sum_{qE(k_2)E(k_3)} P(\vec{q},E(\vec{k}_2),E(\vec{k}_3)) \qquad (1.1.3.5)$$

where $\vec{q} = (\vec{k}_3 - \vec{k}_2)$, $E(\vec{k}_2)$ and $E(\vec{k}_3)$ are chosen to be the independent variables. However $E(k_2)$ and $E(k_3)$ must lay within the thermally

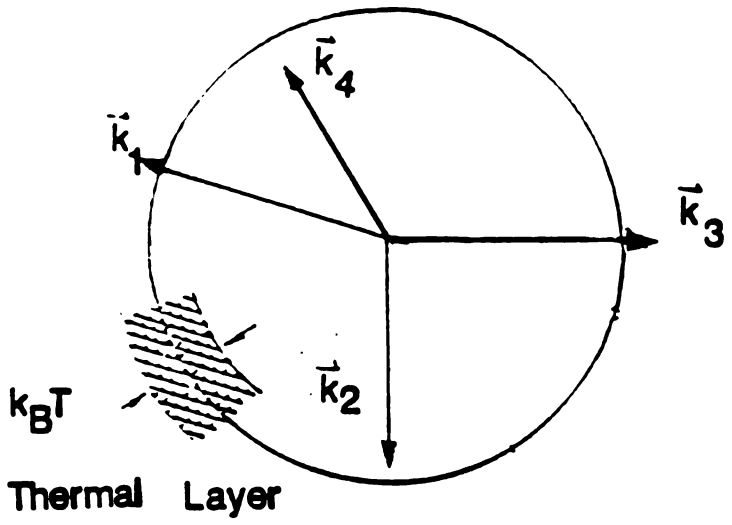

Fig. 1.1.3.1 Schematic diagram of electrons near the Fermi surface. The thermal layer of width=k_BT is also indicated (but greatly exaggerated for clarity).

excited layer of k_BT of the Fermi energy sphere as shown in figure 1.1.3.1. The total available states with these energies is proportional to $(k_BT/E_F)^2$, this leads to

$$\tau_{el-el}^{-1} \propto T^2 \qquad \text{for d=3} \qquad (1.1.3.6)$$

or

$$\rho_{el-el}(T) = AT^2 \qquad \text{for d=3} \qquad (1.1.3.7)$$

The same argument could also be applied to one dimensional system where there is only one independent variable, so that the temperature dependence of resistivity is

$$\rho_{el-el}(T) = AT \qquad \text{for d=1} \qquad (1.1.3.8)$$

In a two dimensional system things are more complicated. When one is applying the above arguments there are three independent variables, the choices could be either $\vec{q}$, E_2 or q, E_2 and E_3, the first will lead to $\rho(T) \propto T$ and the later to $\rho(T) \propto T^2$, the reality must be lie in between these two case. A detailed calculation in a two dimensional system has been carried out by Giuliani and Quinn[9] giving the following result

$$\rho_{el-el}(T) = AT^2 \ln(E_F/k_BT) \qquad \text{for d=2} \qquad (1.1.3.9)$$

which the logarithmic factor has only a weak temperature dependence.

1.1.4 Size Effect on Electrical Resistivity

Electrical conduction is due to the net drift of conduction electrons under the influence of an external electrical field. The resistivity arises from various kinds of imperfections within real metals such as thermal motions of the lattice, impurities, geometrical defects and electron-electron interactions. The electrical resistivity of cubic metals is isotropic and is roughly given by the free electron equation 1.1.1.7 as

$$\rho = mv_F/ne^2l \qquad (1.1.4.1)$$

where l is the electron mean free path. From the above equation one can clearly see that if the dimensions of the sample under consideration are

comparable to the electron mean free path, then its resistivity will be greatly increased due to this geometrical constraint. It was known as early as 1898[24] that the resistivity of metal films was larger than that of bulk specimens. Thomson[25] was the first to suggest that this effect is due to the limitation of electron mean free path by the size of the specimen. The first detailed analysis of the resistivity of a thin metallic film was given by Fuchs[10] based on the space dependence of the Boltzmann transport equation and the idea that the electron mean free path is terminated by a collision at the surface. Assuming a spherical Fermi surface, an isotropic electron mean free path and total random (i.e. diffuse) scattering of the electrons from the surface of a film Fuchs obtained the following equation for film resistivity

$$\frac{\rho}{\rho_B} = \frac{\Phi(\kappa)}{\kappa} \qquad (1.1.4.2)$$

where κ=d/l, d is the film thickness, ρ is the film resistivity and ρ_B the bulk resistivity.

$$\Phi(\kappa) = \frac{1}{\kappa} - \frac{3}{8\kappa^2} + \frac{3}{2\kappa^2}\int_1^\infty \{\frac{1}{t^3} - \frac{1}{t^5}\} e^{-\kappa t} dt \qquad (1.1.4.3)$$

However a somewhat more general theory assumes that when electrons are scattered by the surface of film, a fraction 1-p are scattered diffusively, and fraction p are scattered specularly. When p is independent of the direction of motion of the electrons, the result for electrons is the same as in equation 1.1.4.2 with $\Phi(\kappa)$ replaced by

$$\Phi_p(\kappa) = \frac{1}{\kappa} - \frac{3}{2\kappa^2}(1-p)\int_1^\infty \{\frac{1}{t^3} - \frac{1}{t^5}\} \frac{1-\exp(-\kappa t)}{1-p\exp(-\kappa t)} dt \qquad (1.1.4.4)$$

The limiting form for large κ (thick film) is

$$\frac{\rho}{\rho_B} = 1 + \frac{3}{8\kappa}(1-p) \qquad (\kappa>>1) \qquad (1.1.4.5)$$

and for very thin films

$$\frac{\rho}{\rho_B} = \frac{4(1-p)}{3(1+p)} \frac{1}{\kappa\log(1/\kappa)} \qquad (\kappa<<1) \qquad (1.1.4.6)$$

The single specularity parameter is a very simplistic view and often does not describe the experimental results[11],[12] which require

either temperature dependent p or $\rho_B l_B$. To improve the situation Soffer[13] proposed that a metal surface can be characterized by a root mean square surface roughness h. Assuming all the electrons had the same wavelength λ, and further defining a single surface parameter $r=h/\lambda$ he obtained the following result for an angle-dependent specularity parameter, assuming there is no lateral correlation on the film surface,

$$p(\cos\theta) = \exp(-(4\pi r)^2\cos^2\theta) \qquad (1.1.4.7)$$

where θ is the angle of incidence with respect to surface normal. Using this definition of specularity parameter Soffer obtained the following result

$$\rho_B/\rho = 1 - \frac{3}{2\kappa}\int_0^{-1} du(u-u^3)\frac{(1-p(u))[1-\exp(-\kappa/u)]}{[1-p(u)\exp(-\kappa/u)]} \qquad (1.1.4.8)$$

where $u=\cos\theta$.

1.1.5 Part A--- Size Effect on Temperature Dependent Part of Resistivity - Effect of Surface Scattering

The temperature dependent part part of the resistivity is also drastically affected by the thickness constraint of the sample film. From the discussion of the last section we can write the film resistivity as

$$\rho = \rho_B f(\kappa) \qquad (1.1.5.1)$$

We further define α as

$$\alpha = (1/\rho)(d\rho/dT) \qquad (1.1.5.2)$$

Using equation 1.1.1.7 we obtain the relation $d\kappa/dT=\kappa\alpha_B$, and combined with equation 1.1.5.1 we have

$$\alpha/\alpha_B = 1 + d\ln f(\kappa)/d\ln\kappa. \qquad (1.1.5.3)$$

By using the equation 1.1.4.5 for large κ (thick film) we obtain

$$\frac{d\rho}{dT} = (\rho/\rho_B)(d\rho_B/dT)\left(1-\frac{3(1-p)}{8\kappa+3(1-p)}\right)$$
$$= (d\rho_B/dT)\left(1+\frac{3(1-p)}{8\kappa}\right)\left(1-\frac{3(1-p)}{8\kappa+3(1-p)}\right) \quad \text{for } \kappa>>1 \qquad (1.1.5.4)$$

And in the case of very thin films by using the equation 1.1.4.6, we obtain the following result

$$\frac{d\rho}{dT} = (\rho/\rho_B)(d\rho_B/dT)(1/\ln(1/\kappa))$$
$$= (d\rho_B/dT)\left(\frac{4(1-p)}{3(1+p)}\right)\left(\frac{1}{\kappa(\ln\kappa)^2}\right) \qquad \text{for } \kappa<<1 \qquad (1.1.5.5)$$

Similar results are given for wires[14]. From these two important equations 1.1.5.4 and 1.1.5.5 we draw two conclusions which apply when Eq. 1.1.4.3 and 1.1.4.4 are obeyed. First for both thick ($\kappa>>1$) and thin ($\kappa<<1$) films the form of the temperature dependence of ($d\rho/dT$) is not changed by the size effect. However experimentally this is not always true as we shall see in later discussions. Second, since $p<1$, the magnitude of ($d\rho/dT$) is increased by some factor.

Sambles and Preist[15] also came to the same conclusion for very small κ by applying Soffer's angular-dependent specularity parameter formula (see equations 1.1.4.8). For κ in the range of 0.001 to 10 one can write down the film resistivity from Soffer's formula as

$$\rho = \rho_B + \rho_B\alpha(\kappa,r)\kappa^{-n(\kappa,r)} \qquad (1.1.5.6)$$

where $\kappa=\kappa(T)$ and $\rho_B=\rho_{B0}+\rho_B(T)$, the dependence of parameter n and α have been made explicit, n lies between .3 to 1, α between 0 to 2. From these equations one obtains the increased part of temperature dependent film resistivity as

$$\Delta\rho(T) = (1-n(\kappa,r))\alpha(\kappa,r)\kappa^{-n(\kappa,r)}\rho_B(T) \qquad (1.1.5.7)$$

and $$\rho(T)=\rho_B(T)+\Delta\rho(T). \qquad (1.1.5.7)$$

If one compares the results of these two different approaches it is quite clear that the two conclusions obtained from Fuchs' formula still hold true.

1.1.5 Part B---- Size Effect on the Temperature Dependent Part of the Resistivity Contributed by Other Mechanisms

Normal electron-electron scattering does not contribute to the bulk resistivity in a free electron model even if its scattering rate is two orders of magnitude larger than the umklapp scattering. However Gurzhi[16] suggested that the high normal electron-electron scattering rate does have an influence on size effects. It produces diffusive motions of electrons, which is basically the same as random walk. This kind of motion increases the time needed for an electron to reach the surface where the resistive inelastic scattering of electrons by the surface is taking place. Higher temperature produces more normal electron-electron scattering which means that a longer time is needed for surface scattering to happen. This would reduce the resistivity due to the surface scattering, and the resistivity would decrease as the temperature increases. The opposite of the Gurzhi effect was suggested by Knudsen[17]. At very low temperature, the normal electron-electron scattering rate is very low, but the rare event of this scattering will alter the trajectory of the electrons even though the collision itself does not contribute to the resistivity. Hence scattered electrons will be driven towards the surface where the resistive electron-surface scattering will occur, the net effect is the increase of resistivity by the normal electron-electron scattering. Higher temperature means higher scattering rate, this leads to the increase of surface resistivity with increase in temperature. However these two opposite effects operate in different temperature regions,[52] since the Knudsen effect operates in the region of low electron-electron scattering rate while the Gurzhi effect is effective in the high rate region. For potassium the Knudsen effect is effective only between 3 K to 15 K while the Gurzhi effect is effective between 15 K and 30 K. In both cases

there are only numerical calculations. So these two effects do not have any significance for $\rho(T)$ at T less than 4.2 K.

To explain the large deviation from the T^2 law expected for electron-electron scattering in very thin potassium wires observed by Yu et al.[34], Farrell et al.[18] suggested that even in pure potassium wires localization effects are very important, and resistance of a wire of length L is given by

$$r(L)=(r_s/\nu)\{\exp[\nu r_c(L)/r_s]-1\} \qquad (1.1.5.8)$$

where ν is the number of "distinct" channels and $r_c(L)=\alpha L/l_e$ is the classically calculated additive resistance, and r_s is the scale resistance. Here l_e is the elastic mean free path and α is a constant. Equation 1.1.5.8 gives an exponential dependence of wire resistance on wire length. The coherent interference of electron wave amplitudes scattered by the static disorder of the conductor increases the sample resistance. However the inelastic scattering of electrons destroys the coherence of localized state. Thus the total resistance of the wire is actually decreased by inelastic umklapp el-el scattering. Increasing the temperature increases the inelastic scattering, which in turn reduces the total resistance. In effect the wire breaks into segments, each having its own exponentially increasing resistance, Farrell et al.[18] calculated that in order to explain the experimental results one has to have on the order of 10^3 channels, and their result could only be applied to the thin wires. When thin films are concerned localization theory[18] predicts the following result as

$$\rho(L) = C\ln(L/L_0) \qquad (1.1.5.9)$$

where C is a constant and L_0 is a scale length. Furthermore the localization theory[19] gives a quantum correction to the total resistivity

$$\Delta\rho = \text{constant}\cdot(-\ln(T/Tc)) \qquad (1.1.5.10)$$

where Tc is a characteristic temperature. The equation 1.1.5.9 shows a logarithmic dependence of the length of the film instead of the exponential dependence seen in wires. Thus based on Farrell et al.'s calculations one would not expect to see the same deviation from the T^2 law in thin films.

Kaveh and Wiser[20] proposed yet another explanation for the same experiment results of Yu et al. The idea is based on the simple geometrical arguments shown in figure 1.1.5.1. At very low temperatures an electron originating on the axis experiences a small angle normal electron-phonon scattering, which alters the trajectory of the electron in two different ways, either increasing or decreasing the length traveled by the electron before it has a resistive scattering with the surface. However from figure 1.1.5.1, the two effects are not symmetric and the net result is an increase of the total mean free path for the electrons. Kaveh and Wiser calculated this effect and obtained the following results

$$\Delta\rho_{NEPS} = -\gamma T^5 \qquad (1.1.5.9)$$

where

$$\gamma = 3(\rho_0^2/\rho_{surf}\rho_{imp})(\lambda_{imp}/R)(\beta\theta_D^2)(m/ne^2) \qquad (1.1.5.10)$$

here ρ_0 is the total residual resistivity; ρ_{surf} and ρ_{imp} are the resistivities due to surface and impurities scattering respectively; λ_{imp} is the mean free path due to impurity scattering; R is the radius of the wire; θ_D is the Debye temperature; and β is a constant relating the normal electron-phonon scattering rate to the temperature $\tau_{NEPS}^{-1}(T)=\beta T^3$. When applied to the experiment conditions of Yu et al. they obtained γ as γ=13 fΩ-m/K^5 for d=0.16 mm wire. For thin films one might expect a similar decrease of surface resistivity due to normal electron-phonon scattering. However the film does not have the symmetry existing in a thin wire. One would expect the theory to be the same for the

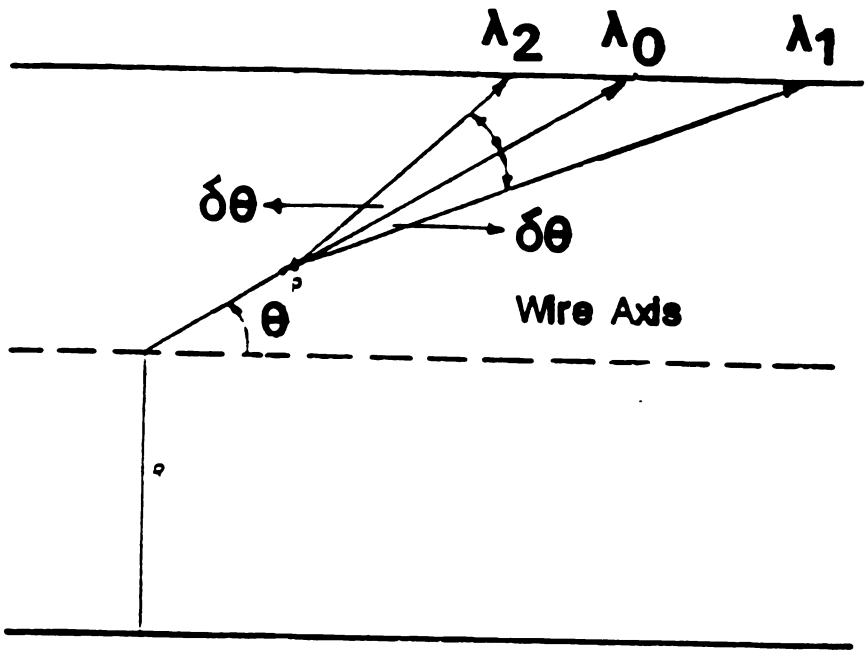

Fig. 1.1.5.1 Normal electron-phonon scattering in a thin wire. The electron undergoes a scatterig in point P, which changes its trajectory with two possible scattering angle $\delta\theta$. The total change of mean free path is $\delta\lambda=(\lambda_1-\lambda_0)+(\lambda_2-\lambda_0)=\lambda_1+\lambda_2-2\lambda_0$, which is positive definite. (See ref.20)

electrons scattered in a plane parallel to the film which includes the direction of the current flow, but the theory would have to be modified for those electrons scattered in the plane of the film.

1.1.6 Temperature Dependent Resistivity Induced by Other Mechanisms

In many investigations the temperature dependence of the resistivity of a metal containing a small concentration of magnetic impurities exhibits a resistivity minimum. At temperatures below the minimum the resistance increases logarithmically as T decreases. Kondo[21] suggested that the magnetic impurity ion forms a localized moment in the metal, and that this magnetic moment interacts with the conduction electrons via a term in the Hamiltonian of the system of the form

$$H_{int} = -J\vec{S}\cdot\vec{s} \qquad (1.1.6.1)$$

where J is the exchange constant and $\vec{S}$ and $\vec{s}$ the spins of the impurity ion and the conduction electron respectively. The scattering of electrons by the local moment through the interaction Hamiltonian in equation 1.1.6.1 is quite different from the previous scattering mechanisms because, during the scattering process, the spin of the conduction electron is flipped over by the magnetic impurity ions. A first order Born-approximation perturbation calculation using equation 1.1.6.1 gives a change of resistivity independent of temperature. However Kondo was the first to find that the second order Born-approximation calculation of local moment scattering led to a divergence of the scattering rate for electrons very near the Fermi surface. The coupling matrix of this interaction could be written as

$$M = \langle\vec{k}',s'| \{ H_{int} + \sum_i \frac{H_{int}\ |i\rangle\langle i|\ H_{int}}{E_0 - E_i} \} |\vec{k},s\rangle \qquad (1.1.6.2)$$

where $|\vec{k},s\rangle$ is the initial state of conduction electrons and $\langle\vec{k}',s'|$ the final state, E_i is the eigenstate energy of intermediate states. The

detailed calculation (For example see W. A. Harrison) led to following result

$$M^2 = (\frac{J}{2N})^2 <Sz>^2 [1 - \frac{J}{2N} \sum_i \frac{2f(\vec{k}i)-1}{E_0 - E_i}]$$

$$= (\frac{J}{2N})^2 <Sz^2> [1 + \frac{JN(0)}{2N} \ln \delta E/E_F] \qquad (1.1.6.3)$$

where N(0) is the density of states at the Fermi surface, Sz is the z-component of local moment, and δE is the energy difference between the initial state and Fermi surface. The result clearly shows the divergence of the scattering rate when δE goes to zero. However at finite temperatures δE is proportional to $k_B T$ and this leads to the dependence of resistivity

$$\rho_{Kondo} = c\rho_1 [1+(J/E_F)\ln(k_B T/E_F)] \qquad (1.1.6.4)$$

where ρ_1 is the first order calculation for one magnetic ion impurity inside metal and c is concentration of impurities. When J is negative the resistivity of the Kondo effect increases logarithmically with decreasing temperature. However, in the Kondo effect there is a strong dependence of the divergence on magnetic fields. This can be understood from the following arguments. When a magnetic field is applied all the spins of the ions are aligned. But the spin-flip of electrons down to up can occur only when there is reduction of spins of ions due to the conservation of the total spin, thus for an electron initially at the Fermi surface energy the intermediate state saw it as if being displaced by the $\delta E = -\mu_0 H$ from Fermi surface energy, from the equation 1.1.6.3 one can see that this reduces the divergence as well as changes the characteristic temperature of the Kondo effect. The more rigorous calculation[22] of the Kondo effect removes the singularity of the resistivity when $T \to 0$.

Another mechanism that gives rise to logarithmic behavior of resistivity results from scattering by a two level system. This was proposed by Cochrane et al.[23] to explain the dependence of resistivity

observed in disordered metals which showed no magnetic field dependence. In order to get a Kondo-like effect they assumed that in an amorphous metal the atoms have two local equilibrium states, and the atoms were free to tunnel between these two states. Just like the magnetic ions with their spins in a Kondo system, this gives the atoms an extra degree of freedom and together with the further assumption that electrons somehow could distinguish these two different positions, the calculation gives

$$\rho_{TWL} = -C\ln[k_B^2(T^2+T_c^2)/D^2] \qquad (1.1.6.5)$$

where C, Tc and D are constants. For an amorphous metal this temperature dependence of the resistivity would disappear with crystallization of sample structure. In our case the potassium metal samples used in our experiment have a well annealed crystalline structure and it is unlikely that the two level theory could be applied.

1.2 Previous Work

In this section a brief history of previous work will be presented. The motivation of our experimental investigation for this dissertation will be discussed.

1.2.1 Potassium and Its Basic Properties

In the last two decades there has been renewed interest[35] in the measurements of the transport properties of alkali metals. These metals are all monovalent with body centered cubic (b.c.c.) structures at room temperature. They have nearly spherical Fermi energy surfaces which do not touch the first Brillouin zone boundaries. Unlike many other metals they have no unfilled d- and f-shells electrons states below the Fermi energy to complicate theoretical calculations. There is no evidence that any of the alkali metals becomes superconducting at low temperature

which means that normal resistivity measurement can be made to very low temperatures. These unique characteristics of alkali metals make them suitable for both extensive theoretical calculations based on our fundamental understanding of solid state physics, and experimental measurement of unprecedented precision at very low temperatures.

Experimentally, among the all the alkali metals, potassium is the most extensively investigated so far. This can be attributed to several unique properties of potassium. Unlike lithium (Li) and sodium (Na) potassium does not undergo a martensitic phase transition when the temperature is lowered from room temperature to the lowest temperature reached. The Debye temperature (θ_D) for potassium is about 100 K, so that its $\rho_{el\text{-}ph}(T)$ is usually negligible below 1.3 K for the bulk metal. Potassium is a solid at room temperature and is chemically much less reactive than rubidium (Rb) and cesium (Cs), so that it is relatively safe to handle and relatively easy to make into samples. Another big advantage of potassium is that it can be obtained with high purity in large quantities from commercial sources.

There exists a large literature[35,36] on theoretical calculations of transport properties of potassium from rather basic assumptions, and good comparisons can be made between the theoretical and experimental results.

We will largely deal with K in terms of conventional nearly free electron theory but it should be noted that Overhauser[37] has long championed the view that the ground state of potassium is a Charge Density Wave (CDW) state which would appreciately modify the transport properties of potassium. If this could be verified it would change our basic understanding of potassium and other simple metals.

1.2.2 Previous Works

Before 1971 it was generally believed that the resistivity of potassium would follow the Bloch-Gruneissen theory which stated that it would be proportional to T^5 at low temperatures. In 1971 Gugan[38] and at the same time Ekin and Maxfield[39] independently reported in their resistivity measurements of high purity potassium that there was a clear violation of the T^5 law. Instead they observed an exponential decrease in resistivity from 4 K to 2 K with decreasing temperature, which was predicted[5] for umklapp electron-phonon scattering when the Fermi surface does not touched the first Brillioun zone boundary. In 1976 van Kempen[40] et al. measured the resistivity of 0.9 mm diameter potassium wires inside polyethylene tubes down to a temperature of 1.1 K with high precision, and concluded that their data could be fitted by the following formula

$$\rho = \rho_0 + AT^s + DT^n \exp(-\theta/T) \qquad (1.2.2.1)$$

where s was between 1 to 2 and n=1, θ=20 K , and A varied from sample to sample by a factor as large as 3.6. This not only confirmed the previous results but also convincingly demonstrated the total absence of the Bloch-Gruneissen T^5 law. If s was chosen as 2 the AT^s term was the first indication of resistivity due to electron-electron scattering which had long been predicted but not observed. Another interesting observation was that when the RRR (residual resistance ratio=R(300)/R(4.2)) was increased by sample annealing at room temperature the coefficient A apparently decreased. In 1978 Rowlands[41] et al. extended the potassium resistivity measurement down to 0.4 K, and found $\rho(T)$ proportional to T^n where n=3/2 for the best fit to the experimental results. However the uncertainty of their data could not rule out a T^2 law out. Bishop and Overhauser[42] explained the $T^{3/2}$ temperature in terms of their CDW theory, which also predicted

the variation of A with different alignments of CDW domains. The many experimental observations of different values of A stimulated theoretical work of Kaveh and Wiser[58] in which they proposed that the coefficient A could vary from sample to sample, or even on the same sample depending on the concentration of anisotropic scatterers, such as dislocations or some other imperfection. In 1978 Levy et al.[43] reported their result of n=2.0 for $\rho(T)$ below 1.4 K and also observed a variation in the magnitude of A.

Armed with a much higher precision for measurements at very low temperature, Lee[44,66] et al. (MSU group) in 1982 measured $d\rho/dT$ of free hanging potassium samples without contacting any oil or plastic tubes of any kind, and confirmed the existence of a $\rho(T)=AT^2$ law due to electron-electron scattering from T=0.35 up to 1.3 K with $A=2.4\pm0.2$ fΩ-m/K^2. There was no large variation of A from sample to sample in their experiments, but there was a deviation from a T^2 law below 0.35 K where $d\rho/dT$ became larger than predicted from T^2 temperature dependence. Lee et al.[44] also measured the resistivity of free-hanging KRb alloys containing 0.077% to 2.24 at% Rb and found the coefficient A increased linearly with ρ_0 . That is, $A=A_0+Ai\rho_0$ where $Ai=(8.5\pm0.3)10^{-6}/K^2$, A_0 for perfect crystal structure. Later on Yu et al.[45] (MSU group) took more complete data on pure K with improved sample conditions and obtained results similar to Lee's. In Figure 1.2.2.1 these results are presented.

It is clear from the results of the above investigators that the resistivity ρ of bulk high purity, well annealed K at very low temperature (0.3 to 4.2 K) is

$$\rho = \rho_0 + AT^2 + DT\exp(-\theta/T) \qquad (1.2.2.2)$$

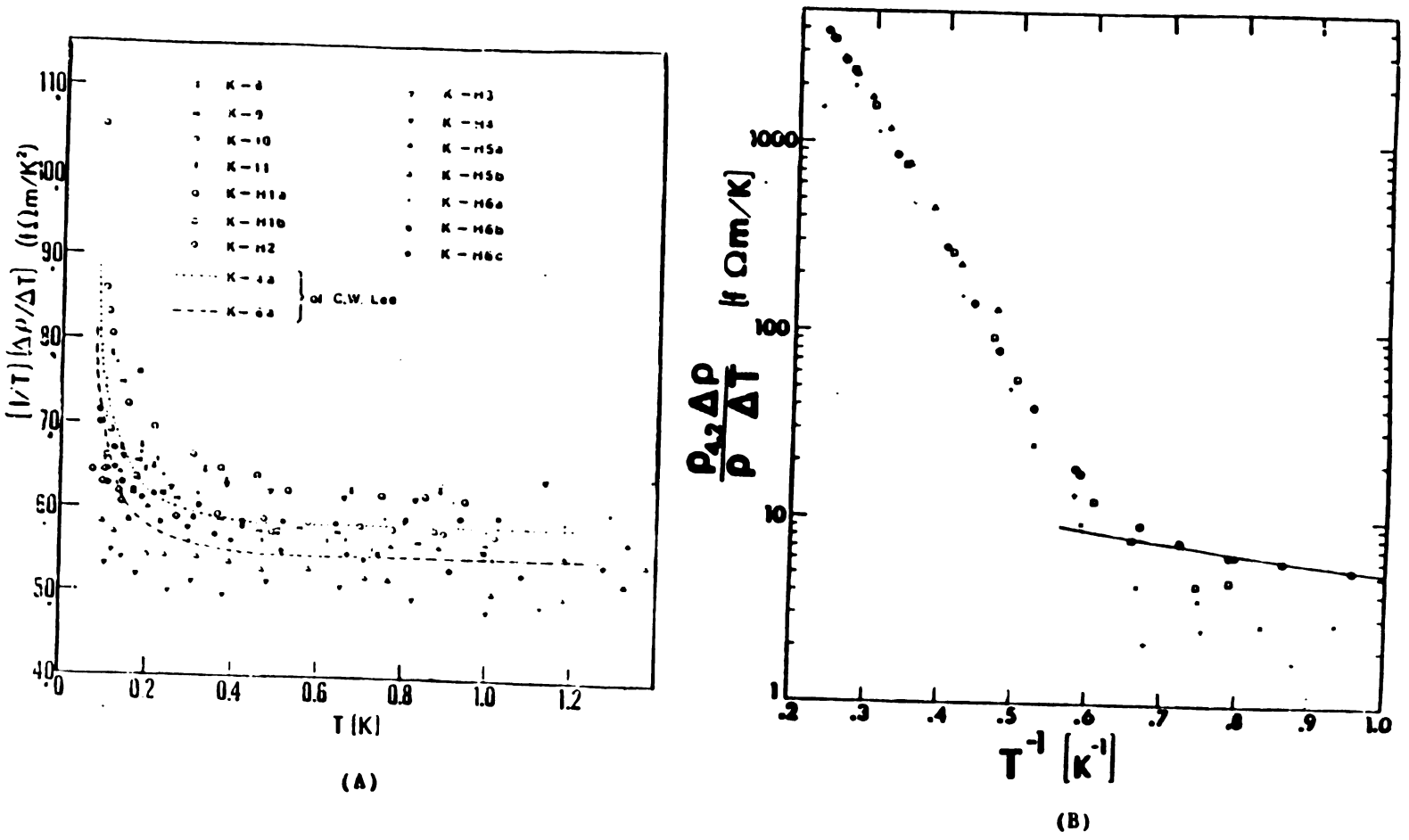

Fig. 1.2.2.1 (A) $(1/T)(d\rho/dT)$ vs. T for free hanging bare high purity thick K samples. (See ref. 45 by Z. Z. Yu). (B) $(d\rho/dT)$ vs. T^{-1} for pure bulk K samples. Notice the logarithmic scale of $(d\rho/dT)$. (See ref. 66 by Pratt et al.)

Representative values of the parameters are A=2.2 fΩ-m/K² (Yu et al) and D=77300 fΩ-m/K and θ= 20.3 K (Haerle et al.[46]). The typical results for high purity bulk K are shown in fig. 1.2.2.1.

However as early as 1971 Gugan[38] had observed substantial changes of $\rho(T)$ between 2 to 4 K in their deformed samples of K, and subsequently Van Kempen et al.[40] and Rowlands et al.[41] In 1982 Van Vucht et al.[47] measured $\rho(T)$ of K down to 0.9 K having twisted his samples at 4.2 K. When they fitted their data with equation 1.2.2.2, they found that the coefficient D of a twisted sample had been increased by a factor of 2 compared with D for well annealed samples. Later Haerle et al.[48] (MSU group) also found an increase of $\rho(T)$ upon deforming their samples, but instead of an increase in the coefficient D observed by Van Vucht et al., they found that the increase could be attributed to an additional term CT^5 with C= 0.30 fΩ-m/K^5, which they attributed to the partial quenching of phonon-drag. Taylor et al.[49] in 1978 and Danino[29] et al. in 1981 provided possible explanations of the partial quenching of phonon-drag in terms of phonon-dislocation scattering, but Gugan argued that these models had too small an effect to account for the observation. In 1982 Engquist[32] and Danino[33] proposed another mechanism, in which electron-dislocation scattering was still responsible for the quenching, but in which anisotropic electron-dislocation scatterings played an important role. This model did not require a very large density of dislocations. However work done by MSU group on deformed K and KRb cast serious doubt on the theory based on anisotropic electron-dislocation scattering. So far there is no definitive model for the quenching of phonon-drag.

Yu et al.[45] (MSU) measured both the resistivity and the thermoelectric ratio of high purity K samples inside polyethylene tubes down 0.07 K, and found that at very low temperatures an additional term

$-b\ln T/T_0$ was needed to explain an observed decrease in $d\rho/dT$ at very low temperature. They showed that this term and the associated anomaly in the thermoelectrical ratio were greatly reduced upon applying a small magnetic field (B~0.1 T). They argued that the logarithmic dependence of $\rho(T)$ at low temperature, and the association of anomaly with thermoelectrical ratio and strong reaction to the magnetic field could be attributed to the Kondo effect.

Yu et al[50] also did a series of measurements on the resistivity of high purity very thin potassium wires and found that there were large deviations from the T^2 law at low temperature. In figure 1.2.2.2 the results for these wires are presented. It can be clearly seen that the largest deviations occurred for the thinnest wires. They also observed that the magnitude of the deviation seemed to be dependent on whether the sample was prepared in an Ar or He atmosphere. Later, Zhao et al.[51] took additional measurements trying to establish the source of the deviations. The additional conclusions from their measurements were that the sample purity was a very important factor in determining the magnitude of the deviation, higher purity resulting in larger deviations. The deviation was enhanced by the corrosion of the surface of the wire. This was probably the source of the difference seen by Yu for samples prepared in Ar and He atmospheres respectively. At the end Zhao confirmed the presence of a size effect in the thin wires.

The deviations observed in Yu's experiments stimulated several theoretical investigations of the source of their. Farrell et al.[18] proposed the model based on the localization model discussed in section 1.1.5. But this model was only valid for the 1 dimensional nature of thin wires, and it also needed a very large number of channels to be comparable with the experimental results.

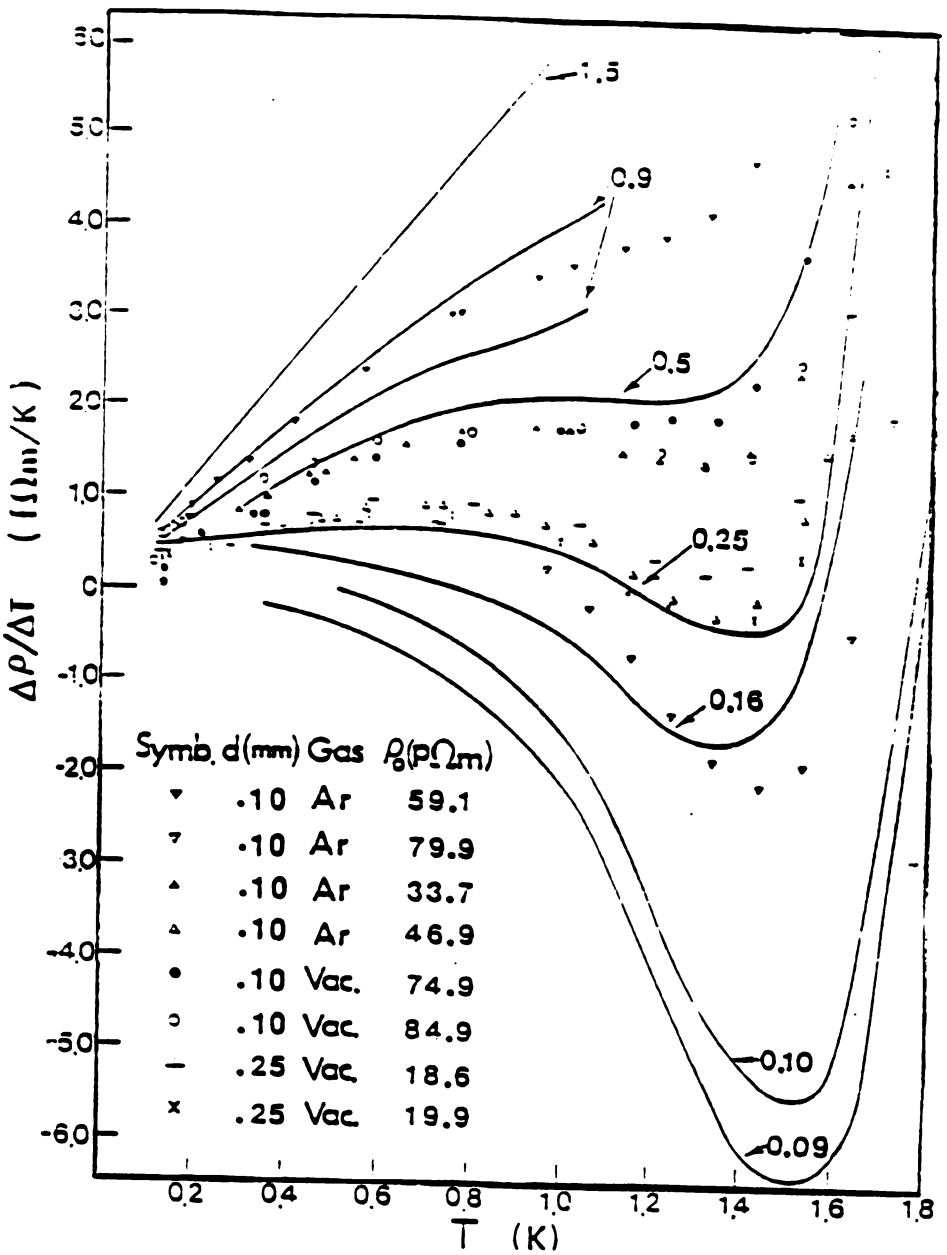

Fig. 1.2.2.2 (dρ/dT) vs. T for thin wires of K, the straight line is the behavior of bulk K. (See ref. 45)

Movshowitz and Wiser[52] did numerical analyses of both Gurzhi and Knudsen effects on K thin wires and concluded that the Gurzhi effect could not be the right explanation for the deviation as Yu et al. first proposed. In 1985 Kaveh and Wiser[20] proposed that it was normal electron-phonon scattering, as discussed in section 1.1.5, that was responsible for the deviation from the T^2 law. Their model proposed a T^5 temperature dependence, and with some adjustable parameters the correct magnitude of deviation was obtained. It was important to note that the underlying physical origin could also be applied to the 2 dimensional nature of thin films, which was not the case for the model proposed by Farrell et al.

It was the work on thin potassium wires by Yu et al. and Zhao et al. that motivated us to see how the size effect would be manifested in the resistivity of thin K films two dimensional nature, and to compare the results with the predictions of various theoretical models. According to CDW[60] model the residual resistivity parallel to $\vec{Q}$ is much larger than it is perpendicularly to $\vec{Q}$. The charge density wave vector $\vec{Q}$ is normal to (110) plane but 45 degree to (100) plane. Hence the CDW model predicted that the residual resistivity of a thin film with (100) planes parallel to the sample surface should be unusually large compared with resistivity in samples with (110) planes parallel to sample surface.

Early experiments[59] on potassium were concentrated on comparing the behavior of residual resistivity versus thickness at fixed temperature with classical thin film theory. Very recently Gridin et al.[53] studied the electrical resistivity of rolled potassium films in the temperature range 4.2-17.4 K. The thickness of their samples was between 3.4 and 69.0 μm. By simply fitting the form of $(T/\theta)^n \exp(-\theta/T)$ they concluded that when θ was fixed, the exponent n of the prefactor in

the umklapp electron-phonon scattering term showed a linear increase as a function of the reciprocal of the film thickness 1/d. And also when n was kept constant, θ showed a similar linear increase as a function of 1/d. However in their analysis they neglected the contribution from normal electron-phonon scattering, which would introduce about 10% systematic error. One also noted that extrapolation of their data to the bulk value did not agree with any previous measurement.

The high accuracy needed to measure the temperature dependent part of the resistivity of potassium coupled with requirement of stable temperature below 4.2 K over long period of time made these measurement hard to achieve. However at MSU the dilution refrigerator equipped with an rf SQUID null voltage detector, coupled with a very high precision current comparator enables us to make measurements of $d\rho/dT$ of a potassium thin film with very high precision. In the next chapter we will discuss the experimental apparatus in detail.

CHAPTER 2 EXPERIMENTAL APPARATUS AND TECHNIQUES

2.1 Introduction

In this chapter we are going to discuss in detail the experimental apparatus used in the measurements. The three most critical pieces of equipment for the success of the measurements deserving special examination, are the dilution refrigerator, glove-box and current comparator.

2.2 Experiment Set Up

2.2.1 Dilution Refrigerator

Since our main interest is in the range from 4.2 K to about as low as possible (mK), we employed a largely locally built continuous flow dilution refrigerator with an operating temperature range from 70 mK to 4.3 K.

After one transfers liquid nitrogen into the Dewar system, it takes about 24 hours for the system to cool down from room temperature to about 77 K, during which time one has to retransfer nitrogen twice to assure a smooth cooling. When the system is at liquid nitrogen temperature a built in ^{3}He-^{4}He mass spectrometer leak detector is used to check if there is any leak in the circulation system of the refrigerator. Only after one is sure that there is no leak whatsoever then the transfer of the liquid helium begins. It takes about 25 liters of liquid helium transfered over a period of two hours to fill the refrigerator system and reach 4.2 K. After pumping the liquid ^{4}He from the 1 K pot, the ^{3}He and ^{4}He mixture is condensed and circulation of the

mixture commenced. It usually takes 6 hours to get down to the 70 mK, which is the lower limit of the system. For the detail working principle of the dilution refrigerator and how it is operated one could see Lounasma's[53] book.

2.2.2 Current Comparator and SQUID

For a typical K sample, the relative resistivity change at 1 K, $\Delta\rho/\rho$, is about 10^{-5} for a temperature change of 0.1 K, and it usually gets smaller when the temperature is lower. To measure $\Delta\rho$ to ≈ 1% , we therefore need a precision ≈ 1 in 10^7. To achieve such a precision we used a commercial high precision current comparator modified by Edmunds et al[54]. In conjunction with this we use a rf SQUID (Superconductor Quantum Interference Device) made by SHE Inc. as a null detector. The SQUID could detect a signal of less than 10^{-15} V or less then 10^{-9} A. To eliminate any possible electrical and magnetic interference from the surrounding environment, several layers of μ-metals are used to shield the refrigerator from magnetic fields. The refrigerator plus measuring equipment is enclosed in a commercial double-layered screened room made by Erik A. Lingren and Associate Inc, to further reduce any possible RF noise which could interfere with the operation of the SQUID. Even though the rf-SQUID is shielded by several layers of μ-metal, the mechanical vibration of the refrigerator system in the earth's magnetic field could induce current which in turn, could show up in the extremely sensitive SQUID system as noise. To prevent this from happening the whole refrigerator system is mounted on a high-gas-pressure vibration isolated supporting table, and all the system pumps are put outside of the screened room and connected with bellow tubes.

2.2.3 Glove-Box and Vaccum System

To handle the very active, and sometimes dangerous alkaline metals we used a commercial argon filled glove-box made by Vacuum Atmosphere Company to our design with a locally built purification system to remove oil and water vapor. The whole system has a nominal oxygen content of less than 0.4 ppm as calibrated by S. Yin, by comparison with another Helium filled glove-box with an oxygen content meter. The time it takes for potassium to oxidize is an indication of how much H_2O contamination is probably in the system. We could not measure the water vapor contamination directly but the potassium keeps shiny for several hours.

Since our main interest is to measure the temperature dependence of the potassium films, we have constructed a high vacuum system inside the glove-box. Within the belljar potassium can be evaporated. Figure 2.2.3.1 shows the evaporation system enclosed inside the glass bell jar, which hangs mono rail style by pulleys from a horizontal rod, so that if can be move horizontally along the length of glove-box. Once it is evacuated, it is independent of the glove-box. The stainless steel flange is connected to the pumping system, and has variety of feedthroughs. Commercial high frequency feedthroughs are used to link the quartz crystal oscillator to the thickness monitor control. A two line water feedthrough is used to cool the quartz crystal. There are two rotation feedthroughs that are used to manipulate the evaporation sources and a shutter. The evaporation source is mounted on a platform with a threaded hole in the center and two smooth guide holes on each side. A threaded rod connected to one of the rotation feedthrough passes through the threaded hole in the platform. Thus by rotating the feedthrough outside the vacuum system one could move the evaporation source back and forth at will. The heater was enclosed by BN wall with bottom and top covered by stainless steel to prevent the radiation loss

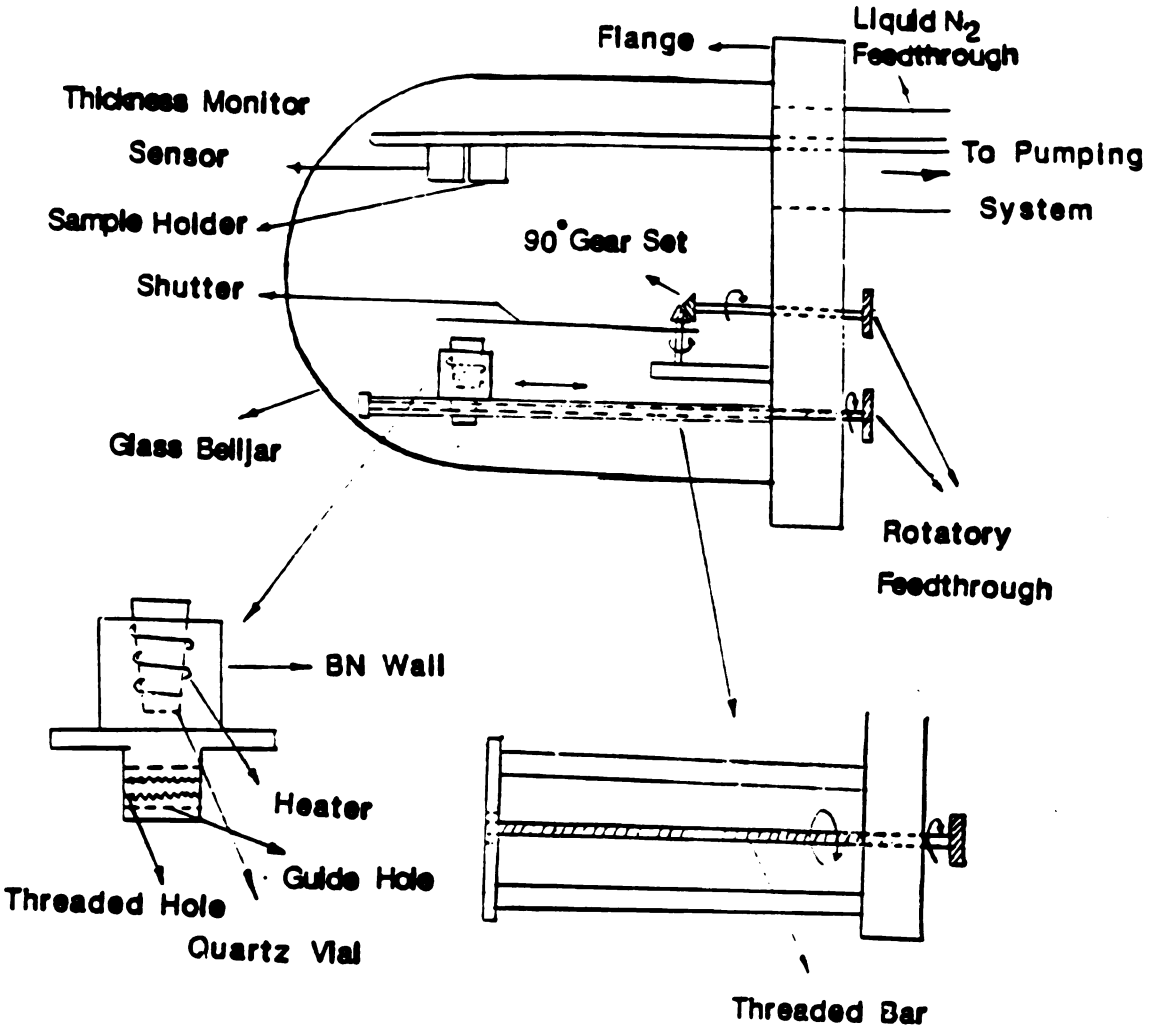

Fig. 2.2.3.1 Evaporation System Enclosed Inside Glass Belljar.

of heat. However there was a hole to be used for heating quartz crystal vial on the top cover. Two 45 degree gears connected to another rotation feedthrough convert the rotations of the feedthrough outside the vacuum into the motion of the shutter. The detail is shown in figure 2.2.3.1.

The glass belljar is connected to a diffusion pump with a liquid nitrogen trap which is backed by a rotary mechanical pump. The whole system is shown in figure 2.2.3.2, the first thermocouple gauge is placed in the belljar and an ion gauge is placed some distance away, near the diffusion pump. With the cooling of the liquid nitrogen one could achieve a high vacuum of the order of 10^{-7} Torr as indicated by the ion gauge.

2.2.4 Sample Can

The sample can is made of two parts. The copper can shown in figure 2.2.4.1 is made of copper with a brass ring hard-soldered to the top. This has a shallow groove to hold an Indium O-ring and 12 threaded holes for screws to attach the top enclosing flange and sample holder. The flange is made of brass with several feedthroughs. The bigger copper feedthrough serves as the cold sink and attachment to the refrigerator mixing chamber. Since it is hard-soldered to the flange, it is both electrically and thermally connected to the flange and copper can. The two thermal feedthroughs are a little more complicated. Each has a stainless steel tube, hard-soldered on the outside of flange, and a long copper rod inside the stainless tube. The copper rod is well annealed, 8 cm long and 3 mm in diameter, and is sealed to the end of the tube by stycast 3850 epoxy, which is both electrically and thermally insulating. At the other end of the copper rod a silver thermal link is spot-welded to connect the mixing chamber and the sample. The poor thermal conductivity of the stainless steel tube and insulation of the

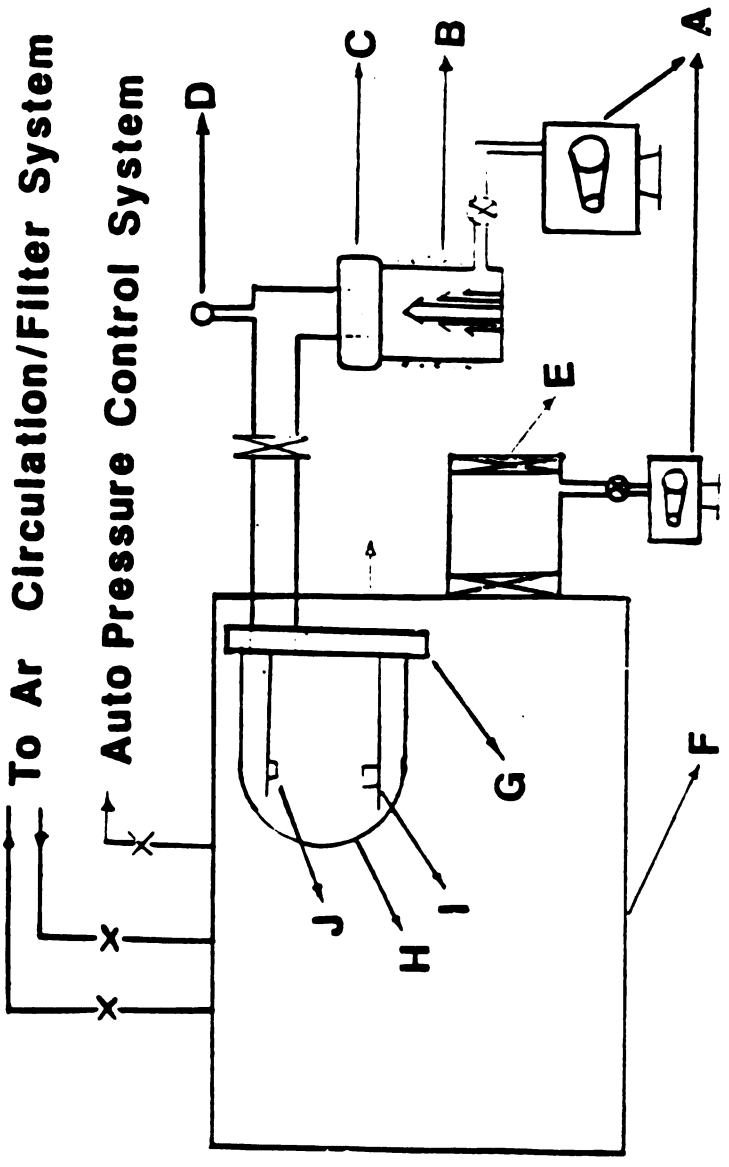

Fig. 2.2.3.2 The Whole Glove-Box with Vacuum Pumping System. (A) Mechanical Rotary Pumps. (B) Diffusion Pump. (C) Liquid N_2 Cold Trap. (D) Thermocouple & Ion Gauges. (E) Transfer Port. (F) Glove-Box. (G) Flange. (H) Glass Bell Jar. (I) K Oven. (J) Sample Holder.

s
e
c
T
s
o
p

2
w
E
t
S
c
a
c
m
s
t

p
i
s
c
f

stycast 3850 epoxy keep the sample isolated from the Sample Can. The electrical feedthrough is similarly constructed but instead of the copper rod, the necessary superconducter wires (Niomax made by IMI Titanium Inc., and Norton Co.) are put into the tube and sealed with stye-cast. Between both ends of the copper coated superconductor wires one has to remove a half inch section of copper coat by acid etching to prevent heat conduction by this layer.

Another part of the sample can is the sample holder shown in figure 2.2.4.1. Since it was originally designed by Yu et al. to measure two wire samples at the same time, it has two separated support structures. Each of them is an independent 4-probe resistance system consisting of two copper voltage lead supports and two copper current lead supports. Since potassium is very reactive with oxygen and water vapor, a sheet of copper coated with a thin layer of potassium was inserted in the can to absorb gases (O_2, H_2O). This was a very effective way to reduce contamination of the potassium sample. Visual inspection and measurement of the change of resistance indicates that the potassium sample changes very little after several days inside the can at room temperature.

Since we are studying the temperature dependence of the transport properties, the precise measurement of temperature is critically important. We use germanium resistance thermometers to measure the sample temperature, the thermometer is attached by copper clamps to the copper rod outside of the sample can. The well insulated copper rod feedthrough ensures that we do measure the sample temperature.

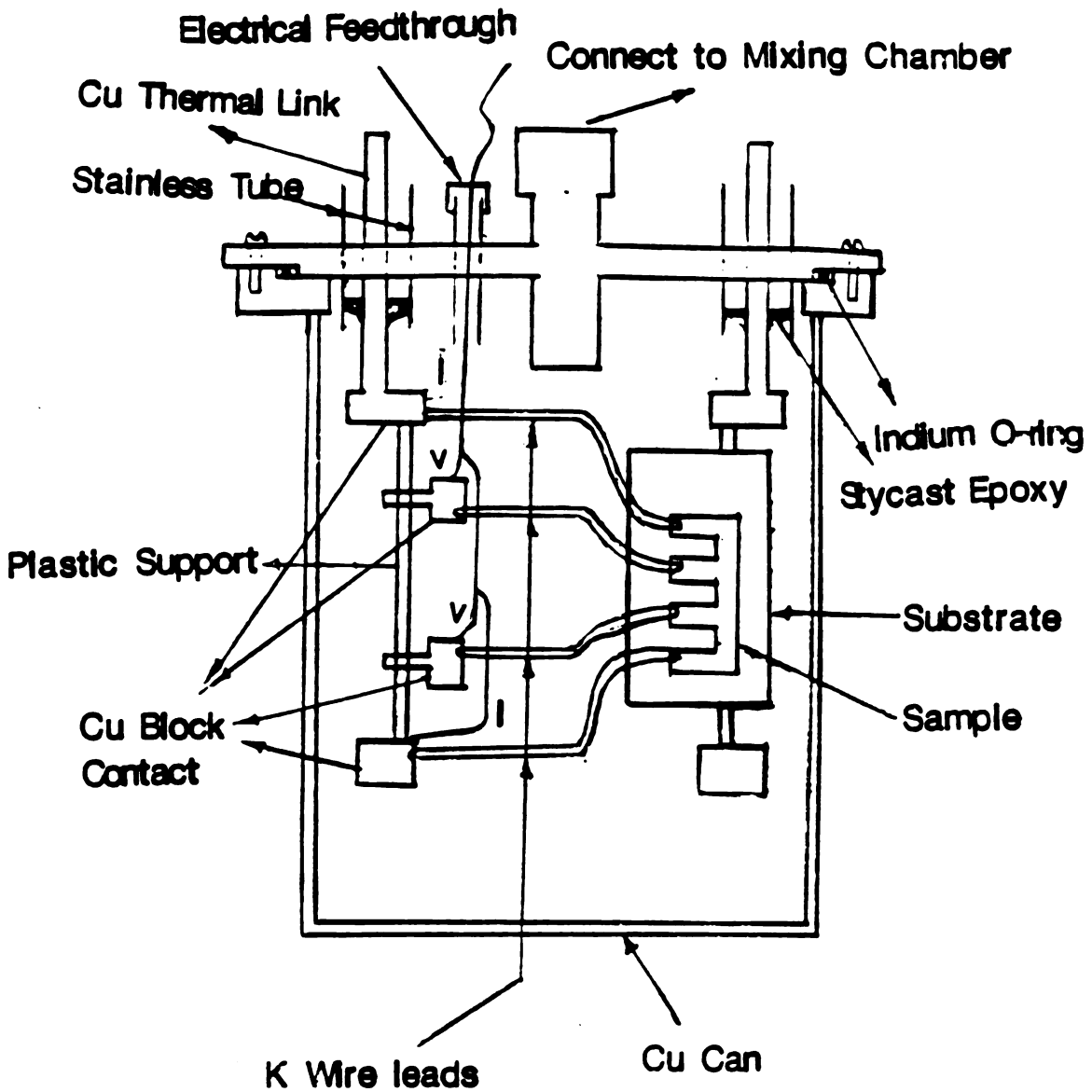

Fig. 2.2.4.1 Sample Can

2.2.5 Thickness Measurements

The thickness of the sample is determined by a thickness monitor, and the results are checked independently by Spectrum Intensity Measurements.

The film thickness monitor is a Temescal Inc. model FTM-3000 which has a quartz crystal sensor. The principle of operation is that mass deposited on the crystal shifts the resonant frequency of the quartz crystal. The monitor which has been equipped with a microprocessor automatically converts resonance shift to mass, and hence from a knowledge of the deposition area to the film thickness.

The other method is totally different from the film thickness monitor. First one puts the sample or the quartz crystal sensor with the deposited film into deionized water to make a KOH solution. Then one makes a series of secondary standard solutions from a very concentrated standard solution from Aldrich Chemical Company, Inc. Using the Blackspectrum IV from Spectrum Inc., one measures the potassium spectrum intensity versus the concentration of the standard solutions. From the graph of intensity versus concentration the sample concentration is easily obtained from measurement of its spectrum intensity. Finally the concentration is converted into the film thickness. The secondary standard and sample were made by mixing standard solution or K film with deionized water. The fluid volum during the experiments was measured by volume beakers and pipettes, which had very poor resolution. Due to the difficulty in making the secondary standards because of the large error in reading the water volume, one introduces very large errors into the measurements. The additional error in making the sample solution, and the intrinsic system errors of the Blackspectrum IV, give a total relative error estimated to

be about 25% of the measurement. The two measurements agree within this experimental uncertainty.

2.2.6 Thermometry

The accurate measurement of temperatures largely depends on the two thermometers, which we call G1 and G2. Both are Lakeshore Cryotronics Germanium resistors. G2 was calibrated by C. W. Lee and M. L. Haerle[55] in three stages. G2 was calibrated against a Cryocal CR50 thermometer calibrated by J. L. Imes and G. L. Neiheisel[56,57], by using the He^3 Vapor pressure as a temperature standard and extrapolating using a CMN susceptibility thermometer to plot the G2 conductance vs. temperature from 0.065 K to 4.2 K. Then the following equation was used to fit the data for temperature calculation,

$$\ln R = \sum_{i=0}^{9} A_i (\ln T)^i \qquad (2.2.6.1)$$

But this standard is only accurate enough for our experiment from 1.3 K to 4.2 K. Below that we have to use other means. For 0.059 K < T < 1.24 K a set of Superconducting Fixed Point Devices SRM767 and SRM768 obtained from National Bureau of Standards is used to get 6 absolute temperature calibration points. A susceptibility thermometer is used to interpolate between the fixed points. By using the same equation (2.2.6.1) mentioned above, these data are used to calculate temperature below 0.5 K. For the temperature between 0.5 K to 1.3 K, a large powder sample of cerous magnesium nitrate and four fixed points were used for calibration and interpolation. Again the same equation (2.2.6.1) is used to fit the data.

G1 was originally calibrated against G2, but after it was used for a while, one of its four leads was broken, and therefore it was configured for a three probe measurement, that is one of the leads

served as both voltage lead and current lead. It is calibrated against G2 for the whole temperature range.

We will discuss in section 2.3.4 how the accuracy of these calibrations was checked against the Wiedemann-Franz Law. An Ag-.1 at% Au alloy wire was used as follows. One end of the alloy (R and R' in fig. 2.3.3.1) was attached to the mixing Chamber of the refrigerator at fixed temperature and the other end of the wire was firmly attached to G2 for measuring the temperature change, when a known thermal current passed through the alloy wire. The product $T\Delta T$ as measured by the calibrated G2 is within the value predicted by the Wiedemann-Franz Law for the known electrical resistance of the alloy with a standard deviation of 1.2%[45]. To further ensure that the calibration does not change during the course of the experiment, the test using the Wiedemann-Franz Law is applied to G1 and G2 while one actually takes data during a run, and this double check guarantees the consistency of the temperature measurement.

The conductance of G1 and G2 were measure by two self balancing SHE conductance bridges (model PCB) with 4-probe configuration, The excitation voltage used in these bridges is from 10 to 100 μV. They are accurate to better than 5%. The differential output of one of these bridges was led into a temperature controller to regulate the temperature of the mixing chamber.

2.3 Measurement Procedure

In this section I will briefly describe the procedure used for the sample preparations and sample measurements.

2.3.1 Cleaning Procedure

In the course of the measurements three kinds of substrates are used, namely the amorphous surface of a microslide glass, <111> oriented surface of a high purity silicon Wafer, and <100> oriented surface of the potassium fluoride (KF). The glass and the silicon are cleaned by the same procedure. First one puts the glass/silicon into a beaker of ethyl alcohol placed inside the chamber of an ultrasonic bath. The ultrasonic power is turn on for about than ten minutes. After that one takes the substrates out of the beaker and puts them into trichloroethane solution to further clean any possible residual oil on the surface of the substrate and then again the substrates were clearned by alcohol solution. After this rigorous cleaning procedure one puts the substrate under a mask which is placed in a vacuum chamber pumped by a turbo molecular pump. Silver is evaporated at a pressure of $5 \cdot 10^{-5}$ torr on to the substrate through a mask to give four strips of thin silver film as four probe leads.

2.3.2 Making Thin Films

After the substrate is cleaned and the Ag leads were made, four thin copper wires were soldered to the silver strip leads, so that later on one could measure the resistance of the film sample in situ during the evaporation. One then covers the substrate with a mask which has the four probe geometry cut out as shown in figure 2.3.2.1. We have used masks made from two different kinds materials. After the substrate is in place it is firmly attached with masking taped. The substrate and mask were placed in the vacuum port of the Glove-Box along with the sample can, necessary tools, and indium O-ring. They would be left there to outgas for several hours before transferring them into the Glove-Box where they were left over night for further cleaning. At the

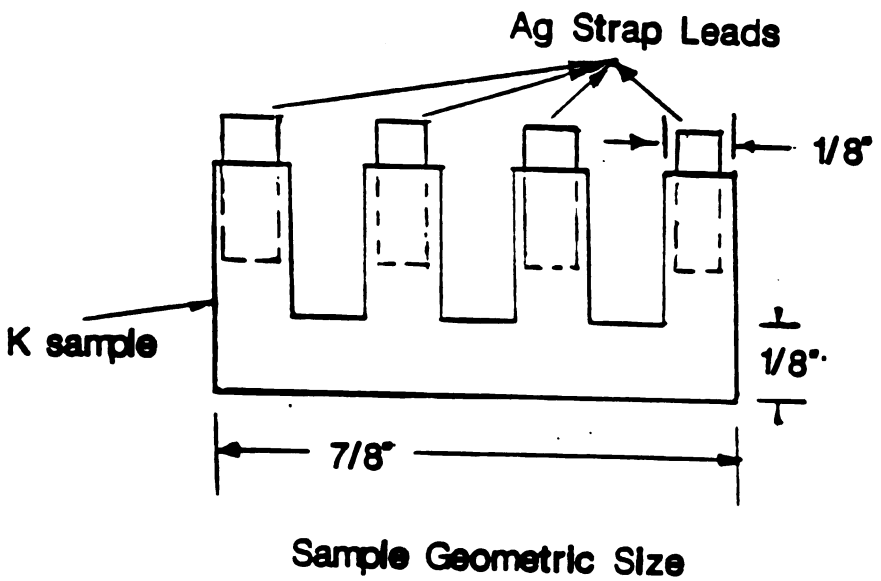

Fig. 2.3.2.1 Geometrical Form of Sample

same time one begins pumping the bell jar. The next day one puts the mask and substrate into the glass jar, and pumps the system down to the a vacuum of 10^{-7}Torr with a liquid nitrogen trapped diffusion pump. This usually takes about 5 or 6 hours. Only then does one begin to evaporate potassium by applying about 3 amperes DC current to the heating wire of the evaporation oven. The evaporation rate for most samples was about 12-20 Angstrom/sec. Later on we realized that fast evaporation made smoother films, so that the evaporation rate was increased to 60-100 Angstrom/sec. It seems that the evaporation rate has no overall effect on our low temperature measurements. During the evaporation one continuously monitors the evaporation by measuring the film resistance and checking the film thickness monitor. Usually the film is not conductive until it is about 2 micron thick (about 20,000 Angstrom).

After the film sample was made, it was put into the sample can, sealed and taken out of the glove-box. The resistance was measured one more time before the sample can was finally put into the dilution refrigerator. It takes about another 24 hours before the sample reaches liquid nitrogen temperature (77 K).

2.3.3 Technique for Resistance Measurement

The detailed thermal and electrical circuits in figure 2.3.3.1 are used to do the measurement. The SQUID (Superconducting Quantum Interference Device) in the circuit is a null detector, and there are here R_m for reference and R_s for sample. For large R_s, a properly chosen inductor has to be used in series with the resistors to keep the circuit relaxation time at approximately one second, in order to reduce the noise and keep the SQUID locking properly. There are three inductors to choose from, with values of 0, 50,and 200 μH respectively. They are made of multifilament Nb-Ti superconducting wires (Niomax CN)

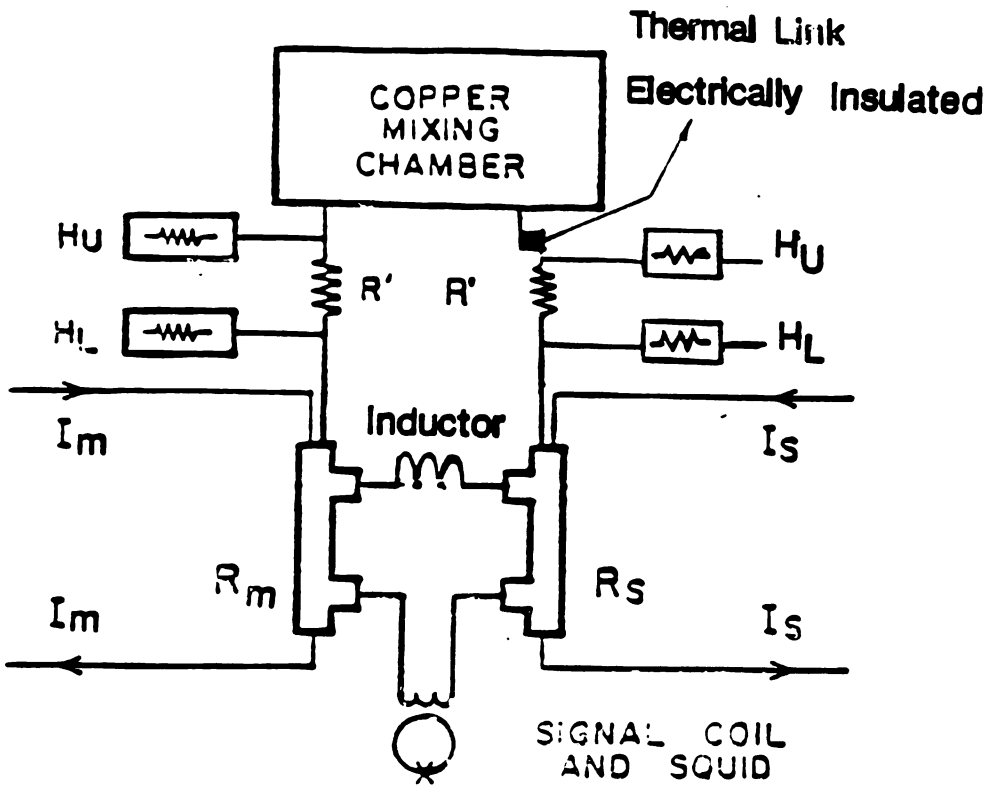

Fig. 2.3.3.1 Thermal Electrical Circuits

having a Tc larger than 4.2 K. The proper choice of inductor turns out two resistors connected in series, we call them, R_m and R_s respectively, to be very crucial to the success of the measurement.

The measurement of resistance is accomplished by measuring the ratio of the two resistors, this is done with the help of the current comparator. First let us call any pair of these resistors R_m and R_s respectively, and corresponding currents from the comparator I_m and I_s. A switch in the current comparator could reverse the direction of the both I_m and I_s simultaneously. I_s and I_m have the relation of $I_s=C/I_m$, where C can be obtained directly to 1 part in 10^7 from the dials of the current comparator. To eliminate any possible thermal EMFs generated within the circuit, a standard current reversal technique is employed as follows.

The currents going through R_m and R_s in one direction generate a voltage V^+ in the SQUID circuit

$$\begin{aligned} V^+ &= I_m R_m - I_s R_s + V_T \\ &= I_m R_m - C I_m R_s + V_T \end{aligned} \qquad (2.3.3.1)$$

where V_T stands for any thermal EMF. One then reverses the current to give

$$\begin{aligned} V^- &= -I_m R_m + I_s R_s + V_T \\ &= -I_m R_m + C I_m R_s + V_T \end{aligned} \qquad (2.3.3.2)$$

One then adjusts the comparator switch setting such that we have

$$V^+ = V^- \qquad (2.3.3.3)$$

$$I_m R_m - C I_m R_s + V_T = -I_m R_m + C I_m R_s + V_T \qquad (2.3.3.4)$$

$$2 I_m R_m = 2 C I_m R_s \qquad (2.3.3.5)$$

$$C = \frac{R_m}{R_s} \qquad (2.3.3.6)$$

which is independent of the influence of thermal emfs.

At 4.2 K, the absolute value of R_s and R_m were obtained from their respective ratios with a known standard resistor R_{st}, which has the

values of 1.134 $\mu\Omega$ at 4.2 K. Then these values are used to calculate the residual resistance ratio, or RRR,

$$RRR=\frac{\rho(295K)}{\rho(4.2K)}=\frac{R(295K)}{R(4.2K)} \qquad (2.3.3.6)$$

Then assuming there is no changes in geometry of the sample, we get

$$\rho(4.2K)=\frac{R(4.2K)}{R(295K)}*\rho(295K)=\frac{\rho(295K)}{RRR} \qquad (2.3.3.7)$$

For potassium samples the above formula becomes

$$\rho(4.2K)=\frac{7.19\ \mu\Omega\text{-cm}}{RRR} \qquad (2.3.3.8)$$

The above describes in detail the direct measurements of resistance of the samples, however this direct approach has its very serious deficiency due to the physics of the resistivity. Assuming that there is no large deviation for high purity potassium samples from Matthiessen's Rule, one could write down the resistivity in two parts, one, the so called residual resistivity which is caused by all the defects inside the samples, is independent of the temperatures; the other is dependent on the temperature so that we have following equation

$$\rho_{total}=\rho_{residual}+\rho(T) \qquad (2.3.3.9)$$

And in general the ratio of $\rho(T)/\rho_{total}$ is about 10^{-5} at about 1 K. $\rho(T)$ will usually be written as the sum of terms representing several temperature dependent mechanisms, the results of fitting these terms to the data yield parameters highly dependent on the chosen value of ρ_0. To avoid arbitrariness in the choice of ρ_0, we choise to measure the $d\rho_{total}/dT$ directly since from (2.10) we have

$$\frac{d\rho_{total}}{dT}=\frac{d\rho(T)}{dT} \qquad (2.3.3.10)$$

and it is independent of the residual resistivity.

For a typical experiment, we use a Ag-Au alloy as R_m, which has a resistance of 16 $\mu\Omega$ and a R_s has a resistance of the same order of magnitude. After one cools down the system to liquid Helium temperature and starts circulation of the mixture, the above mentioned procedure is

performed to get $\rho(4.2\ K)$. Then one lowers the mixing chamber of the refrigerator to some fixed T by using a temperature controller and gets

$$C(T)=\frac{R_s(T)}{R_m(T)} \qquad (2.3.3.11)$$

To measure the $d\rho/dT$ experimentally, one puts a small heating current through either R_s side of H_U or U_L to raise the $R_s(T)$ to $R_s(T+\Delta T)$, and at the same time one uses the differential output signal from the conductance potential bridge, which is used to measure the temperature of R_m, to keep the temperature of R_m constant, so that one gets

$$C(T+\Delta T)=\frac{R_s(T+\Delta T)}{R_m(T)} \qquad (2.3.3.12)$$

and from equation 2.12 one has

$$\Delta C(T)=C(T+\Delta T)-C(T)=\frac{R_s(T+\Delta T)}{R_m(T)}-\frac{R_s(T)}{R_m(T)}$$

$$=\frac{1}{R_m(T)}\times(R_s(T+\Delta T)-R_s(T))=\frac{1}{R_m(T)}\times\Delta R_s(T) \qquad (2.3.3.13)$$

considering Eq. 2.12, we further have

$$\frac{\Delta C(T)}{C(T)}=\frac{\Delta R_s(T)}{R_s(T)}=\frac{\Delta\rho_s(T)}{\rho_s(T)} \qquad (2.3.3.14)$$

which is of the order of 10^{-5} at 1 K and there is little error introduced for the following equation

$$\rho_0\times\frac{1}{C(T)}\times\frac{\Delta C(T)}{\Delta T}=\frac{\rho_0}{\rho_s(T)}\times\frac{\Delta\rho_s(T)}{\Delta T}\approx\frac{d\rho}{dT} \qquad (2.3.3.15)$$

Here ρ_0 is either $\rho_s(4.2\ K)$ or $\rho_s(1.2\ K)$ for the different temperature range. So we obtain the relation

$$\frac{d\rho}{dT}=\lim_{\Delta T\to 0}\frac{\rho_0}{C(T)}\times\frac{\Delta C}{\Delta T} \qquad (2.3.3.16)$$

which is the experimental value we measure.

The current used in the experiments usually ranged from 5 mA to 50 mA depending on how large R_s was. As long as there is no significant Joule Heating by the current, the largest possible current is chosen in order to achieve greater accuracy. One also has to use different currents to ensure that there is no current dependence.

2.3.4 The Techniques for G measurement

In the last section we described in detail how $d\rho/dT$ is measured against temperature with high accuracy. In this section we are going to briefly discuss another related important quantity, the thermoelectric ratio G.

As mentioned in chapter 1, the resistivity could be defined as

$$\rho=\frac{E}{J}\Big|_{\nabla T=0} \qquad (2.3.4.1)$$

and the thermoelectric ratio as

$$G = \frac{j}{q}\Big|_{\vec{E}=0} \frac{I}{Q}\Big|_{E=0}. \qquad (2.3.4.2)$$

Assuming that the Wiedemann-Franz law is valid as pointed out in chapter 1. Then the thermopower S is

$$S=G\kappa\rho=GL_0\ T \qquad (2.3.4.3)$$

where L_0 is ideal Lorentz number, T is temperature.

The G measurement closely follows the definition of equation 2.3.4.2. A heater with resistance R_G is attached to the sample. A small current I_G is passed through the heater so we have a heat current of $\dot{Q}=I_G^2R_G$, which produces a thermo-electric voltage V_G detected by the SQUID. To cancel out this voltage we apply a current I_s, and since we have $I_s=C\times I_m$ then

$$G=\frac{CI_m}{I_G^2R_G} \qquad (2.3.4.4)$$

we use a Dale resistor as the heater, which has a relative stability of 0.1% below 4.2 K. Usually we set the I_G/current to 5 mA.

For Potassium films we did no G measurements, because the substrate and the film have the same order of magnitude of thermal conductance.

Chapter 3 Experimental Results

In this chapter we present and discuss the experimental results of our measurements on thin films. The major portion of the discussion is devoted to the understanding of 2 dimensional size effect on electron-electron scattering and electron-phonon scattering, and the differences between 3-D, 2-D and 1-D systems, characterized by the ratio of their geometric size to the electron mean free path. Some other experiments will be discussed at the end of this chapter.

The bulk potassium resistivity $\rho(T)$ has been measured by many different groups and the measurements are relatively well understood. A typical recent result for both the T=1.3 to 4.2 K by Pratt et al.[66] and 0.1 to 1.3 K by Yu[45] is shown in figure 1.2.2.1. For bulk potassium $\rho(T)$ from T=1.3 to 4.2 K is dominated by umklapp electron-phonon scattering, and can be described by the semi-emprical equation

$$\rho_{el\text{-}ph}(T)=DT^{n}EXP(-\frac{\Theta}{T}) \qquad (3.1.1)$$

Here D is a constant and Θ is a characteristic temperature, and n is a coefficient. The quantities of n and Θ are not independent but rather correlated with $n\geq 1$, there is no rigorous theoretical calculation to give a firm value of n and Θ. Here we take $n=1, \theta=20.3$ (K) and D=77300 ($f\Omega$-m/K) which are obtained by fitting the experimental data by M. Hearle[46].

For T=0.3 to 1.3 K the dominating contribution to $\rho(T)$ comes from electron-electron scattering. From simple phase space arguments[36] given in chapter 1

$$\rho_{el\text{-}el}(T)=AT^2 \qquad (3.1.2)$$

The best value of A from experimental data is 2.2 ($f\Omega$-m/K²)[45]. For T<0.3 K the slight upturn of the data is not well understood, but it is thought to be the contribution from inelastic electron-dislocation interaction[45].

Yu[50] et al. have measured many potassium wire samples of different sizes, which are comparable to the electronic mean free path at very low temperature. Their data, shown in figure 1.2.2.2, indicate very large deviations from the T^2 law. The origin of this deviation is not clearly understood yet. (See the discussion in chapter 1).

3.1 Crystal Structure of K Films on Different Substrates

Crystalline potassium at room temperature has a body-centered cubic (b.c.c) structure with a lattice constant of 5.34 Å.[61] The bulk pure potassium was deposited on a substrate by thermal evaporation inside a high vacuum belljar. Three kinds of substrates were used in our experiments. They were amorphous microslide glass, high purity crystalline Si, and crystalline KF cleaved at a (100) surface. Among them the crystalline KF is unique because its lattice constant is 5.347 Å[61], which is almost the same as the potassium lattice constant.

The structures of the K film on these substrates were determined by x-ray diffraction. We used a very versatile θ-2θ scanning x-ray machine (Rotaflex made by Rigaku, USA Inc.) to do the measurements. The machine has a resolution of Δq=0.003 $Å^{-1}$, but the initial position of q=0 has to be adjusted every time one uses it, which sometimes can result in a shift of initial position as large as 0.02 $Å^{-1}$. In our setup the wave vector $\vec{q}=\vec{k}-\vec{k}'$ was normal to the surface of the sample; here $\vec{k}$ and $\vec{k}'$ are the wave vectors of incident and reflected x-ray beams. The x-ray diffraction was done in air at room temperature, and it often took

several hours to complete one scanning run for K films. Since the potassium is very reactive in air, it took less than 1 minute to completely oxidize a 10 μm thick K film when it was exposed to air. Great care was therefore taken to prevent the oxidation of the K film. The sample was left inside the glove-box filled with Ar gas after the deposition of K onto the substrate. Then we coated the K film with paraffin wax which had a lower melting point than potassium. Furthermore we put another layer of vaccuum grease on top of the wax to prevent possible oxidation through small cracks within the wax. After this procedure the K film could exist for about 24 hours without visible oxidation when the whole ensemble was exposed to air.

The condition that all scattered x-rays interfere constructively is given[62] by

$$\vec{G}\cdot\vec{q} = 2\pi n \qquad (3.1.1)$$

where $\vec{G}$ is a reciprocal lattice vector, $\vec{q}$ is the difference of wave vectors of incident and reflecting beams ($\vec{q}=\vec{k}-\vec{k}'$), and n is an integer. For a b.c.c. structure Eq. 3.1.1 becomes

$$q = (n\cdot 2\pi)(h_1^2 + h_2^2 + h_3^2)^{1/2}/a \qquad (3.1.2)$$

where $(h_1h_2h_3)$ is the Miller index. But not all reciprocal vectors that satisfy Eq. 3.1.2 will have a peak diffraction because the unit cell of b.c.c. has two atoms (more than one). A detailed calculation of the intensity for a diffraction of b.c.c structure results in[60]

$$I\propto [1+\cos\pi(h_1+h_2)+\cos\pi(h_1+h_3)+\cos\pi(h_2+h_3)]^2 + [\sin\pi(h_1+h_2)+\sin\pi(h_1+h_3)+\sin\pi(h_2+h_3)]^2 \qquad (3.1.3)$$

By using the Eqs. 3.1.2 and 3.1.3 we can predict the q values for the diffraction peaks for potassium.

In figure 3.1.1 we present x-ray diffraction data for a 10 μm thick K film coated with wax and grease on a glass substrate. In figure 3.1.2 we present the result for a glass substrate coated with wax and grease

without K film for abackground check. In both cases we see a large peak at q=1.49 A^{-1}, but only with the K film do we see a large sharp peak at q=1.63 A^{-1} whereas for the background there exists a small peak at q=1.58 A^{-1}. When we compare fig. 3.1.1 and 3.1.2 we see that the large peak at q=1.63 A^{-1} must come from the diffraction of the K film. Assuming a=5.34 Å for the lattice constant of K and using equation 3.1.2 we get q=1.66 A^{-1} for diffraction from (110) planes, in good agreement with our experimental result. However due to the low intensity of x-ray diffraction for a K film on a glass substrate we did not see the peak for second order diffraction at q=2•1.63 A^{-1} for the (220) direction. For the diffraction from a K film on Si substrate, there is a possibility that peaks could come from the diffraction by the Si substrate. In table 1 we calculated the q values of possible diffraction peaks from Si substrate, one can see that none of them match the peaks measured in experiments.

In fig. 3.1.3 we show the result of x-ray diffraction of a 10 μm thick K film coated with wax and vacuum grease on a Si substrate. And in fig. 3.1.4 we present the result of x-ray diffraction, as a background check, of wax and grease on a Si substrate without a K film. In both figures we see two peaks at q=0.9 A^{-1} and q=1.5 A^{-1}respectively, but only in the x-ray diffraction with the K film we do see a sharp strong peak at q=1.65 A^{-1} and another small peak q=3.30 A^{-1}. A further scan of the same K film sample was made near q=3.30 A^{-1} to see the detail of that small peak. The result is shown in figure 3.1.5. Notice the small oscillation in the background is just a polynomial fit between the data points to guide the eye when we plotted the figure. Comparing these three figures (3.1.3, 3.1.4 and 3.1.5) we conclude that the two peaks at q=1.65 A^{-1} and q=3.30 A^{-1} must come from x-ray diffraction of 10 μm thick K films. Using the same analysis as for a K

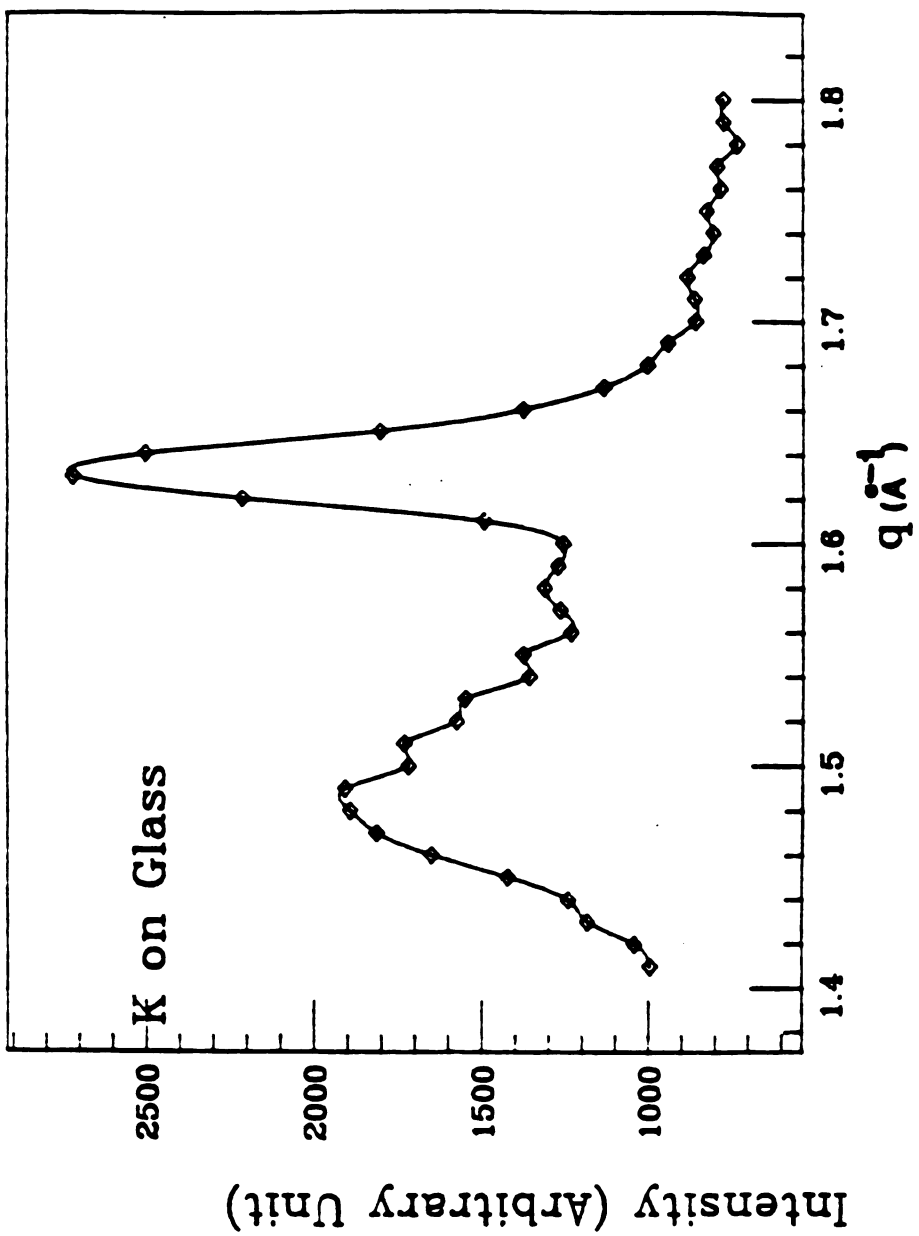

Fig. 3.1.1 X-ray diffraction of a K film coated with wax, and grease on a glass substrate.

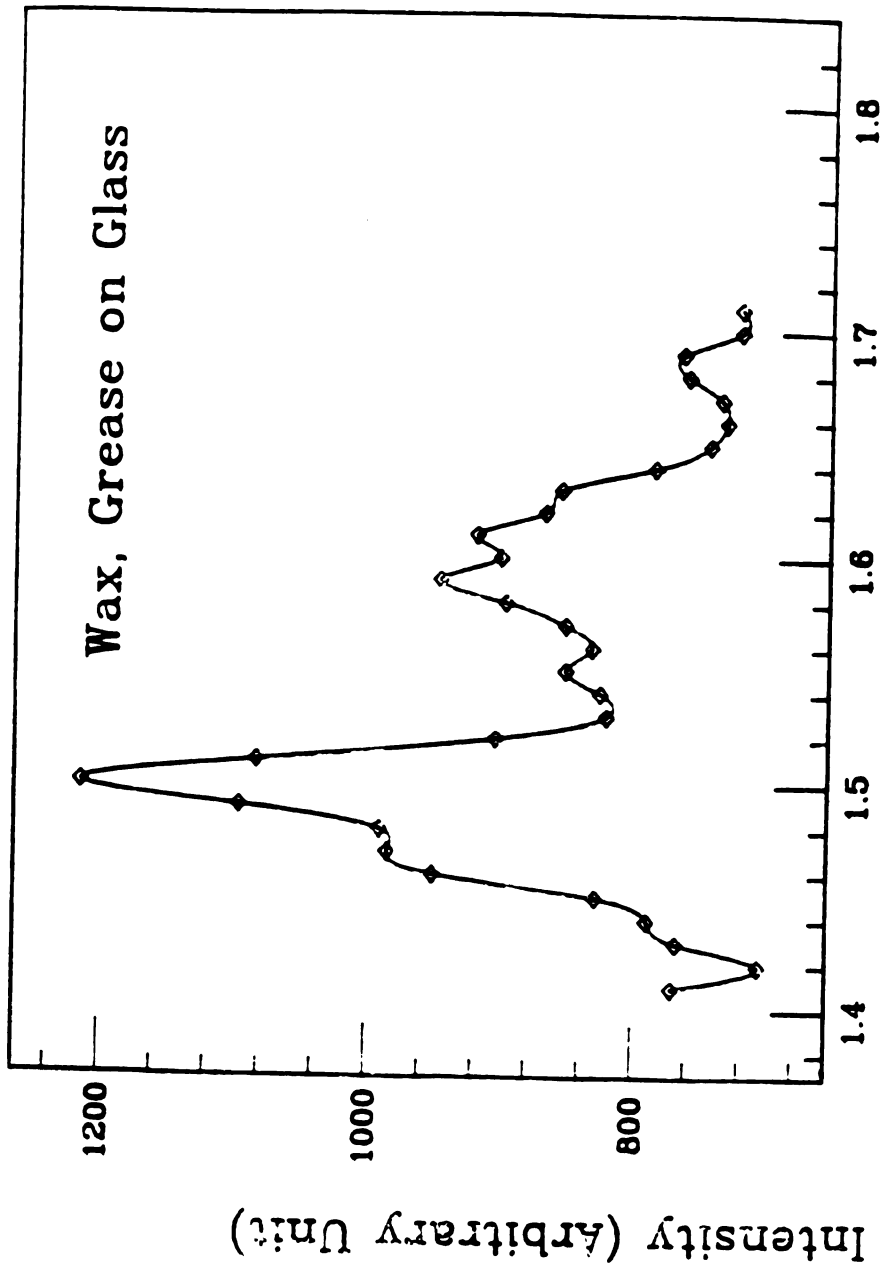

Fig. 3.1.2 X-ray diffraction of background check for glass substrate coated with wax and grease.

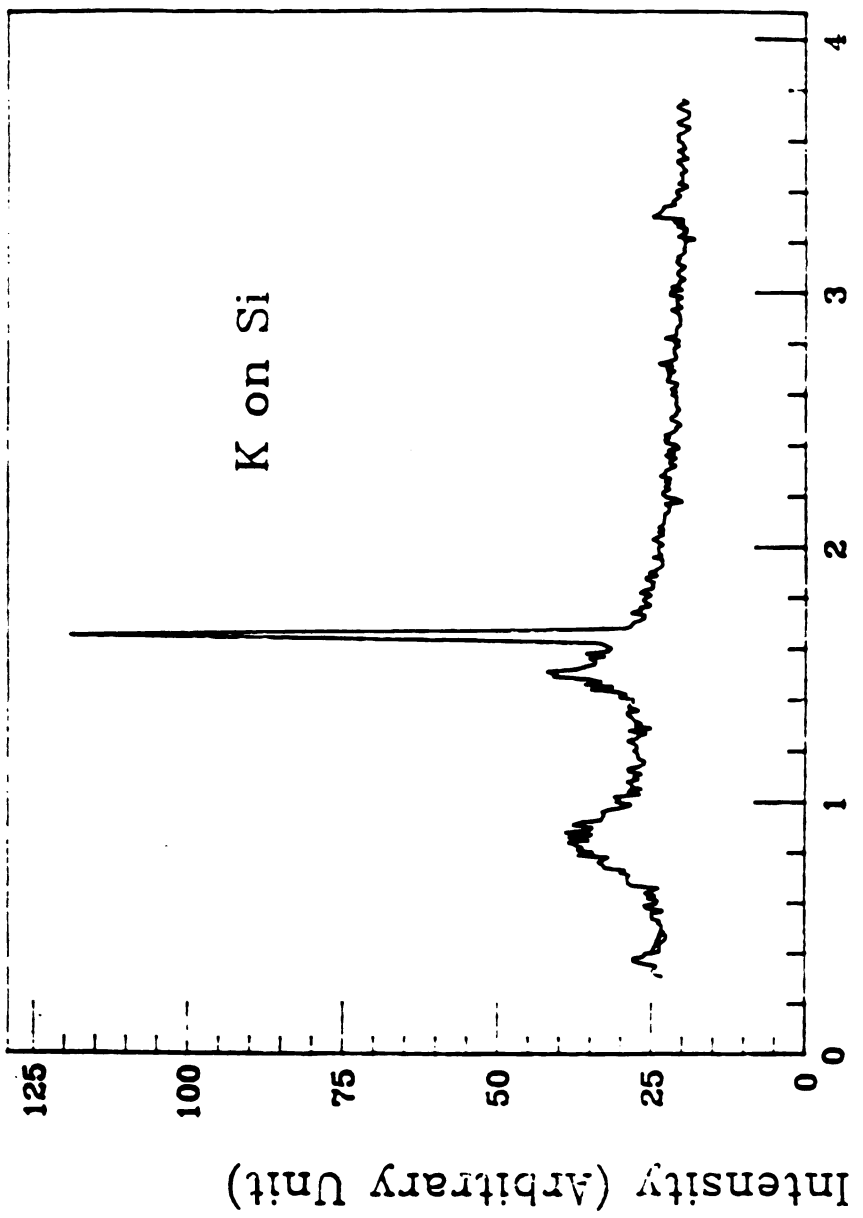

Fig. 3.1.3 X-ray diffraction of a K film coated with wax, and grease on a Si substrate.

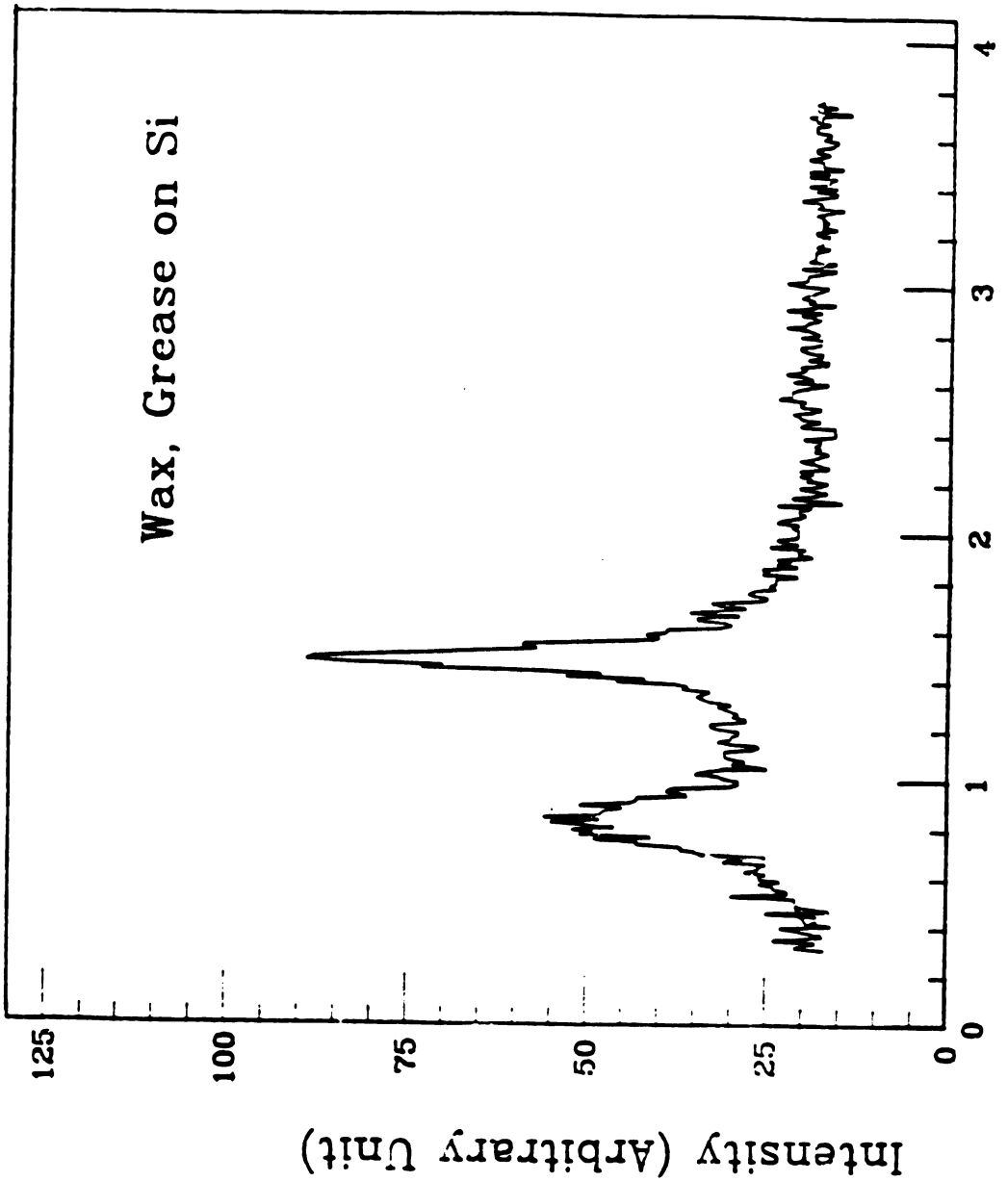

Fig. 3.1.4 X-ray diffraction of background check for Si substrate coated with wax and grease.

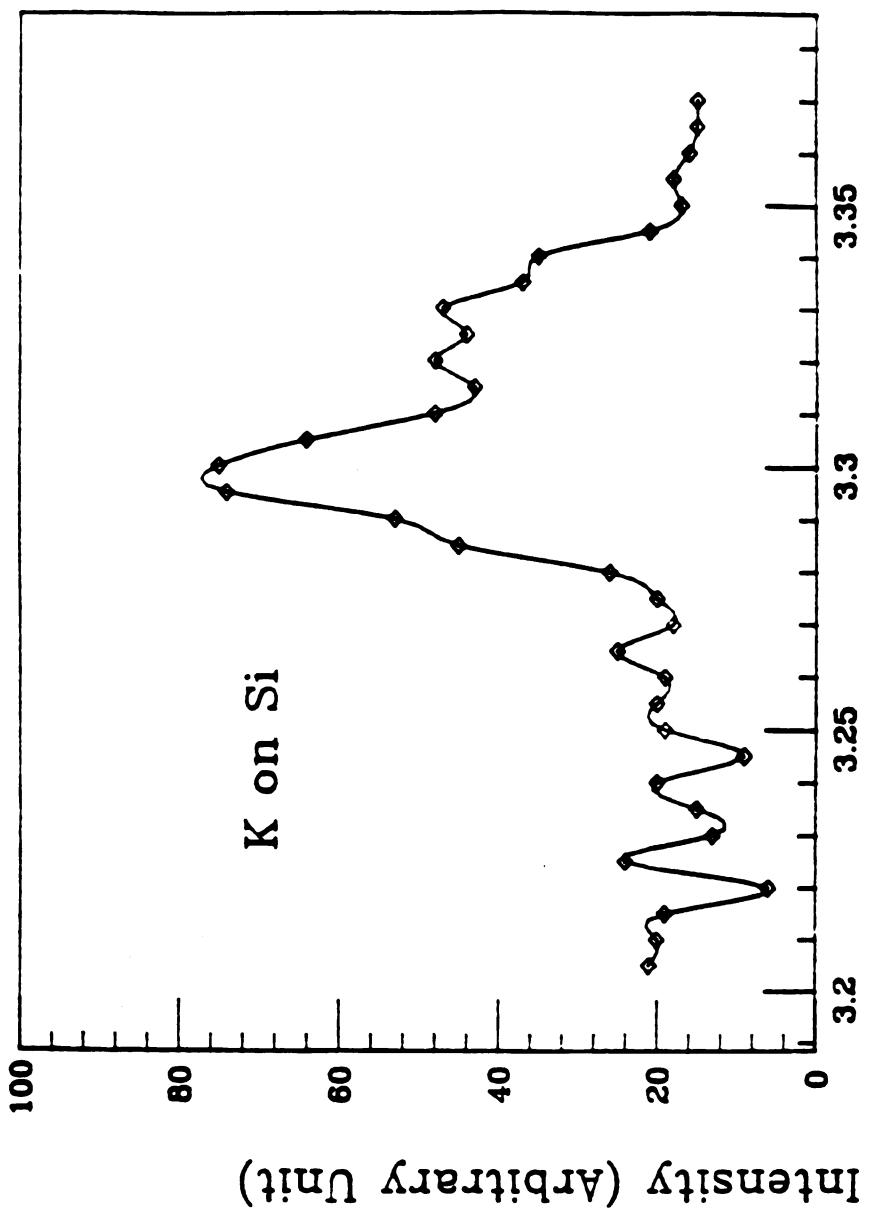

Fig. 3.1.5 Details of the peak in Fig. 3.1.3 at q= 3.3 $Å^{-1}$.

film on a glass substrate we conclude that the two peaks were the diffraction from (110) and high order (220) planes. No direct comparison of the x-ray intensity can be made from the graphs which are plotted against arbitrary units, but it should be noticed that the x-ray intensity at the peaks for a K film on a Si substrate is much stronger than those for a K film on a glass substrate. For both Si and glass substrates the position of the peaks agrees very well considering the uncertainty in the initial position of q=0. We also use the relative positions of the two diffraction peaks from a K film on Si substrate to determine the lattice constant of K. This minimizes the the effect of zero errors. Using the equation 3.1.2 we obtain

$$a=2\pi\cdot 2^{1/2}/(q(220)-q(110)) \qquad (3.1.4)$$

from which a=5.385 Å for thin K film, which is in good agreement with the literature. However we only scan the one particular $\vec{q}$ direction, there is the possibility that the diffraction peaks could come from the Si substrat, in table 1 we listed possible peak values for Si substrate. We can see that none of them match the peak values obtained from our experiment.

From the x-ray results we conclude that the K films deposited onto microslide glass and crystalline Si substrates have a preferred direction of <110> normal to their surfaces. This is not hard to understand since the b.c.c. structure has the largest distance between the successive layers in this direction, the so called "easy direction", which requires minimum energy for the growth of film.

G.-A. Boutry and H Dormont[63] had measured the x-ray diffraction of K films deposited onto a crystalline KF substrate cleaved along a (100) surface. They concluded that due to the close match of lattice constants of KF and K the the K film grew with the (100) planes parallel to the surface. We have also taken an x-ray diffraction scan of a 5μm

thick K film deposited onto a crystalline KF, which was cleaved parallel to (100) surface inside the Ar filled glove-box before the potassium deposition. In fig. 3.1.6 we present a total scan of this sample. From this figure we see there exists three strong sharp peaks. However upon detailed examination we found that each peak actually consisted of two peaks. In figure 3.1.7 we present the detail of these three main peaks seen in the total scan (fig. 3.1.6). Of these Fig. 3.1.8 is anomalous, in that the peak at q=4.64 A^{-1} cannot be identified as belonging to K or KF, and the double peak at ≈ 4.82 A^{-1} is not precisely where it should be expected at ≈ 4.7 A^{-1} from fig. 3.1.6. We presume the double peak represents these lines from K and KF. From the diffraction data of a K film on Si substrate we know the lattice constant of a K film is a=5.385 Å. Assuming the same constant here and using the equation 3.1.2 and 3.1.3 we calculated possible q values for the diffraction peaks. Since the KF was single crystal and the normal direction of its surface was <100>, and the wave vector $\vec{q}$ in our experimental setup was also normal to the surface of KF substrate, the only peaks we could see must come from reciprocal vectors parallel to <100> direction, i.e. (200), (400) and (600) etc. We have listed six peaks from the experimental data in table 2, along with corresponding calculation of peaks for K film and KF substrate. We did not see any peaks at q=1.650 A^{-1} when we first made the scan as routine check, but unfortunately records were not kept, and repetition was impossible due to a major x-ray machine breakdown. But from fig. 3.1.6 we did not see the peak at q=3.300 A^{-1}. These two peaks correspond to (110) and (220) as in the case of K on film on Si substrate. Comparing the experimental data with the calculation we conclude the peaks we see from x-ray diffraction came from (200),(400) and (600) of KF and K film respectively. The tentative assignments of peaks are also listed in table 3.1.1. This is in good agreement with

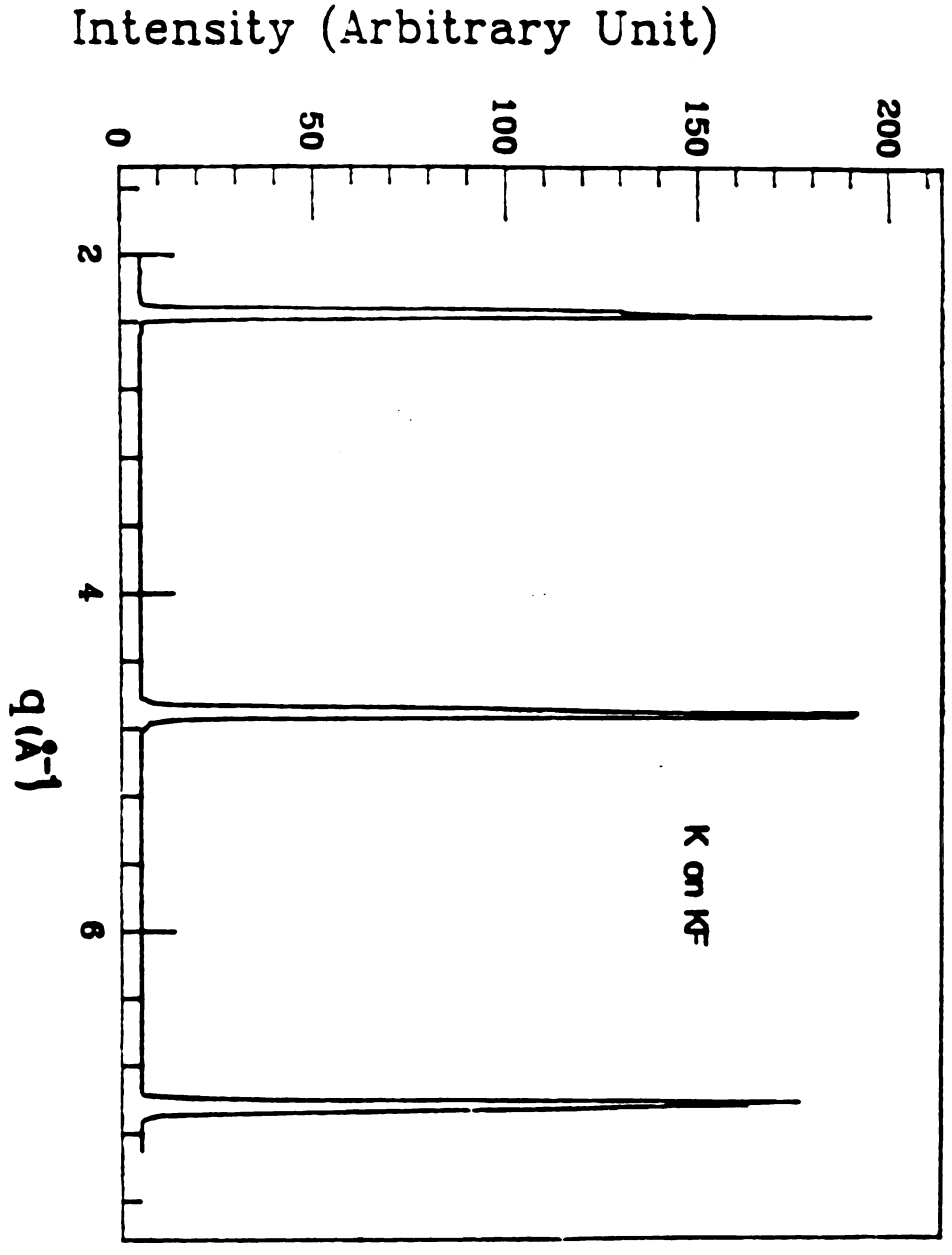

Fig. 3.1.6 X-ray diffraction of a K film coated with vax, and grease on a KF substrate.

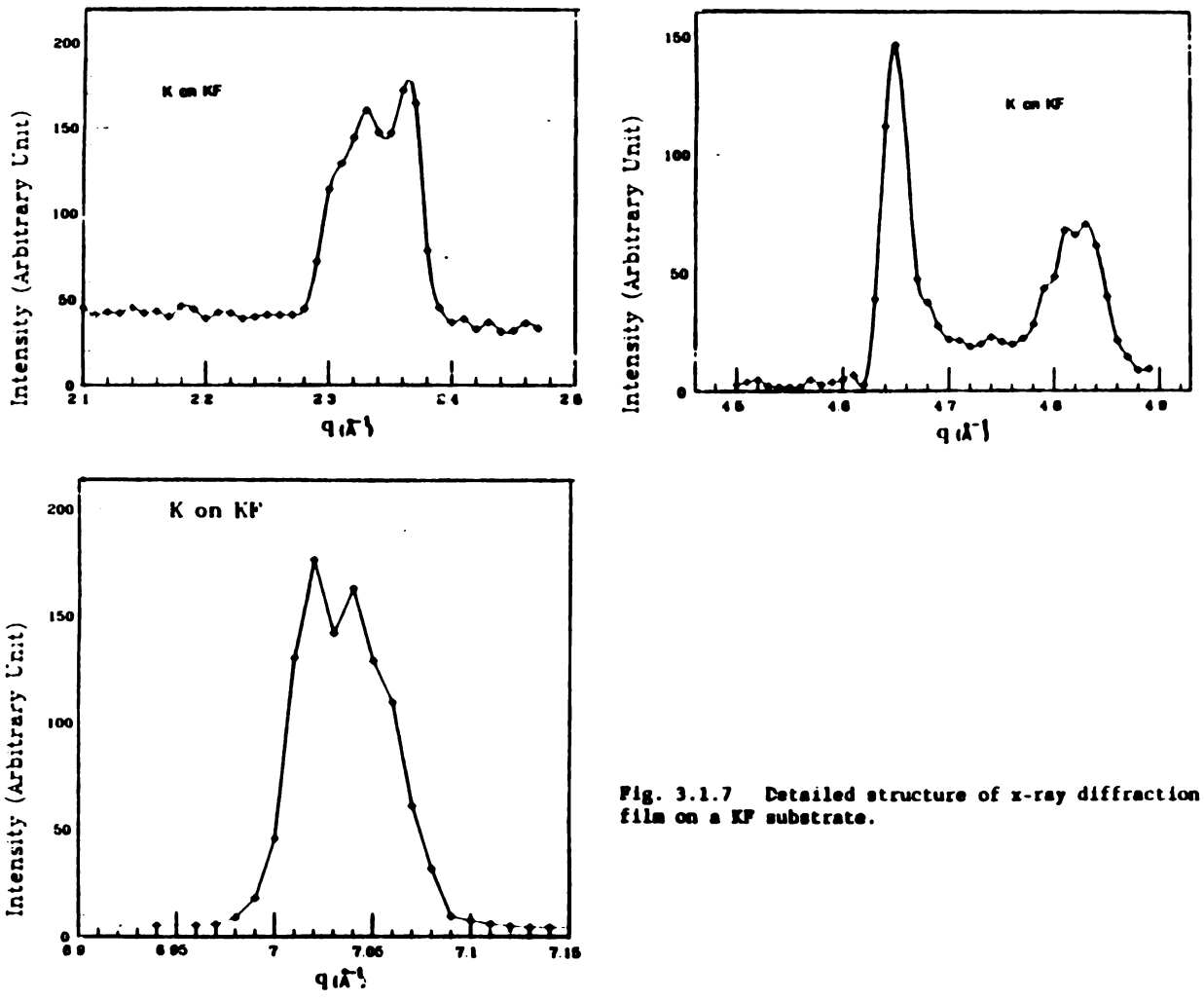

Fig. 3.1.7 Detailed structure of x-ray diffraction of a K film on a KF substrate.

Table 1 Calculated peak valued for Si and KF

For Si		For KF	
Planes (h_1,h_2,h_3)	q (A^{-1})	Planes (h_1,h_2,h_3)	q (A^{-1})
1,1,1	2.004	1,1,1	2.035
2,2,0	3.272	2,0,0	2.350
1,3,1	3.837	2,2,0	3.324
2,2,2	4.008	3,1,1	3.890
4,2,2	5.668	2,2,2	4.074
3,3,3	6.012	4,0,0	4.700
		6,0,0	7.049

Table 2 Peak values of X-ray diffractions

Substrates	$q(A^{-1})$	Planes (h_1,h_2,h_3)	Comment
Glass	1.63	1,1,0	
Si	1.65	1,1,0	
Si	3.30	2,2,0	
KF	2.33	1,0,0	From K Film
KF	2.36	1,0,0	From KF
KF	4.65	2,0,0	From K
KF	4.82	Not Clear	Anomalous
KF	7.02	6,0,0	From K
KF	7.04	6,0,0	From KF

Boutry et al.

The results of our x-ray diffraction data show that K films on amorphous glass and crystalline Si substrates prefer an orientation with (110) planes parallel to the surface, whereas K films prefer (100) planes parallel to the surface when deposited on single crystal KF cleaved parallel to (100).

3.2 $\rho(T)$ for K films on Glass Substrates at T=1 to 4.2 K

We have done a series of experiments on potassium films on microslide glass substrates. The data consist of two parts; Thoso obtained from a conventional 1.3-4.2 K cryostat and these obtained from a dilution refrigerator.

Preliminary experiments were done inside a conventional 1.3-4.2 K dewar cryostat connected to a large mechanical pump. By using a conventional condom pressure controller, one could control the temperature of the liquid helium bath into which the sample can was submerged. In this way the temperature could be varied from 4.2 K to approximately 1.5 K. The voltage meter (180 Digital Nanovoltmeter made by Keithley Instruments Inc.) which we used in these measurements had a nominal resolution of 1 nV, and an actual resolution of 15 nV. As pointed out in chapter 2, this precision is not enough to give very reliable measurements, especially at the lower temperatures. Also these measurements were not done with a potassium coated copper sheet to absorb the contaminating gases, so that the sample itself was seriously eroded. Combining these deficiencies it is clear that these data are not as good as the data which were taken with the dilution refrigerator and SQUID system, and they are only serve the purpose of giving some preliminary feeling for the task at hand.

Part of the data taken with the dilution refrigerator over the range 1.7 K to 4.2 K were measured by comparing the resistance of K film with a standard 1% AgAu Alloy sample as given below.

Defining $$C(T)= \frac{R(K,T)}{R(AgAu,T)} \qquad (3.2.1)$$

so one has

$$R(K,T))=C(T)\cdot R(AgAu,T)$$

$$=C(T)\cdot(R_0(AgAu)+R_T(AgAu)) \qquad (3.2.2)$$

and $$\frac{\rho(T)}{\rho_0} = \frac{R(T)}{R_0} \qquad (3.2.3)$$

then from equ. 3.2.3

$$\frac{d\rho}{dT} = \frac{\rho(T_2)-\rho(T_1)}{T_2-T_1} = \frac{\rho_0(K)}{R_0(K)} \cdot \frac{R(K,T_2)-R(K,T_1)}{T_2-T_1}$$

and from eq. 3.2.2

$$\frac{d\rho}{dT} = \frac{\rho_0(K)}{C_0R_0(AgAu)}\cdot\{ \frac{R_0(AgAu)(C(T_2)-C(T_1))}{T_2-T_1} + \frac{C(T_2)R_{T_2}(AgAu)-C(T_1)R_{T_1}(AgAu)}{T_2-T_1}\}$$

$$=\frac{\rho_0(K)}{C_0}\cdot\frac{\Delta C(T)}{\Delta T} + \frac{\rho_0(K)\{(C(T_2)R_{T_2}(AgAu)-C(T_1)R_{T_1}(AgAu))\}}{C_0R_0(AgAu)\Delta T} \qquad (3.2.4)$$

From M. Khoshnevisan et al.[64] and eq. 3.2.3 we get

$$R_T(AgAu)= \frac{BT^nR_0}{\rho_0(AgAu)} \qquad (3.2.5)$$

where we accept the BT^n obtained by Khoshnevisan et al.[64] for silver as being good approximation to $\rho(AgAu,T)$. Implementing the parameters given in Edmunds et al.[65] and Khoshnevisan's paper one calculated that the second term in equation (3.2.4) is about 1% of the first term at 1.5 K and 0.1% at 4.2 K for the thickest K (76 μm) film, which is the worst case. So we can neglect the second term in equation (3.2.4) without introducing appreciable error at high temperature and

$$\frac{d\rho}{dT} = \frac{\rho_0}{C_0}\cdot\frac{\Delta C}{\Delta T} \qquad (3.2.6)$$

In our experiments we assume that for a potassium film at room temperature the resistivity is

$$\rho(RT)=7.19 \quad \mu\Omega\text{-cm} \tag{3.2.7}$$

and

$$\rho(4.2)=\frac{\rho(RT)}{RRR} \tag{3.2.8}$$

where RRR stands for the resistance ratio of room temperature resistance to liquid helium temperature resistance.

In figures 3.2.1 we present a set of data obtained from the measurements done in the conventional dewar system. Considering the large uncertainty discussed previously, these data could only serve as very preliminary data hinting at the behavior of thin K films at these temperatures, and indicating considerable irreproducibility. For more precise measurements we went to the dilution refrigerator and to improve the reproducibility we added the K coated Cu foil. In figures 3.2.2 we present another set of data obtained from the measurements done in the dilution refrigerator. A logarithmic scale is used on the y-axis and 1/T is plotted on the x-scale. There are two prominent features of the data; first these data are clearly consistent with an exponential dependence of the resistivity on 1/T at high temperatures; second the data are generally larger than the value obtained for the bulk K measurement, and have the general trend that the thinner the film the larger the $d\rho(T)/dT$. The bulk value shown in Fig. 3.2.2 were obtained as follows. We assume a resistivity of the form of eq. 3.2.9, then from Haerle's data for high temperature (1.3 K and up) we obtain the values for D and θ, and from Yu's data (below 1.3 K) we obtain the value for A,

$$\rho_{bulk}(T)= AT^2+ DT\exp(-\frac{\Theta}{T}) \tag{3.2.9}$$

Hence

$$A = 2.2 \quad (f\Omega\text{-m/K}^2)$$

$$D = 77300 \quad (f\Omega\text{-m/K})$$

$$\Theta = 20.3 \quad (K)$$

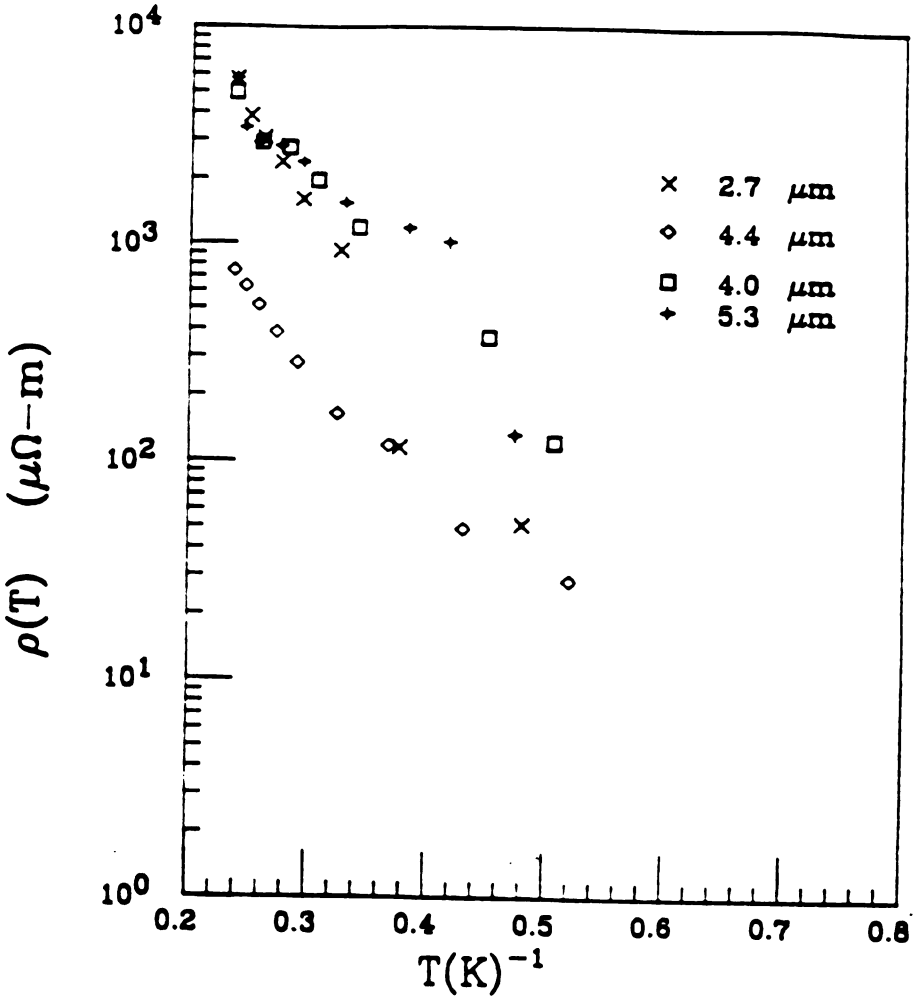

Fig. 3.2.1 ρ vs. T for measurement done on devar for K on glass substrate. (See text.)

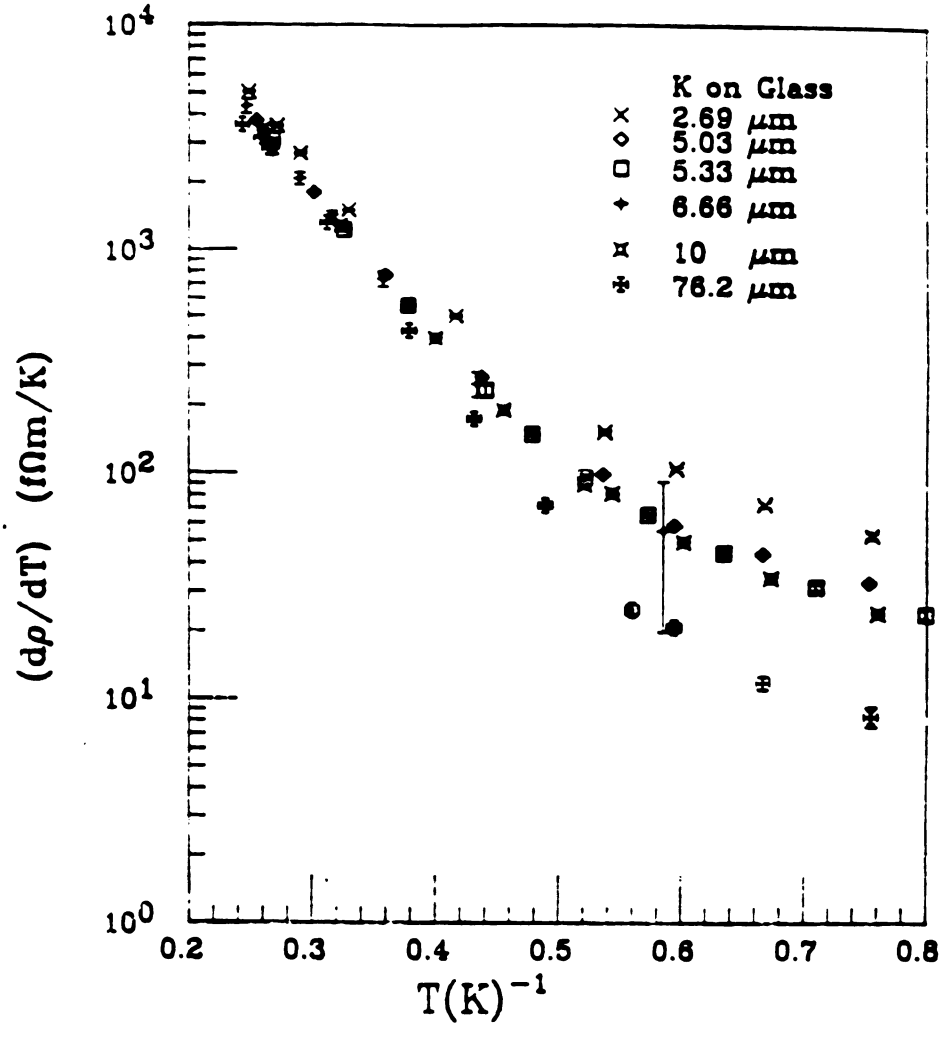

Fig. 3.2.2 $(d\rho/dT)$ vs. T^{-1} for K films on the glass substrates.

The existence of very large difference between $d\rho_{film}(T)/dT$ and $d\rho_{bulk}(T)/dT$ at the higher temperatures suggests that there is a size effect which increases the resistivity of the $\rho_{el\text{-}ph}$ part. As we discussed in chapter 1 for bulk potassium there exists a "phonon-drag" effect resulting from the non-equilibrium of the phonon gas at these low temperature, which effectively suppresses the T^5 term in the resistivity contributed by normal electron-phonon scattering processes. One way for the restoration of the T^5 dependence is to create imperfections, which would strongly interact with the phonon gas so that it is essentially in an equilibrium state. The two dimensional nature of our thin films might produce one of these mechanisms. If this is true then the difference between $\rho_{film}(T)$ and $\rho_{bulk}(T)$ should follow the T^5 dependence of normal electron-phonon scattering, assuming that the umklapp electron-phonon scattering contribution is the same for both bulk potassium and the thin film. This may be a gross assumption which we will consider further later. From Equation (3.2.9) we get,

$$\Delta(d\rho_{diff}/dT)=d\rho_{film}/dT - d\,\rho_{bulk}(T)/dT$$
$$=d\rho_{film}/dT - \frac{d}{dT}\{2.2T^2+77300T\exp(-\frac{20.3}{T})\}\ (f\Omega\text{-}m/K) \qquad (3.2.10)$$

In figure 3.2.3 $\Delta(d\rho_{diff}/dT)/T^4$ vs T is presented. If the T^5 Law is observed then $\Delta d(\rho_{diff}/dT)/T^4$ should be a horizontal straight line.

From the figure one can clearly see that for the film thickness of 6.25 μm and 10.0 μm the T^5 law is followed rather well, but for the thinner films there is a systematic tendency at lower temperature towards a power law smaller than 5, (This is not easily seen, but considering if $\Delta[d\rho/dT]/T^4=2A/T^3+5C$, $\Delta[d\rho/dt]/T^4$ will then clearly increase as $T\to0$.) and for the thickest sample just the opposite is true. But if one plots the $\Delta(d\rho_{diff}/dT)/T^3$ for the thinest sample, and $\Delta(d\rho_{diff}/dT)/T^5$ for the thickest sample as in figures 3.2.4, the results

are worse than $\Delta(d\rho/dT)/T^4$ plot beside there is no firm theoretical ground to justify these plots.

One possible explanation for the upturn at low temperature in figure 3.2.3 is that at these low temperature the contributions from electron-electron scattering is not negligible, and what is more important is that the coefficient of electron-electron scattering may not be equal to bulk potassium value of 2.2 fΩ-m/K^2. The upturn could result from the increasing contribution from el-el scattering. The change in A will be discussed in detail in later sections, but for now notice that there are two terms contributing to the difference of $\Delta(d\rho/dT)$,

$$\Delta\{\frac{d\rho}{dT}\} = 2(A_{film}-A_{bulk})T+5CT^4$$
$$= 2\Delta AT + 5CT^4 \qquad (3.2.11)$$
$$\frac{\Delta(d\rho/dT)_{diff}}{T^4} = \frac{2\Delta A}{T^3} + 5C \qquad (3.2.12)$$

In fig. 3.2.6 we plotted the data according to the eq. 3.2.12. And from the slope we obtained the coefficient A_{film}.

Besides the scatter of the points, there are other reasons why we can not positively say there is a true T^5 law. For example, except for the thickest films, the coefficients of T^5 for the films are several times larger than theories[6,39] predicts (C=0.55 fΩ-m/K^5) for the normal electron-phonon scattering contribution without any phonon drag. Furthermore we do have to consider the assumption made in equ. 3.2.10, Kaveh and Wiser[6,26] have predicted that the phonon drag effect should also effect the umklapp electron-phonon contributions by reducing the equilibrium $\rho^U_{el\text{-}ph}$ by about 40 percent. In other words when the phonon drag effect is depressed by the thin film boundary scattering, $\Delta\rho_{diff}$ should also include the contribution from these umklapp process. Another difficulty comes from the three runs we have done for the same sample with about ten days in between the runs. In figure 3.2.5 we plot

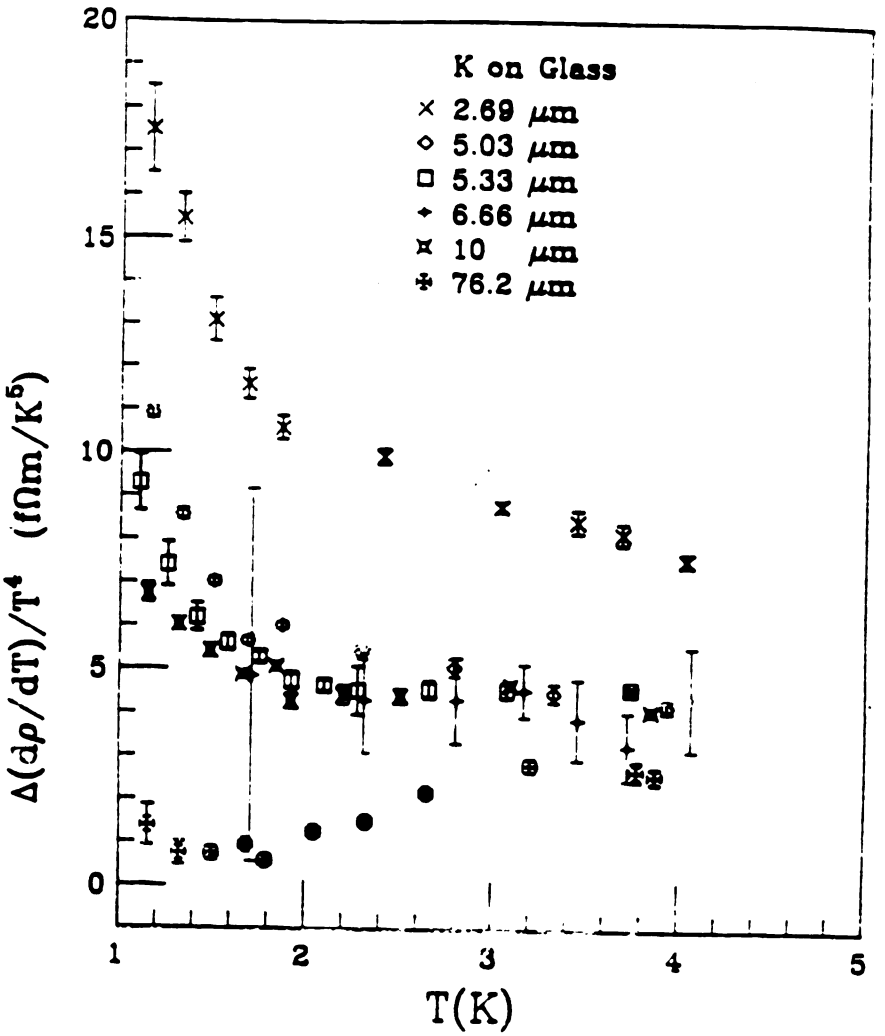

Fig. 3.2.3 Plotting $[\Delta(d\rho/dT)/T^4]$ vs. T to test the existence of T^5 term.

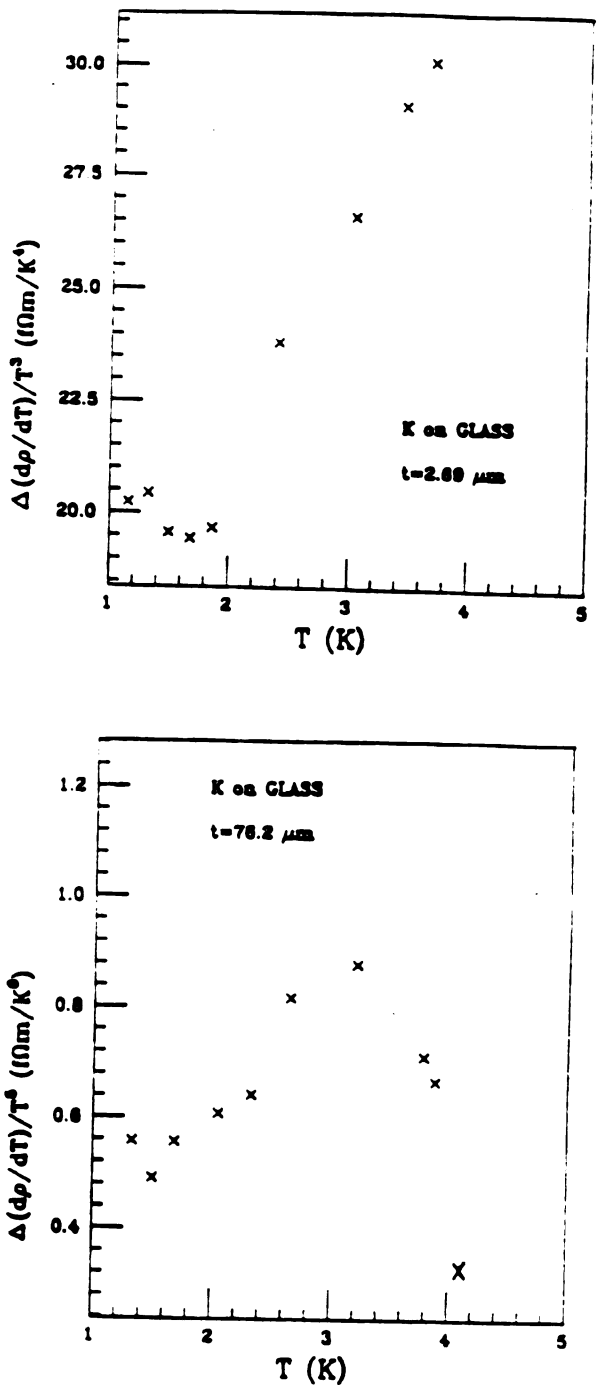

Fig. 3.2.4 Plot $[\Delta(d\rho/dT)]/T^n$ (n=5 or 3) vs. T to test for other possible temperature dependence.

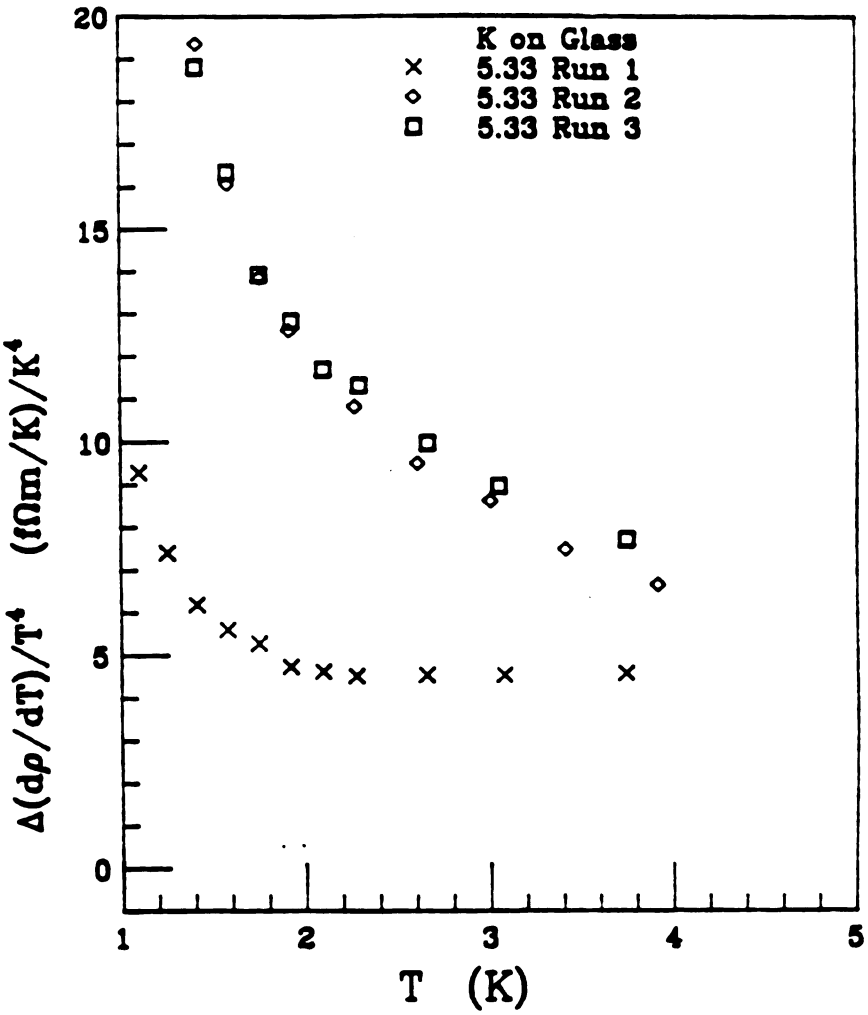

Fig. 3.2.5 Three runs for the same 5.33 μm sample on a glass substrate.

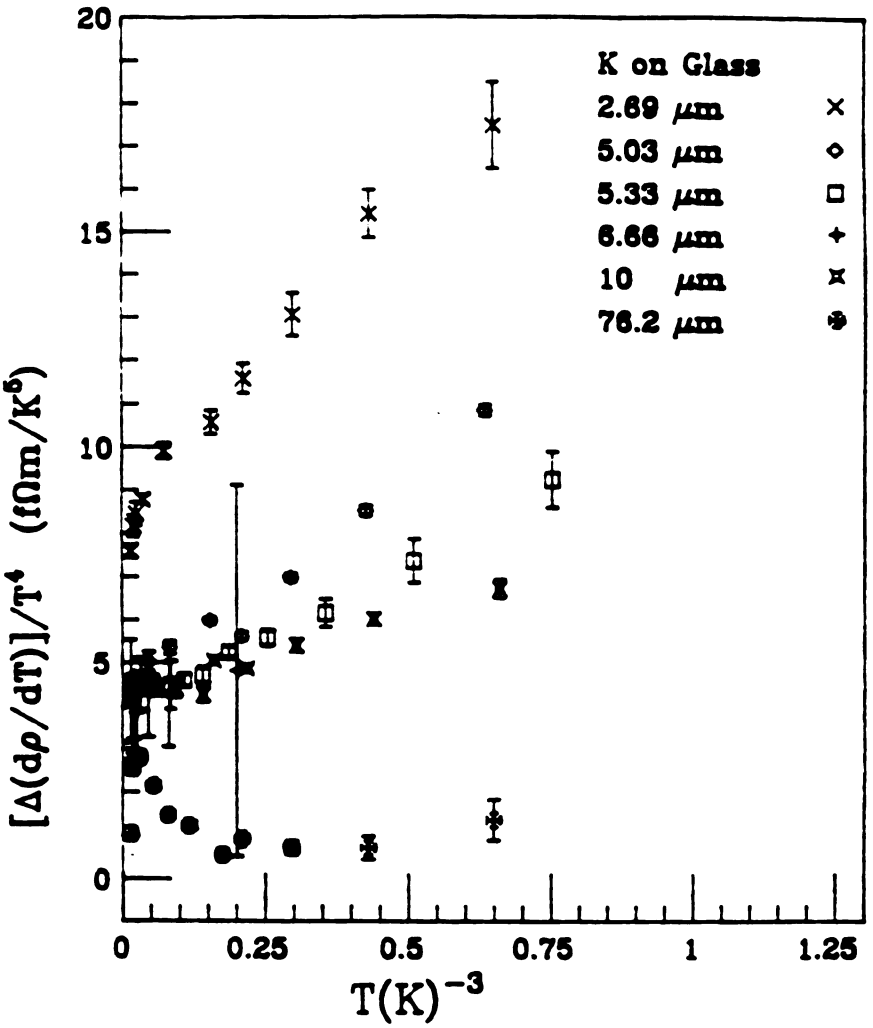

Fig. 3.2.6 $[\Delta(d\rho/dT)/T^4]$ vs. T^{-3} to obtain the slope 2A.

them as $\Delta(d\rho_{diff}/dT)/T^4$ vs T, the result of the last two runs are almost same but they are very different from the first run. One possible explanation is that the first run was carried out right after the sample was made, when this sample may have had a very large island structure, whereas for the last two runs many days later, this island structure may have been annealed out. Evidence supporting this idea can be seen in table 3. The RRR of the second run is larger than that of the first run in spite of the corrosion the sample has endured during these days, and similar effects are frequently seen in bulk K. The RRR is rather similar for the second and third runs which is consistent with the idea that most of the structure had been annealed out already during the first and second run. Also from the figure 3.2.5 we could see that coefficients A and C for the second and third runs are rather large.

3.3 $\rho(T)$ for K film on Si Substrates at T=1 to 4.2 K

There were several advantages in choosing Si as a substrate. The most important one is that Si substrates are magnetically much cleaner than the microslide glass we used in the previous section. As we will see in the discussion of the lower temperature results, the glass substrate apparently has a lot of magnetic impurities at the surface. The Si substrates used in our experiment were slightly doped and have the order of 1 Ω-cm electrical resistance at room temperature. They have (111) planes parallel to the surface and, unlike the glass substrates, they have very few magnetic impurities. The cleaning procedure for the Si wafer, as pointed out in chapter 2, was the same as for the glass substrate. For samples on Si substrates, we measured the temperature differential of the resistivity versus temperature directly in the way discussed in chapter 2,

$$\frac{d\rho}{dT} = \frac{\rho(4.2)}{C} * \frac{\Delta C}{\Delta T} \qquad (3.3.1)$$

The great advantage of this method is that the large uncertainty associated with the determination of ρ_0 is avoided, and we could carry out calculations similar to those in the last section to see the effect of the 2 dimensional nature of the problem.

As pointed out in chapter 2, the temperature dependent part of the resistivity for the bulk potassium could be written as following

$$\rho(T) = AT^2 + DT\exp(-\frac{\theta}{T}) \qquad (3.3.2)$$

so the differential of $\rho(T)$ is easily calculated as

$$\frac{d\rho}{dT} = 2AT + D\exp(-\frac{\theta}{T}) + DT\exp(-\frac{\theta}{T})(\frac{\theta}{T^2})$$

$$= 2AT + D\exp(-\frac{\theta}{T})\{1+\frac{\theta}{T}\} \qquad (3.3.3)$$

One can see from equation (3.3.3) that for the temperature range 1.3 K to 4.2 K the exponential dependence of the umklapp contribution dominates $d\rho/dT$, giving behavior very similar to that of $\rho(T)$ itself. Figure 3.3.1 gives the results of the measurements for the potassium film on the Si substrates, notice the y-axis has a logarithmic scale and 1/T is plotted along the x-axis. The data clearly demonstrate the exponential nature of $d\rho/dT$ at high temperature. However following the pattern for the potassium films on glass substrates, all the measurements of $d\rho/dT$ were larger than those for bulk potassium, and the thinner the sample was, the larger was $d\rho/dT$. The largest of all the measurements that was done on film of the thickness of 2.6 μm.

If we assume that the contribution from umklapp electron-phonon scattering is the same for the films as for the bulk potassium, then as in the case of K films on glass substrates, the difference between the films and the bulk could be explained by the suppression of the "phonon drag" effect, and the corresponding restoration of the T^5 law, so that thus the left side term of equation 3.3.5 is a constant,

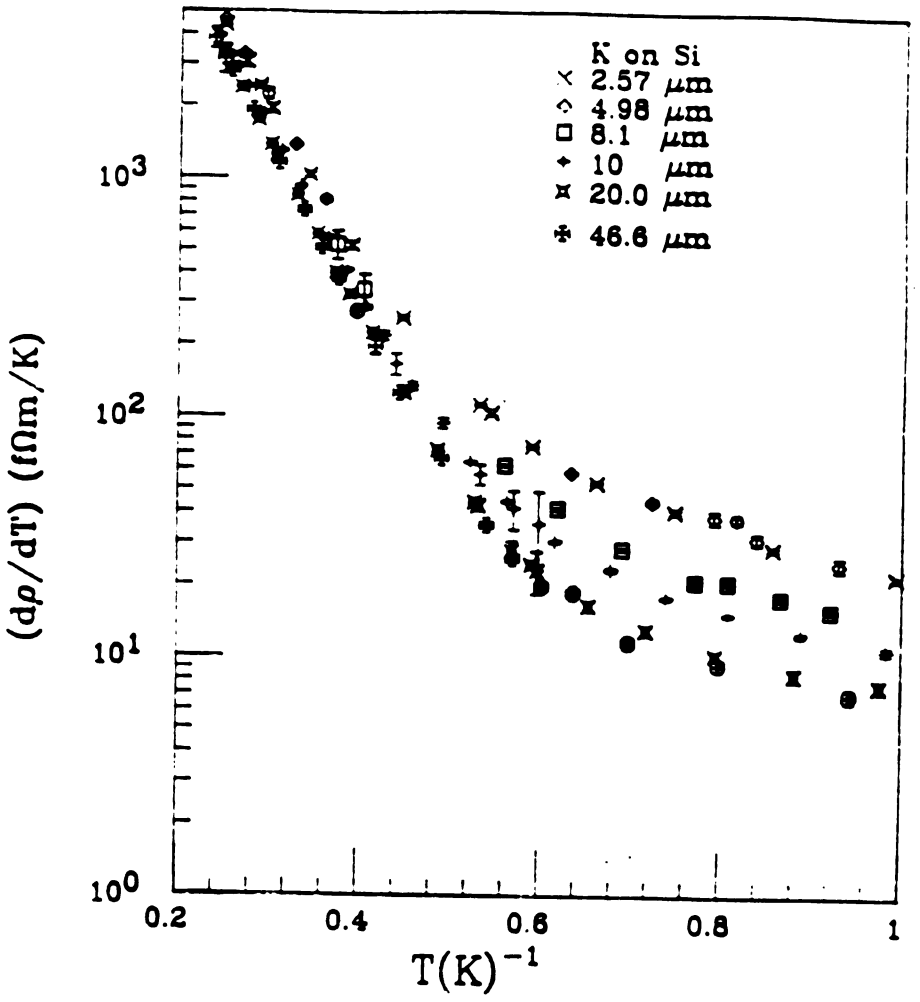

Fig. 3.3.1 (dρ/dT) vs. T^{-1} for K films on Si substrates.

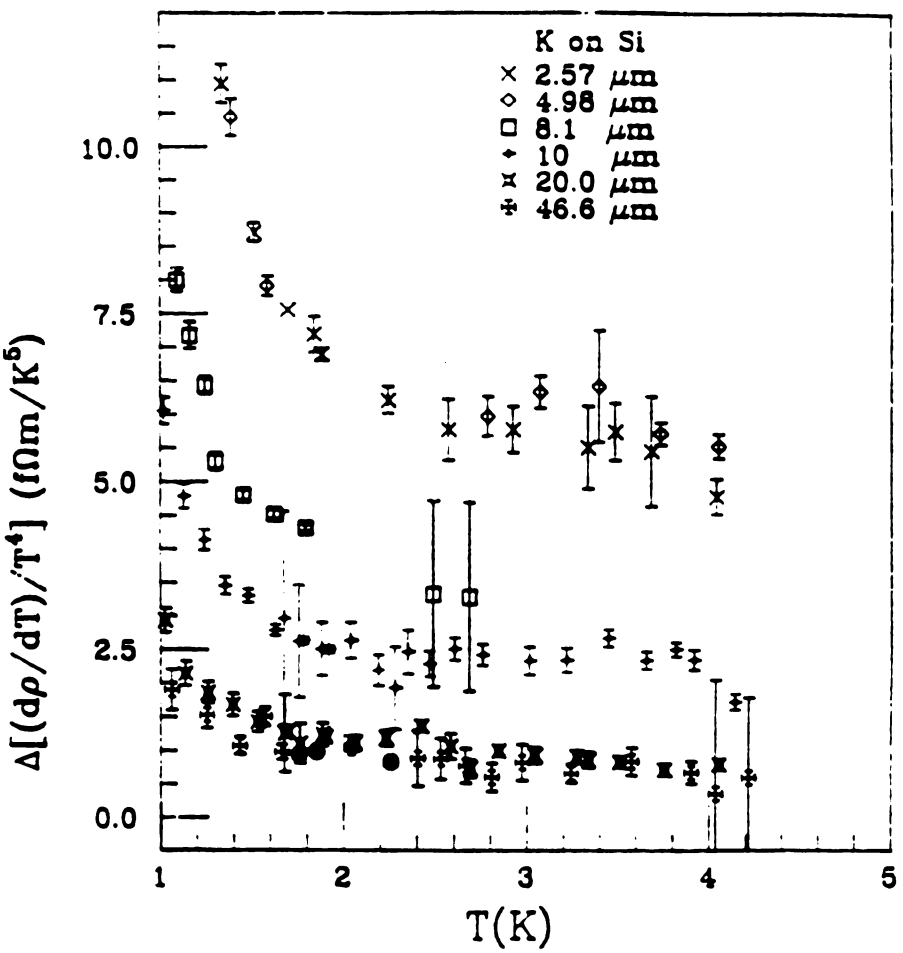

Fig. 3.3.2 $[\Delta(d\rho/dT)]/T^4$ plotted against T to test for existence of T^5 term.

$$\Delta\{\frac{d\rho}{dT}\}_{diff} = \frac{d\rho}{dT}_{film} - \frac{d\rho}{dT}_{bulk}$$
$$= \frac{d}{dT}(CT^5) = 5CT^4 \qquad (3.3.4)$$

from this we get

$$\frac{\Delta(d\rho/dT)_{diff}}{T^4} = 5C \qquad (3.3.5)$$

equal to 5 times the coefficient for the T^5 law. In figure 3.3.2 we plot $\Delta(d\rho/dT)/T^4$ versus T for the K films on Si substrates. In doing so we use the same parameters for bulk potassium as in the last section, i.e. A is 2.2 fΩ-m/K^2, D is 77300 fΩ-m/K, and Θ is 20.3 K.

From figure 3.3.2 we see that except for the two thinnest samples of 2.6 μm and 5.0 μm, the T^5 law is fairly well observed from temperature of 1.6 K to 4.2 K. And below 1.6 K all the samples show a systematic up turn. For the two thinnest films, there is no clearly observed constant region. Over the entire temperature range they show a power law less than T^5. As a possible candidate in fig. 3.3.3 we plotted $\Delta(d\rho/dT)/T^3$ versus T for these two thinnest sample. A horizontal straight line would indicate a T^4 power law. From the plot, one sees clearly that there is no region where $\Delta(d\rho/dT)/T^3$ is a constant, and on the contrary the power law behaviour is much closer to T^5.

As in the case of K films on the glass substrates the upturn in fig. 3.3.2 is produced by the T^2 term from electron-electron scattering, and we can use the eq. 3.2.12 to obtain the coefficient A. In figure 3.3.4 we have plotted $\Delta(d\rho/dT)/T^4$ versus $1/T^3$, the slope should give us the value of ΔA. In this way we got the A and C's for the corresponding film thickness listed in table 3 and 5. In figure 3.3.5 we again plot $\Delta(d\rho/dT)/T^4$ versus T for the 2.57, 8.1, 10 and 20 μm samples along with these calculated from eq. 3.3 7, using the values listed in table 3.2. One can see that the fitting is reasonable well within the uncertainty of the measurements.

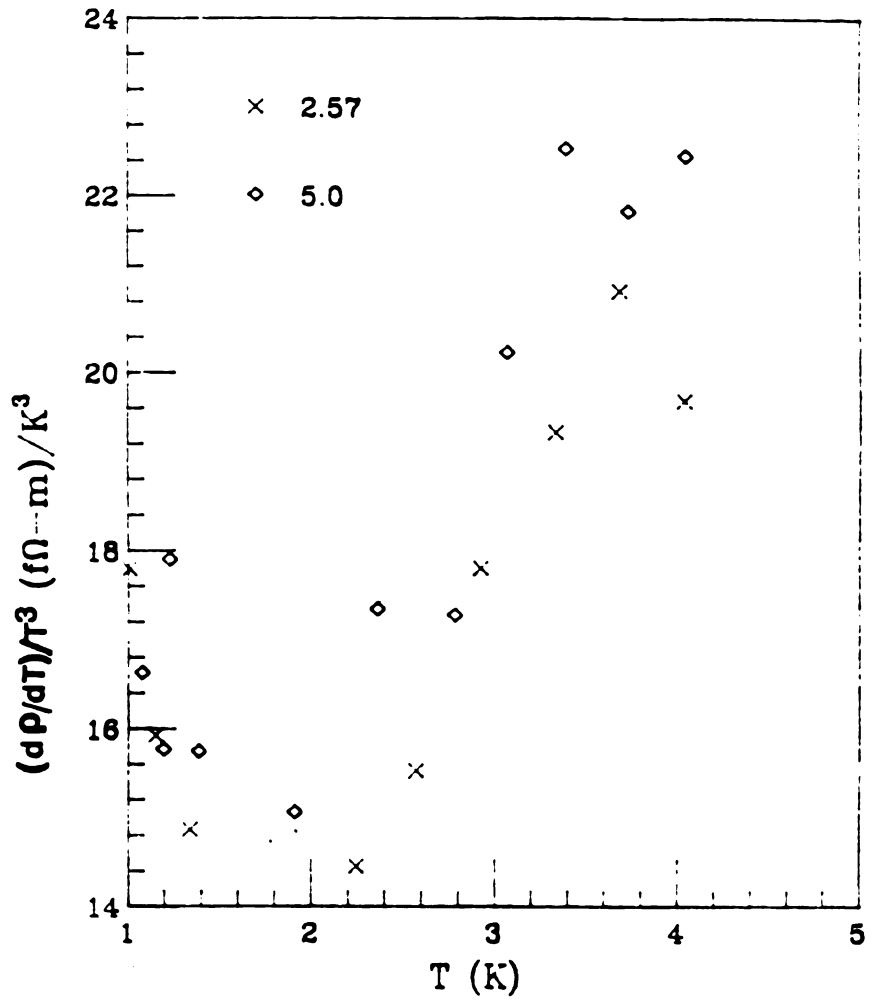

Fig. 3.3.3 plotting $\Delta[(d\rho/dT)]/T^3$ vs. T to test possible T^4 dependence.

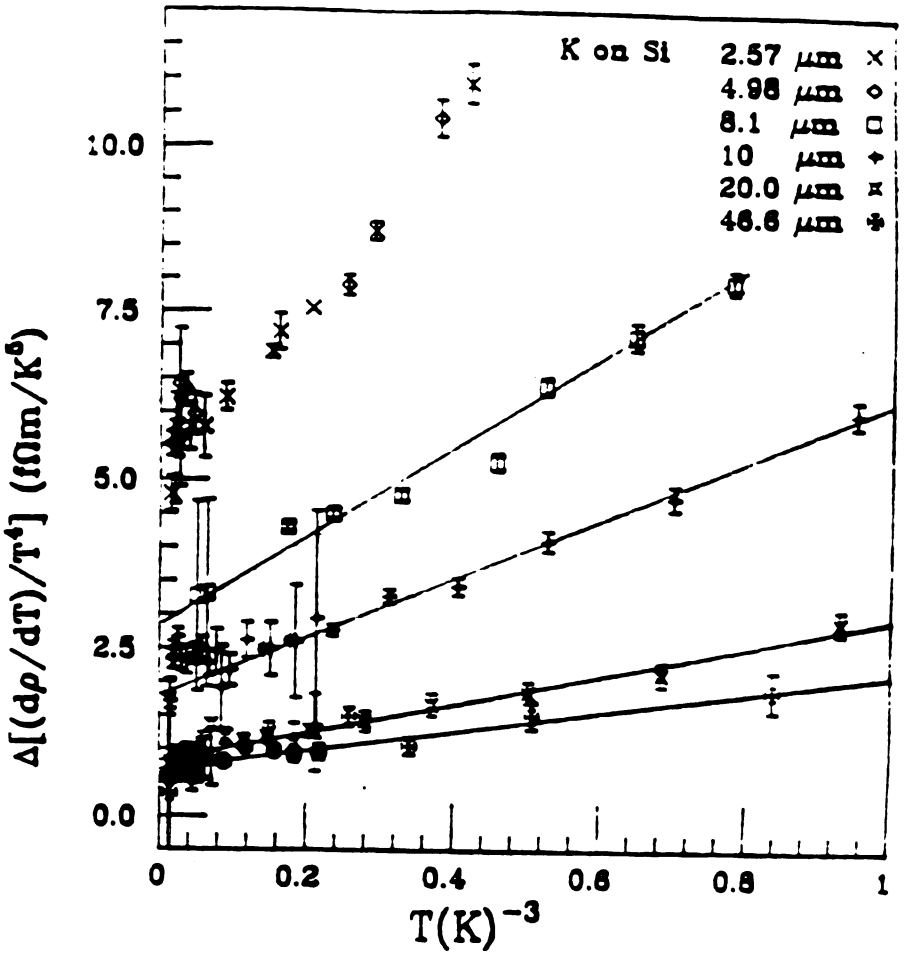

Fig. 3.3.4 $[\Delta(d\rho/dT)/T^4]$ vs. T^{-3} to obtain the slope 2A.

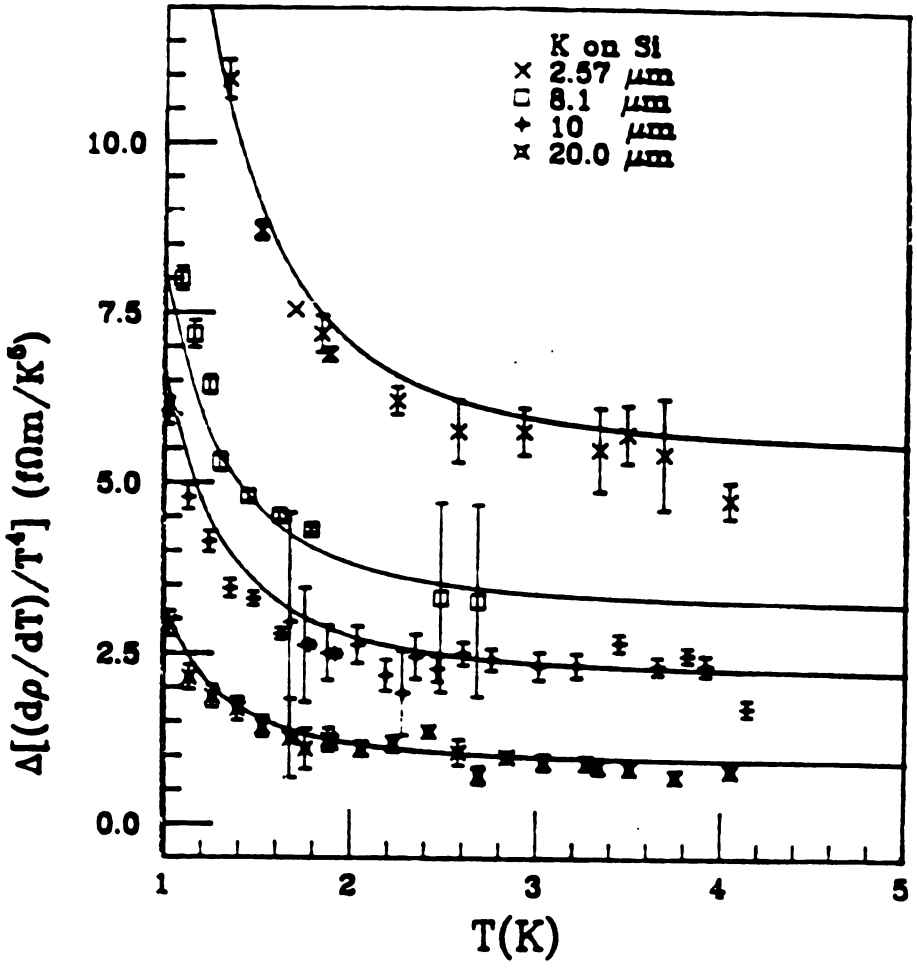

Fig. 3.3.5 The solid line is the fit curve for different thickness. The upturn at low temperatures is produced by the AT^2 term.

To a large extent the same difficulties encountered in the last section for the interpretation of the data also exist for potassium films on Si substrates, and I will not discuss them again here.

3.4 $\rho(T)$ for K films on KF substrates at T=1 to 4.2 K

The third kind of substrate we used was the cleaved surface of a KF single crystal. The lattice constant of crystalline KF is almost the same as crystalline K. The idea behind choosing this crystal as substrate is to see if there would be any significant difference of behavior of $\rho(T)$ for different film orientations. The films deposited on KF single crystal cleaved parallel to (100) planes have the preferred orientation of (100) parallel to the surface as opposed to the preferred orientation of (110) parallel to the surface on the glass and Si substrates. In section 3.1 we presented our confirmation of the preferred (100) K film structure on the KF crystal by x-ray diffraction.

Overhauser[42,60] has proposed that the ground state of K metal should be a charge density wave (CDW) as opposed to the conventional view of a nearly free electron gas. The different orientation of the wave vector $\vec{Q}$ of CDW, in turn the different orientation of K films, should give significant difference in potassium transport properties as discussed in chapter 1. The CDW theory predicts that the ρ_0, and $\rho(T)$ should be quite different for films with (100) planes parallel to the surface than those with (110) planes parallel to the surface. The residual resistivity should be much larger for (100) films than for the (110) ones, and the scattering of electron-phason (collective excitations of CDW) would result in a $T^{3/2}$ term. The resistivity measurements of (100) structure films on KF should indicate whether these prediction are true.

Figure 3.4.1 is a plot for the measurements on K films on KF substrates. Just like K films on Si substrates, it clearly shows the exponential nature of the umklapp contribution to the resistivity at the higher temperatures. Notice that what we measure is the differential of the resistivity, as in the last section, so the equations 3.3.4, 3.3.6 and 3.3.7 also apply here. Figures 3.4.2 and 3.4.3 are plots similar to those in the last section, but there are substantial differences in the resistivity contributions at the lower temperatures. From figure 3.4.2 we see the following different behavior:

First it seems that the thickness of the potassium film samples makes no great difference to the coefficient of the T^5 term. The results are rather similar for the two samples even though their thickness is an order of magnitude different.

Second the coefficient of of the T^5 term is very small for the 4.26 μm thick sample. This is in contrast to the thin K films on Si and on microslide glass substrates where there is a very large increase of T^5 component associated with decrease of sample thickness. But the values for the thick sample on KF substrate are rather comparable to those obtained for Si and microslide glass substrates.

Third the upturn of the of $\Delta(d\rho/dT)/T^4$ near 1 K, which is so prominently displayed for K films on Si substrates, is surprisingly absent for the thin K sample, and only present in the 45.8 μm thick sample.

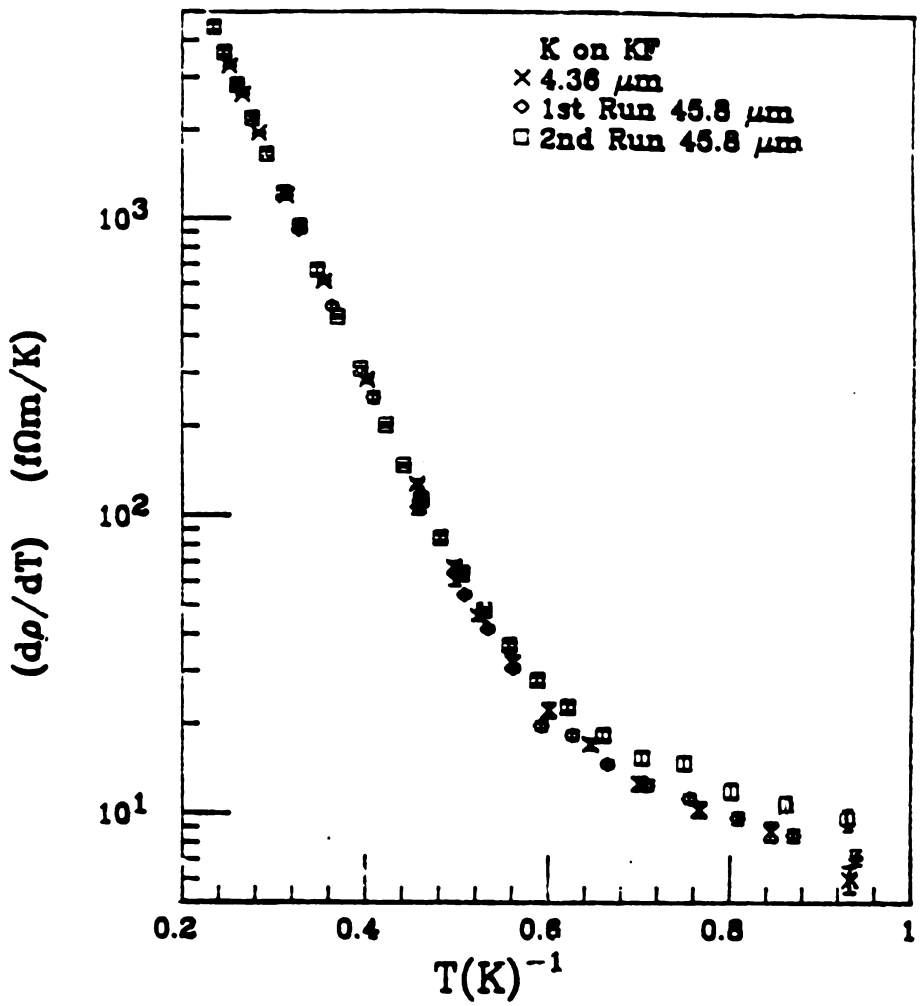

Fig. 3.4.1 $d\rho/dT$ vs. T^{-1} for K films on KF substrates.

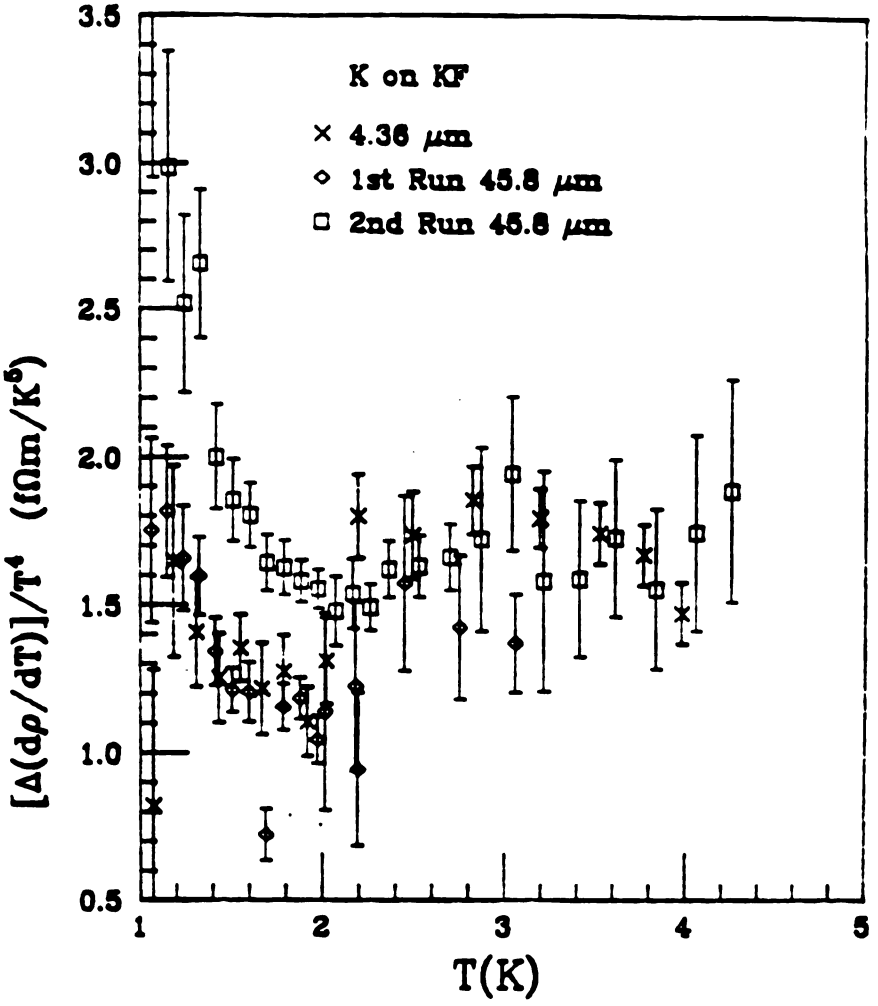

Fig. 3.4.2 Plotting $[\Delta(d\rho/dT)/T^4]$ vs. T to test the existence of T^5 term. (Note the scale on the figure is = 4 times greater than in fig. 3.3.2).

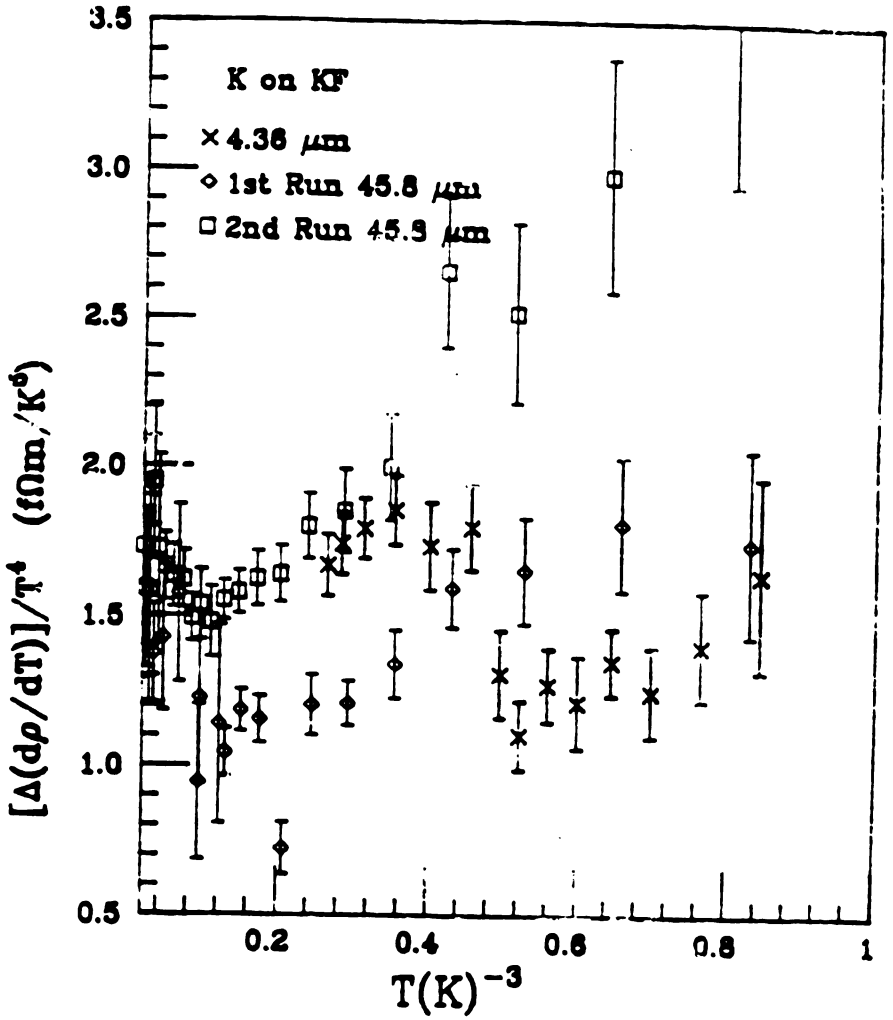

Fig. 3.4.3 $[\Delta(d\rho/dT)]/T^4$ vs. T^{-3} to obtain the slope 2A.

For the first and second difference, one possible explanation is that the nature of the substrate is very different between the KF on one hand, Si and microslide glass on the other. The KF substrate is a very good single crystal, and more importantly the lattice constant of KF is 5.34 Å, and the lattice constant of K single crystal is 5.385 Å, and both KF and K are BCC structure and have cubic symmetry, so they are very well matched at the interface. But the lattice constant of Si single crystal is 5.43 Å, it has a diamond structure which is quite different from BCC structure, and the microslide glass is in an amorphous state, and has no simple structure. The importance of lattice constant and lattice structure match is evidenced by the fact that the K films on KF substrates have (100) parallel to the surface instead of (110) orientation for K films on Si and microslide glass substrates, which has a larger distance between the layers. The very good match in the boundary of K and KF could result in the scattering of phonons by the interface between K and KF is being very much reduced. In turn the interface is less effective in depressing the phonon drag, as discussed in 3.4, so that the coefficient of the T^5 law for that of the thin film should not be very much different from the thick film and should be quite small, but the quantitative comparison is very difficult to calculate.

3.5 Discussion of Results for T=1 K to 4.2 K

We have measured $d\rho/dT$ of K films on three kinds of substrates, the K films with surface parallel to (110) planes on amorphous Microslides Glass and single crystal Si, and K films with surface parallel to (100) planes on (100) cleaved KF single crystal, for which (100) planes are parallel to the surface. The results of these measurements are presented in figures 3.5.1 for C, the coefficients of the T^5 term

presumally due to normal electron-phonon scattering, and in figures 3.5.2 for the coefficients A of the T^2 term due to umklapp electron-electron scattering.

The coefficients A of the T^2 term will be compared with the low temperature data later. In figure 3.5.1 we see the film thickness dependence of the coefficient C of the T^5 Law. There is very large scatter of the data, especially for Glass substrates, for which the measurement techniques were not so well developed as those for Si substrates. However still for both the Si and Glass substrates the thickness dependence is appreciable and roughly proportional to the inverse of film thickness. For the KF substrate, there is no real difference due to film thickness variation. Another very puzzling behavior is the result of the three measurements of the 5.33 μm thick film on glass substrate. Both the A and C value increased dramatically after the first run, especially the value of A which increased by a factor of three. At same time their RRR value also slightly increased in the second run even though its room temperature resistance has increased after the first run, which is frequently observed in bulk K samples. The values of A and C are basically the same for the second and third run. All values of C and related information are listed in table 3.

Since the theory[26,27] also predicted that the umklapp term $\rho^U_{el\text{-}ph}$ should also be reduced to $\simeq$ 60% when phonon drag is effective, one would expect that when the phonon drag effect was suppressed by the surface scattering, the value of $\rho^U_{el\text{-}ph}$ would be increased similar to the behavior of $\rho^N_{el\text{-}ph}$(i.e. T^5 term). Assuming the increase of $d\rho/dT$ for the thin films is coming from both $\rho^U_{el\text{-}ph}$ and $\rho^N_{el\text{-}ph}$, one can write down the resistivity of film as

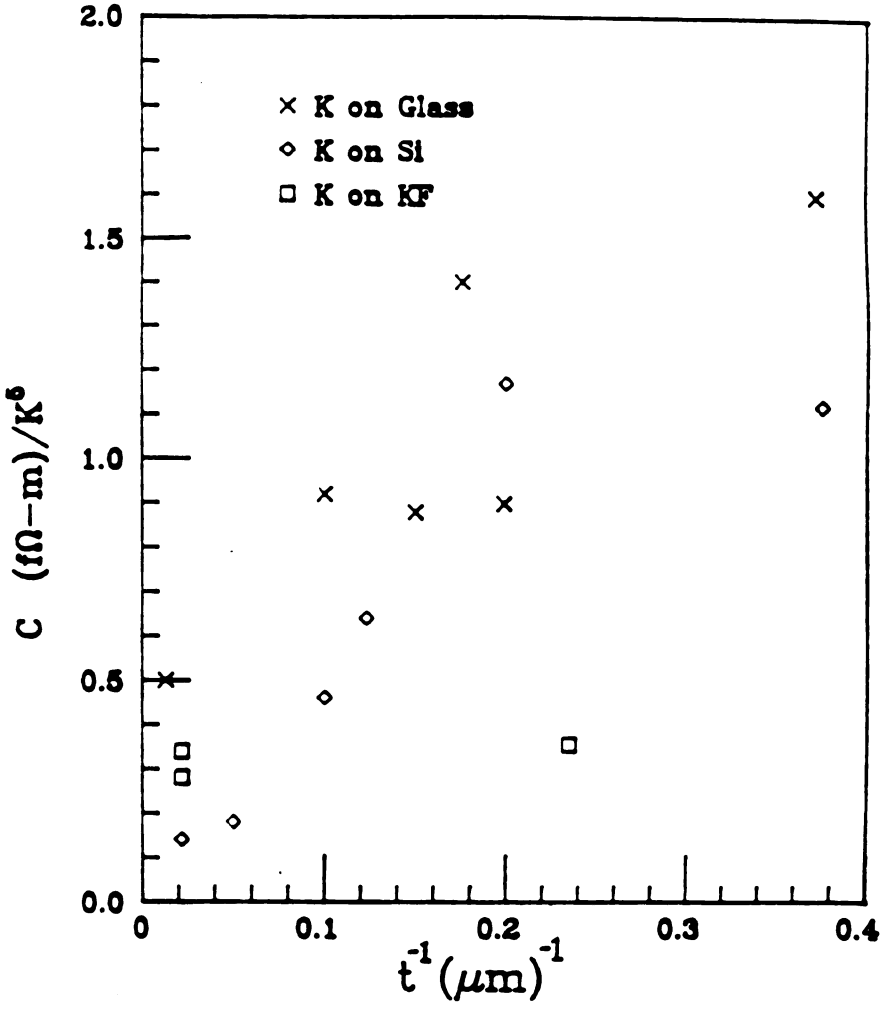

Fig. 3.5.1 Coefficient of T^5 term vs. inverse of the film thickness.

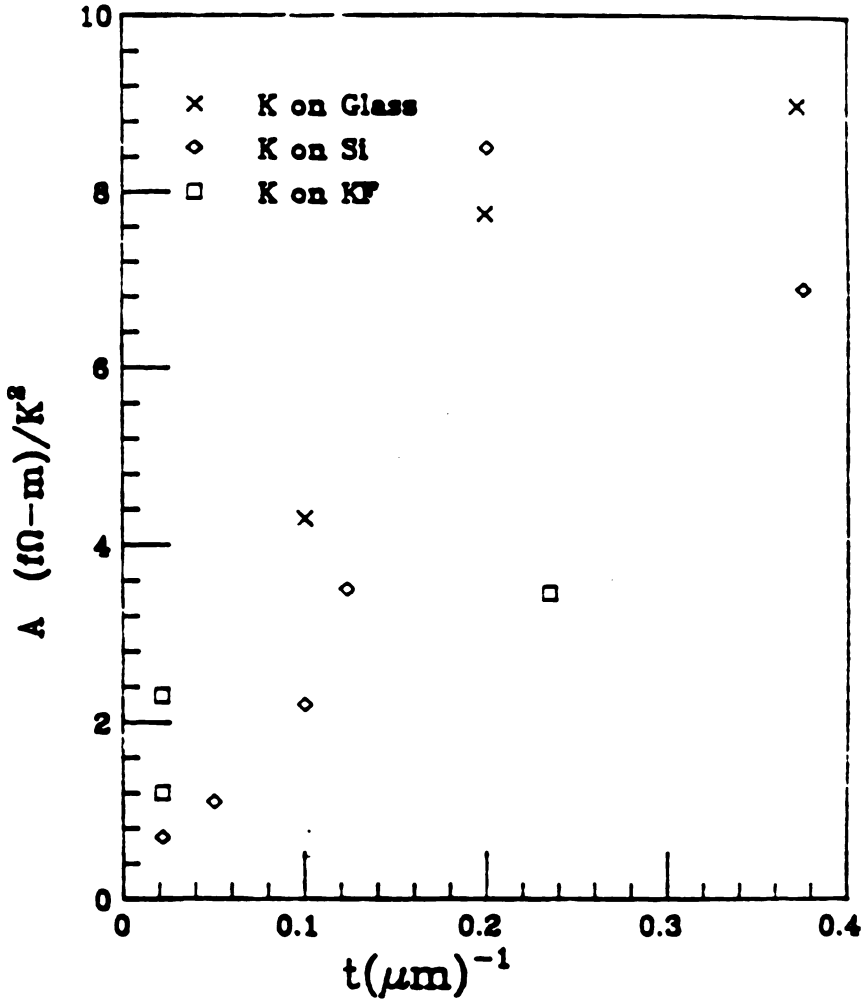

Fig. 3.5.2 Coefficient of T^2 term vs. inverse of film thickness.

Table 3 Values of C from the experimental data, here we assume that the value of D is same for films as for bulk K.

t(μm)	days at RT	RRR	ρ_0(nΩ-cm)	C(fΩ-m/K^5)	Substrates
2.69	0.5	203	35.4	1.6	Glass
5.03	0.5	725	9.9	0.9	Glass
5.33(#1)	0.5	365	19.6	0.9	Glass
5.33(#2)	7.5	413	17.4	1.3	Glass
5.33(#3)	20	432	16.6	1.5	Glass
5.68	0.5	714	10.1	1.4	Glass
6.66	0.5	1235	5.82	0.9	Glass
10	0.5	930	7.73	0.9	Glass
76.2	0.5	1139	6.31	0.5	Glass
2.57	3	423	17.0	1.1	Si
4.98	0.5	407	17.6	1.3	Si
8.1(#1)	0.5	1329	5.39	0.49	Si
8.1(#2)	7.5	1024	6.99	0.63	Si
8.1(#3)	20	842	8.54	0.67	Si
10	0.5	981	7.29	0.29	Si
20	0.5	2280	3.14	0.26	Si
46.6(#1)	0.5	1908	3.77	0.17	Si
46.6(#2)	11.5	1963	3.66	0.34	Si
4.36	0.5	419	17.2	0.32	KF
45.8(#1)	0.5	1688	4.26	0.23	KF
45.8(#2)	19	1722	4.18	0.28	KF

Table 4 Fit the experimental data by least square method to obtain the coefficients of C and D.

t(μm)	D(fΩ-m/K)	C(fΩ-m/K^5)	Substrate
2.57	64300	1.37	Si
4.98	66000	1.42	Si
8.1(#1)	68600	0.74	Si
8.2(#2)	66800	0.74	Si
8.1(#3)	80200	0.54	Si
10	74300	0.52	Si
20	76000	0.19	Si
46.6(#1)	74100	0.20	Si
46.6(#2)	75500	0.43	Si
2.69	58000	2.07	Glass
5.03	70700	1.00	Glass
5.33(#1)	85300	0.65	Glass
5.33(#2)	42100	2.32	Glass
5.33(#3)	50300	2.26	Glass
10.0	76900	0.80	Glass
76.2	66100	0.71	Glass
4.36	75200	0.37	KF
45.8(#1)	86300	0.11	KF
45.8(#2)	78400	0.30	KF

$$\rho(T)=AT^2 + CT^5 + D\exp(-\theta/T) \qquad (3.5.1)$$

where A can be obtained from the low temperature data. We did a least square fit using eq. 3.5.1 to obtain the coefficients of C and D while θ is fixed at 20.3 K. The result is listed in table 4. From the table one can see that instead of D increasing with decreasing in film thickness, D varies little compared with the coefficient C and actually has the tendency of decreasing. This result is in total contradiction to what we expected from the predictions of theory. This justifies our previous analysis of fixing D at the bulk K value while only C changes with the film thickness. The suppression of phonon drag effect only resulted in the increase of resistivity contributions from normal electron-phonon scattering only.

3.6 $\rho(T)$ of K films on Glass Substrates at T=0.1 to 1.3 K

As we discussed above, at temperatures lower than 1.3 K, the dominant contribution to $\rho(T)$ comes from umklapp electron-electron scattering, which has the following form

$$\rho_{el\text{-}el}(T)=AT^2 \qquad (3.6.1)$$

As we have seen, the coefficient A for bulk pure potassium is about 2.2 $\pm$ 0.3 ($f\Omega$-m/K^2) as shown in figure 1.2.2.1, and for thin wires there are very large deviations from the simple square law of eq.3.6.1 as shown in figure 1.2.2.2. In between these 3D and 1D extremities we have here investigated the properties of a 2D geometry, a very thin film deposited on various substrates. The thinnest film is about one order of magnitude smaller than the diameter of the thinnest wire investigated by Z. Z. Yu[45] and J. Zhao[51], and the thickest film is roughly comparable to the diameter of their thinnest wires. In this section we will present the results of measurements done on films deposited on Microslides Glass substrates.

If equation 3.6.1 is obeyed there,

$$\frac{d\rho_{el\text{-}el}(T)}{dT} = 2AT \qquad (3.6.2)$$

and the plot of $d\rho_{el\text{-}el}/dT$ vs T should be a straight line passing through the origin. Furthermore

$$\frac{d\rho_{el\text{-}el}(T)}{TdT} = 2A \qquad (3.6.3)$$

so the plot of $d\rho_{el\text{-}el}/TdT$ vs T should be horizontal straight line.

In figure 3.6.1 we have plotted data according to equation 3.6.2; the solid line is the behavior of $\rho(T)$ for bulk potassium. Comparing this figure with figure 1.2.2.2 we immediately see that there is substantial difference between the 2D and 3D, 2D and 1D cases. First $d\rho(T)/dT$ goes negative below T=0.4 to 0.6 and remains negative to the lowest temperature, which means that there is a resistivity minimum at a temperature of ≈ 0.5 K, as shown in figure 3.6.2 (Notice that the vertical scale in this figure nicely illustrates the part in 10^7 precision of these measurement); Secondly there is no variation of monotonic increase of $d\rho/dT$ with T as seen in the data of thin wires; and thirdly the analysis which follows indicates that the behavior of the coefficient A of the T^2 Law for these low temperature data is similar to that derived from the high temperature data, namely the thinner the film, the larger the value of A. In figures 3.6.3 and 3.6.4 following equation 3.6.3 we plot $(d\rho_{el\text{-}el}/dT)/T$ vs T. The two figures are identical except for the scale. One can clearly see the large negative value of $(d\rho(T)/dT)/T$ at lowest temperature attainable in fig. 3.6.3, and we see that there is no flat region in the data which implies that other mechanisms extend down into the region where electron-electron scattering predominates in the bulk K samples. It is clear from these two figures that there is another term which is effective at very low temperature and has a negative contribution to the resistivity.

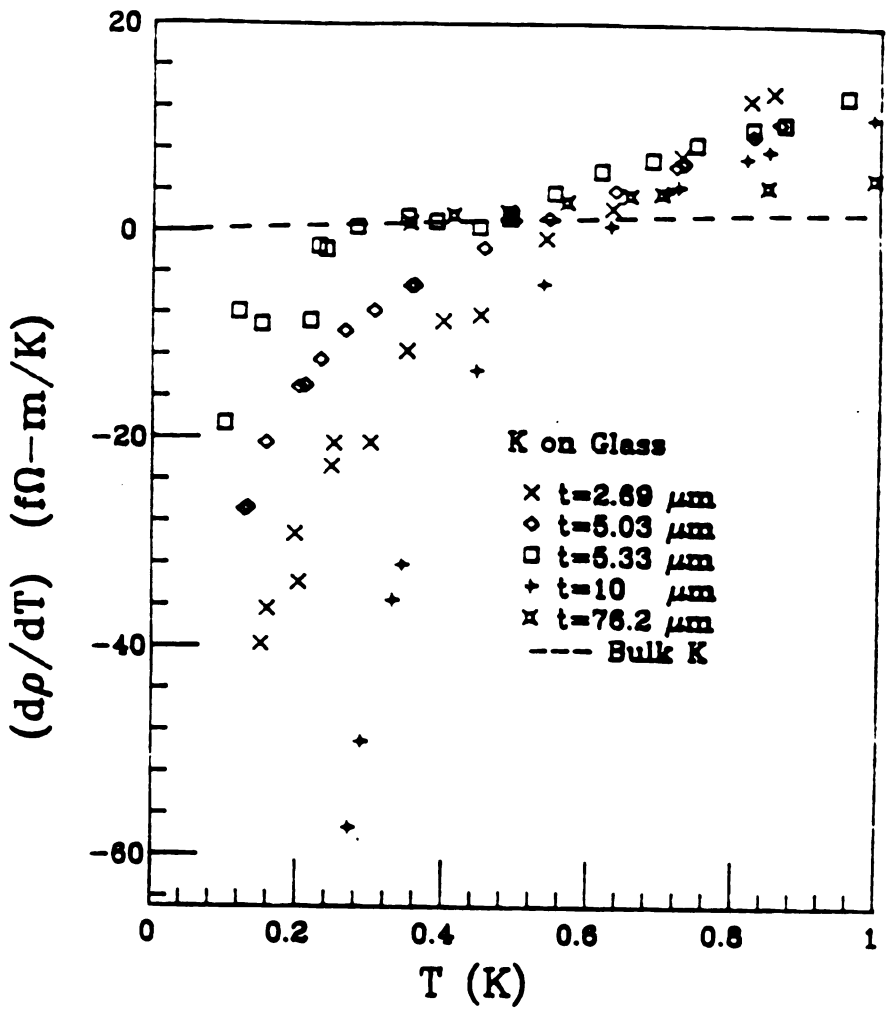

Fig. 3.6.1 (dρ/dT) vs. T for K films on glass substrates.

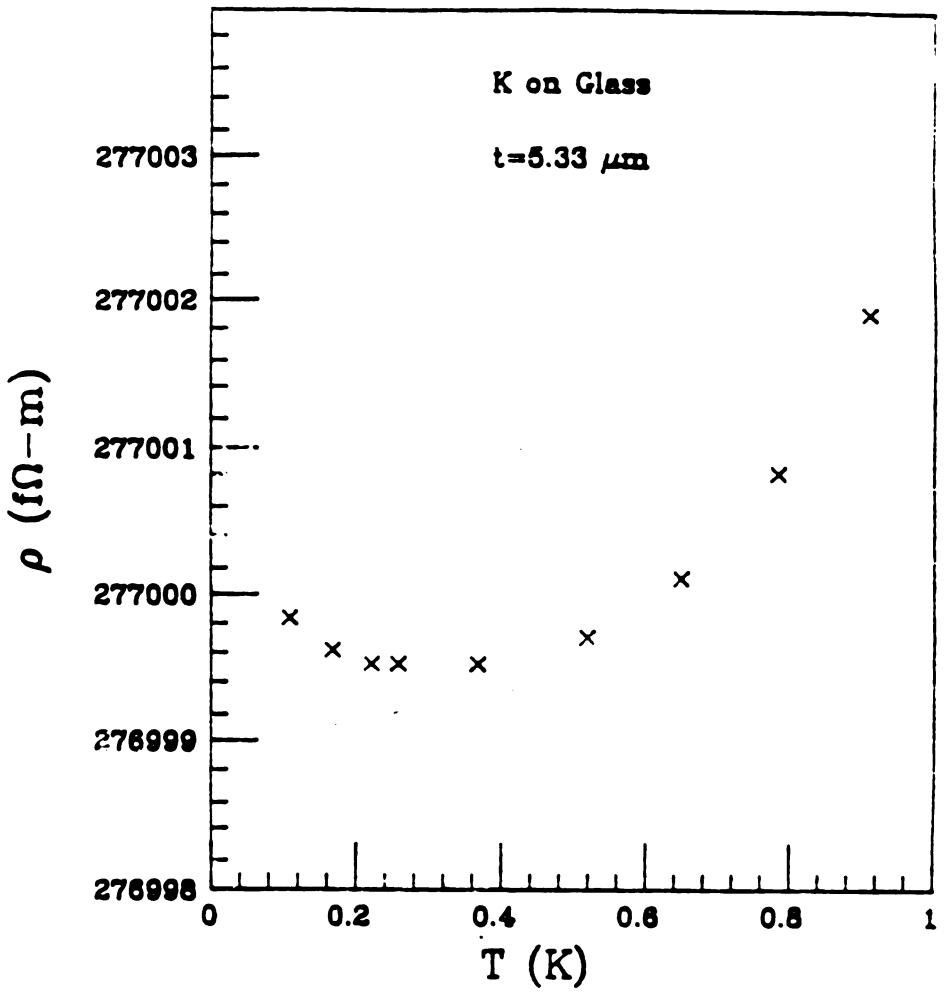

Fig. 3.6.2 ρ vs. T for a 5.33 μm thick film on a glass substrate. Note the resistivity minimum.

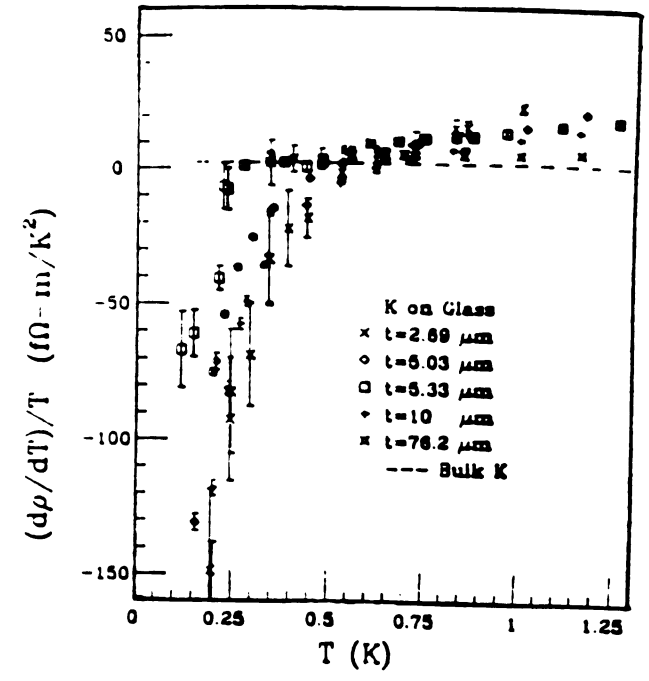

(A)

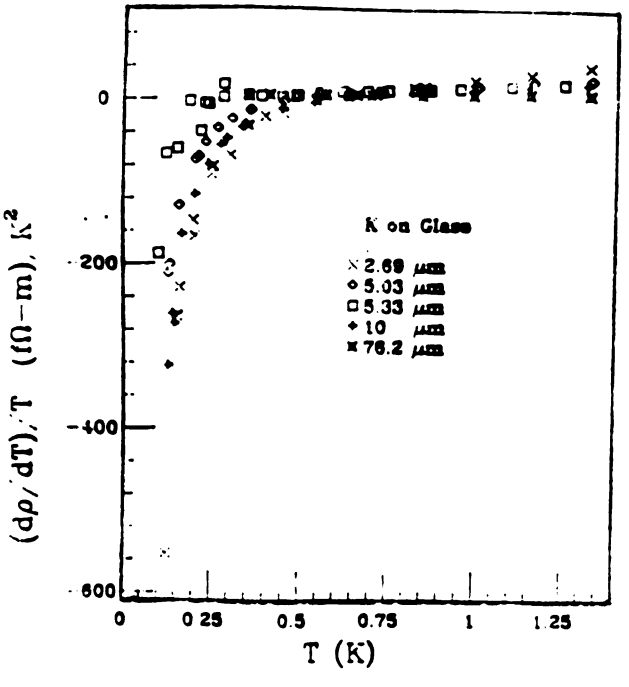

(B)

Fig. 3.6.3 $(d\rho/dT)/T$ vs. T for K films on glass substrates. (B) is in large scale.

Assuming that this term arises from the Kondo effect we can write down the resistivity of a K film on a Glass substrate below 1.5 K as follows,

$$\begin{aligned}\rho &= \rho_0 + \rho(T) \\ &= \rho_0 + \rho_{el\text{-}el}(T) + \rho_{el\text{-}ph}(T) + \rho_{extra}(T) \\ &= \rho_0 + AT^2 + CT^5 - B\ln(T/T_K) \qquad (3.6.4)\end{aligned}$$

where T_K is a constant called the Kondo temperature. From equation 3.6.4 we get

$$\begin{aligned}\frac{d\rho}{dT} &= \frac{d\rho(T)}{dT} \\ &= 2AT + 5CT^4 - \frac{B}{T} \qquad (3.6.5)\end{aligned}$$

We can further simplify this equation at low temperature as follows. The ratio of the differentials for $\rho_{el\text{-}ph}(T)$ and $\rho_{el\text{-}el}(T)$ is

$$\begin{aligned}\frac{d\rho_{el\text{-}ph}(T)}{dT} \Big/ \frac{d\rho_{el\text{-}el}(T)}{dT} &= \frac{5CT^4}{2AT} \\ &= \frac{5C}{2A} T^3 \qquad (3.6.6)\end{aligned}$$

If one uses the value of C obtained from the high temperature part of the data, then the largest possible value of this ratio at 1 K is 34%, and at 0.7 K it is about 11%, but it is only 4% at 0.5 K, so the $\rho_{el\text{-}ph}(T)$ term can be neglected for temperatures lower than 0.7 K. Equation 3.6.5 becomes

$$\frac{d\rho(T)}{dT} = 2AT - \frac{B}{T} \qquad (3.6.7)$$

and further we have equations

$$\frac{d\rho(T)}{TdT} = 2A - \frac{B}{T^2} \qquad (3.6.8)$$

and

$$T\frac{d\rho(T)}{dT} = 2AT^2 - B \qquad (3.6.9)$$

According to equation 3.6.8, $(d\rho/dT)/T$ is linear in $1/T^2$. In figure 3.6.4 we see that the data obey Eq. 3.6.8 well. The slope of the data gives the value of B. Similarly according to the equation 3.6.9 $T(d\rho/dT)$ is linear in T^2. In Fig. 3.6.5 we made the plot corresponding to eq. 3.6.9. The values of A is obtained from its slope. We can also compare the value of the A's obtained from the different temperature

regions and indeed the values of A are generally compatible for both regions. This confirms that indeed the upturns seen in figures of $[\Delta(d\rho/dT)/T^4]$ vs. T at temperature region 1 K to 4.2 K are produced by electron-electron scattering, and the T^5 law is well observed in these figures. This is a further confirmation of the suppression of "phonon drag". All values of A and B are listed in table 5.

As in section 3.2, we also repeated 3 runs for the same 5.33 μm thick sample in the low temperature region with about 4.5 and 6.5 days respectively in between the runs. Figure 3.6.6 shows the results plotted according to equations 3.6.7, 3.6.8 and 3.6.9. There is very large difference in the temperature region higher than 0.2 K between the first and second runs but little or no difference between the second and third runs. The common intercept in figure 3.6.4 indicates that there is no essential difference in the logarithmic term, this contrasts to A which changes very significantly between run 1 and run 2. This difference for A and B will be discussed later when we discuss the origin of this logarithmic term.

3.7 $\rho(T)$ for K films on Si Substrates at T=0.1 to 1.3 K

In this section we present the data for K films on Si substrates at low temperature. Unlike the amorphous microslide glass substrate, the Si substrates are made of single crystal wafer. They apparently contain much fewer magnetic impurities. In figure 3.7.1 and figure 3.7.2 we plot data according to equations 3.6.7 and 3.6.8. From these two figures we can clearly see the T^2 term from 0.75 K down to ≈0.2 K, and lower than 0.2 K we see there is slight down turn, but this down turn is much smaller in magnitude than that of the K films on glass substrates. (Note the 4:1 difference in vertical scales for figures 3.6.1 and 3.7.1). From figure 3.7.2 we obtained the coefficient of T^2

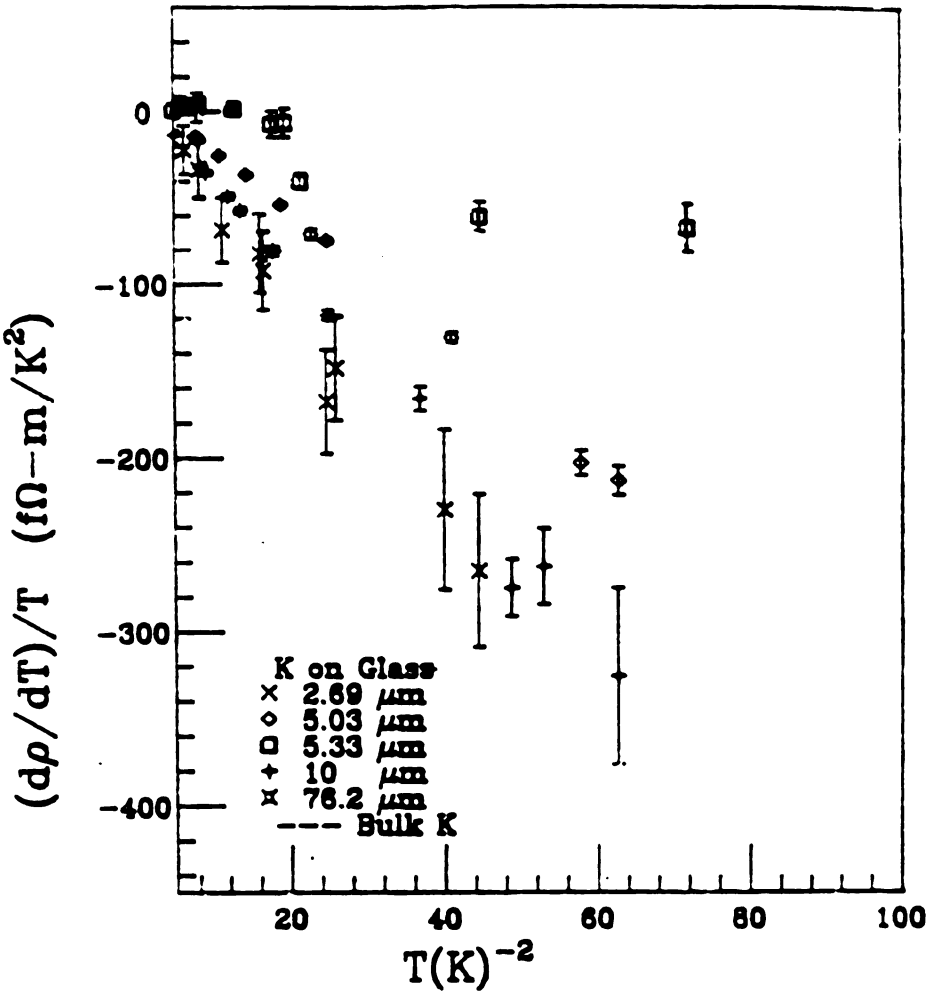

Fig. 3.6.4 $(d\rho/dT)/T$ vs. T^{-2}. The coefficient of the Kondo-like term is obtained from the slope.

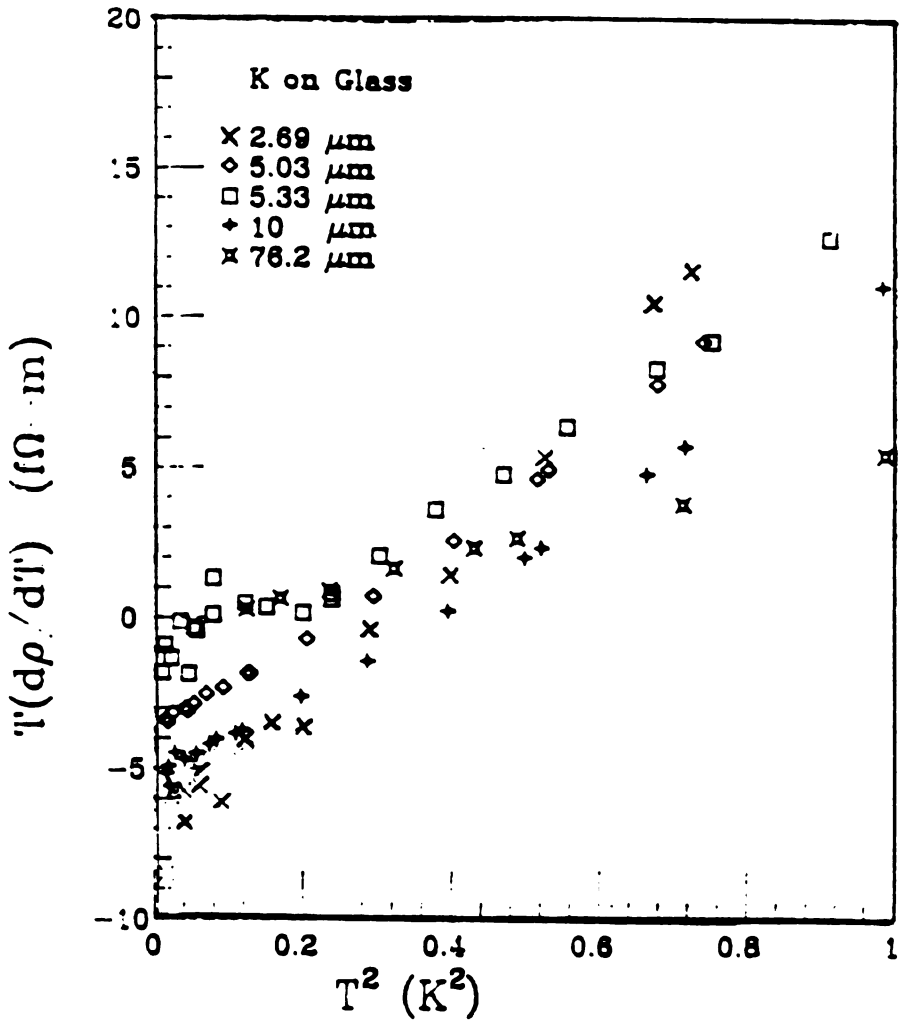

Fig. 3.6.5 T(dρ/dT) vs. T^2. 2A is obtained from the slope.

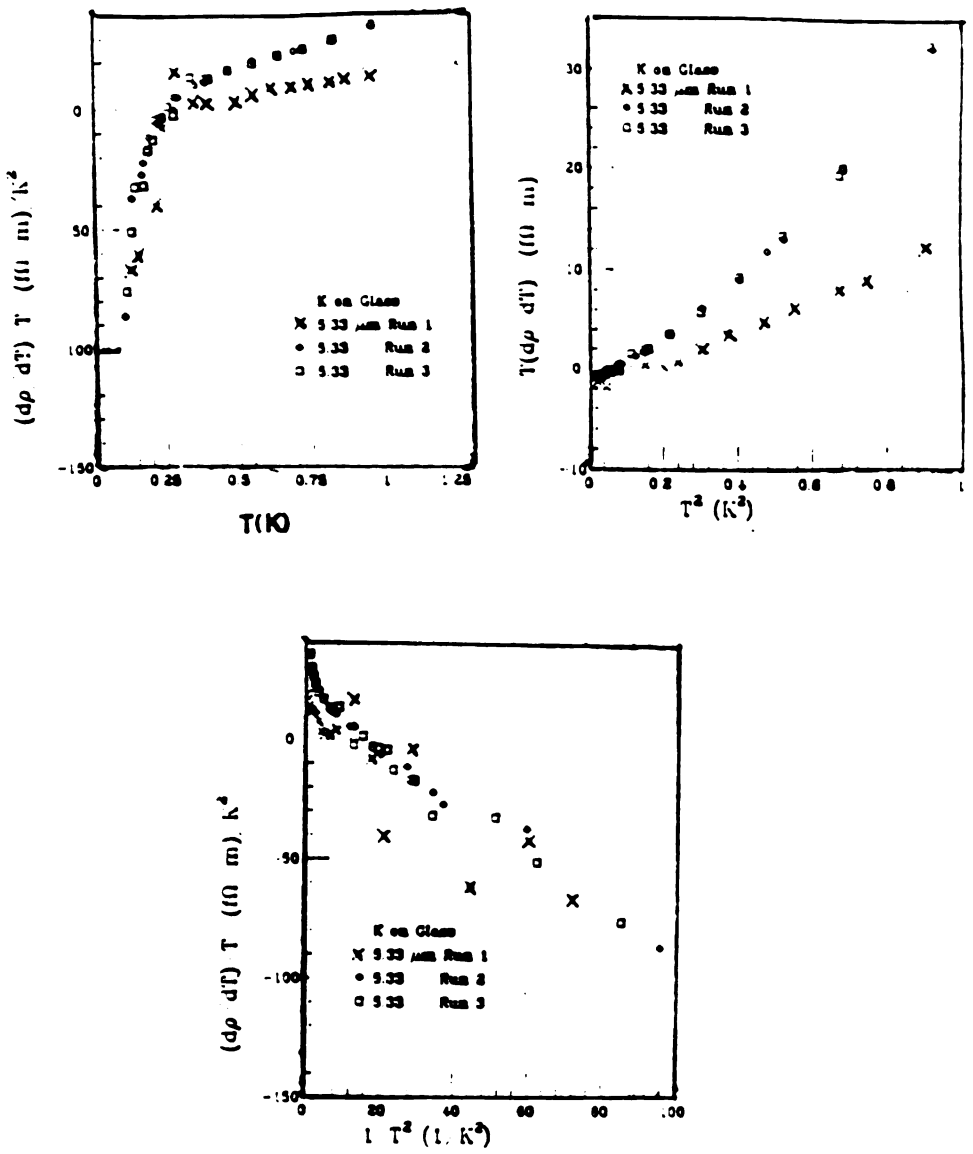

Fig. 3.6.6 Three runs for the same 5.33 μm thick film on a glass substrate.

term. We also plotted the data in figure 3.7.3 and figure 3.7.4 according to equations 3.3.8 and 3.3.9 for the data. From these two figures we obtained values of A and B, as in the case of Glass substrate. From table 5 listing all the coefficients obtained temperature regions, we see that the values of A are quite compatible for both high and low temperature regions, and the B value is very small in comparison with the coefficients we measured of samples on Glass substrates.

3.8 $\rho(T)$ for K films on KF substrates at T=0.1 to 1.3 K

As pointed out in section 3.4, single crystal KF has a very close match in lattice constant with potassium metal, and it is easily cleaved in a (100) plane. Consequently K films deposited on single crystal KF substrates have a <100> direction perpendicular to the substrate, as opposed to the <110> direction for K films deposited on microslides glass substrates and single crystal Si substrates. It is interesting to see if there is any substantial difference in behavior of $\rho(T)$ of K for the different film directions, especially in the light of Overhauser's predictions concerning charge density waves.

In figure 3.8.1 we present data plotted according to equations 3.6.7 and 3.6.8. We see that the 4.36 μm thick film behaves very similarly to the films on glass substrates. They have large down turns for temperature less than 0.3 K. Before the second run of the 45.8 μm thick sample it was first transferred back to the belljar, which was then filled with several τ pressure of pure oxygen, and sample stayed there for several hours. However the surface of the K film was still shiny and no visual effect was observed. But after admission of a few torr of air containing water vapor the sample surface became completely white while its room temperature resistance increased by 14%. There is

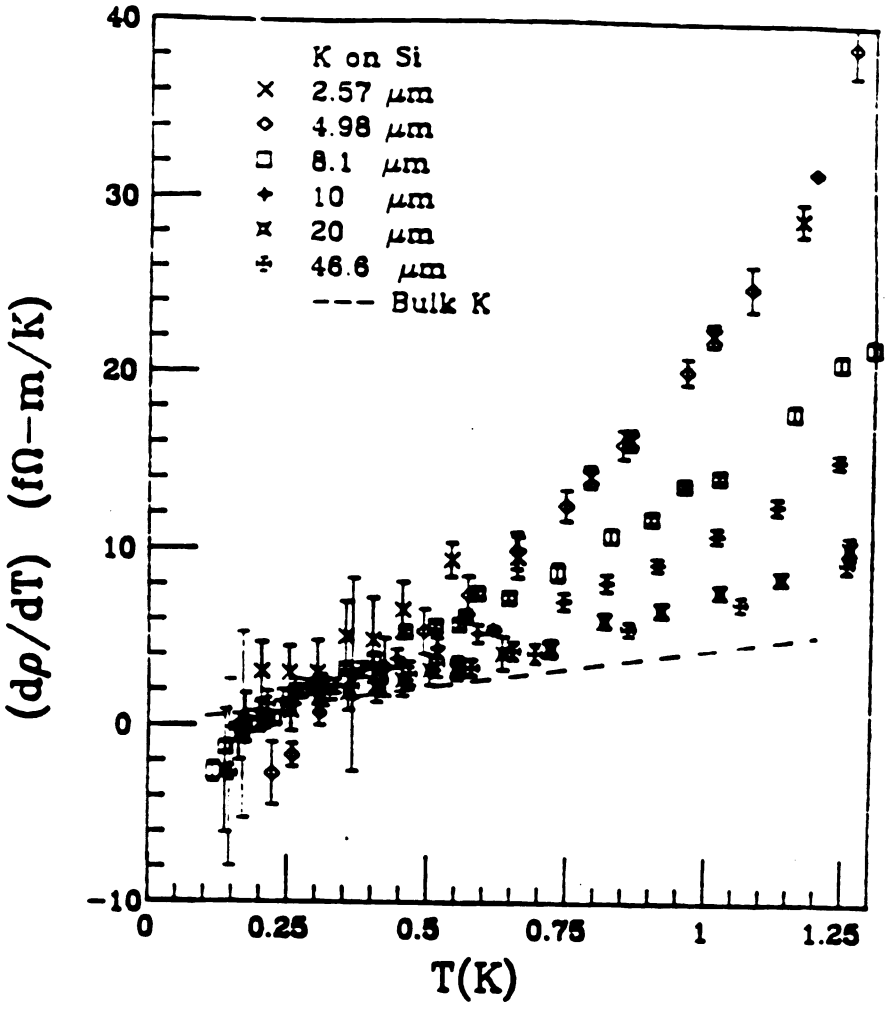

Fig. 3.7.1 (dρ/dT) vs. T for K films on Si substrates.

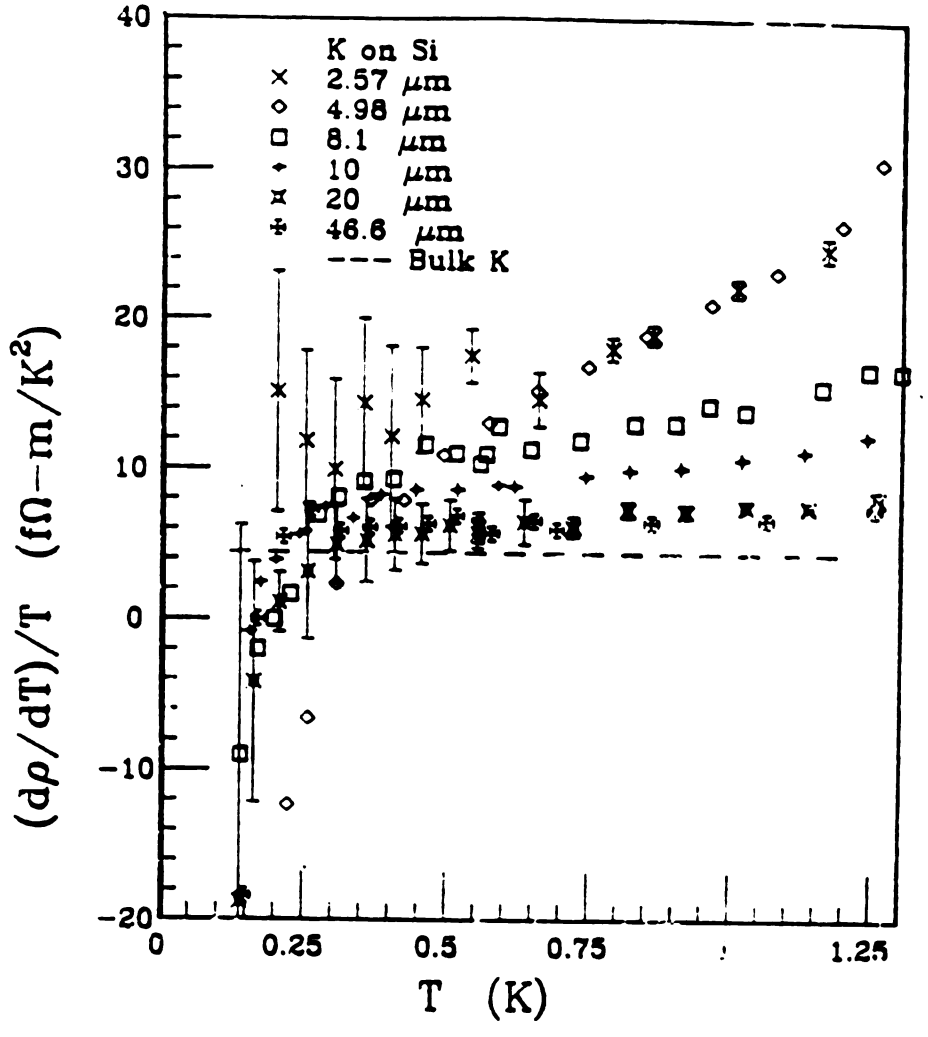

Fig. 3.7.2 $(d\rho/dT)/T$ for K films on Si substrates. The horizontal straight is the behavior of bulk K.

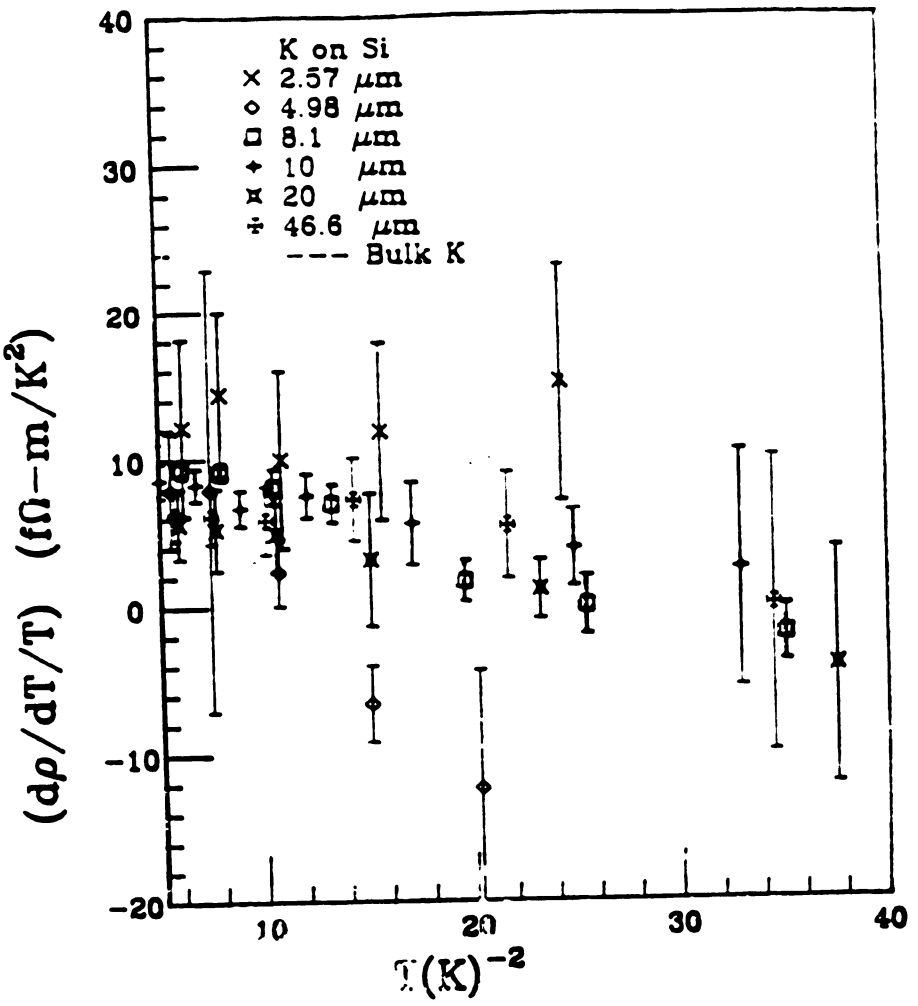

Fig. 3.7.3 $(d\rho/dT)$ vs. T^{-2}. The Kondo-like effect are small on the scale of the error bars.

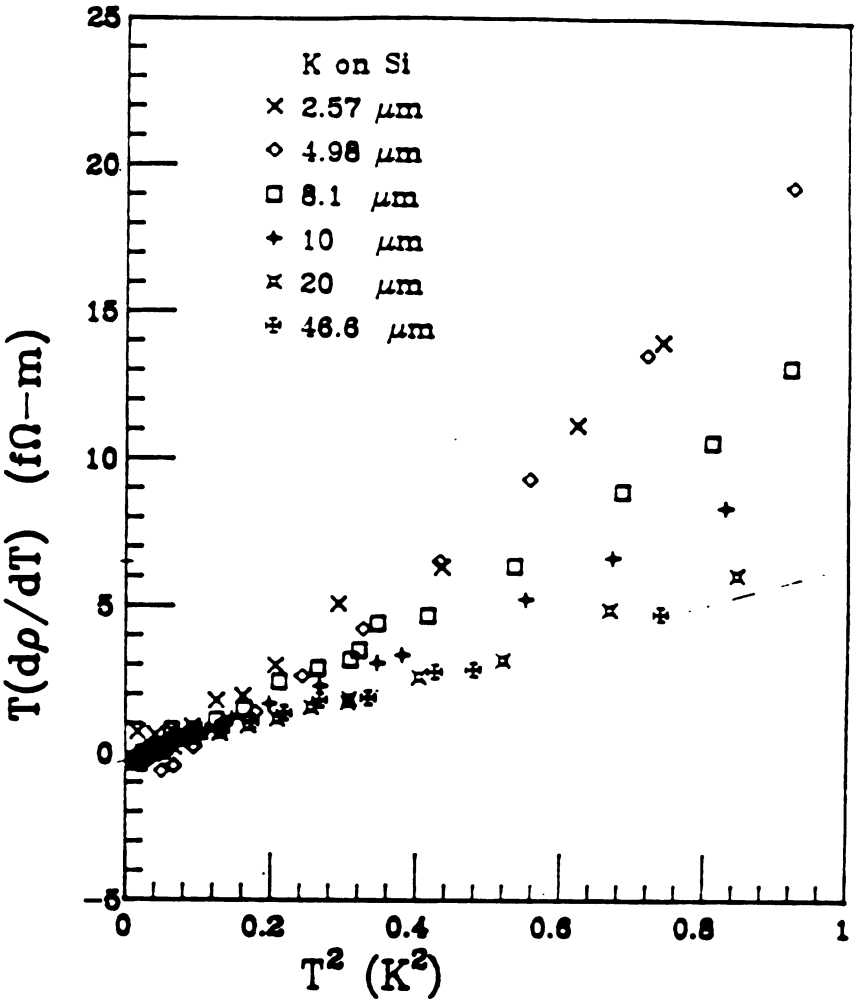

Fig. 3.7.4 $T(d\rho/dT)$ vs. T^2 to obtain the slope 2A.

a peak at T=0.25 K before the large down turn for the second run of 45.8 μm thick sample. Even taking into account the large experimental error, it seems to be a real peak. It is reminiscent of results for pure Li where a peak occurs because of competition between Kondo effect and the inelastic scattering of electrons by dislocations. There is some evidence of a smaller peak in the first run.

In figures 3.8.2 and 3.8.3 we plotted data according to equations 3.6.8 and 3.6.9. From these two figures we obtained the coefficients of A and B for the 4.36 μm thick film. As in the case of glass substrates, at very low temperature, the logarithmic behavior is very well followed, and no unusual deviation is observed, but for the 45.8 μm thick film, it is no longer suitable to use equations 3.6.5, 3.6.8 and 3.6.9 to describe the behavior because of the complication of the peak near T=0.25 K, but nevertheless we obtained the approximate value of their coefficient B by this way. One can still obtain the value of A between 0.6 K and 1.2 K by using the equation for processing high temperature data,

$$\frac{d\rho(T)}{T^4 dT} = \frac{d}{T^4 dT}\{AT^2 + CT^5\}$$
$$= \frac{2A}{T^3} + 5C \qquad (3.8.1)$$

In figure 3.8.4 we plot the data according the equation of 3.8.1 and from this figure we obtained both the coefficients of A and C. The coefficient C is also compatible with the value derived from the high temperature part of the data. We list all coefficients for K films on KF substrates in table 3 and 5.

From these tables one can see there is no substantial dependence of the coefficients of A and C on sample thickness, but the thinner film does have a much larger logarithmic term than the thick ones.

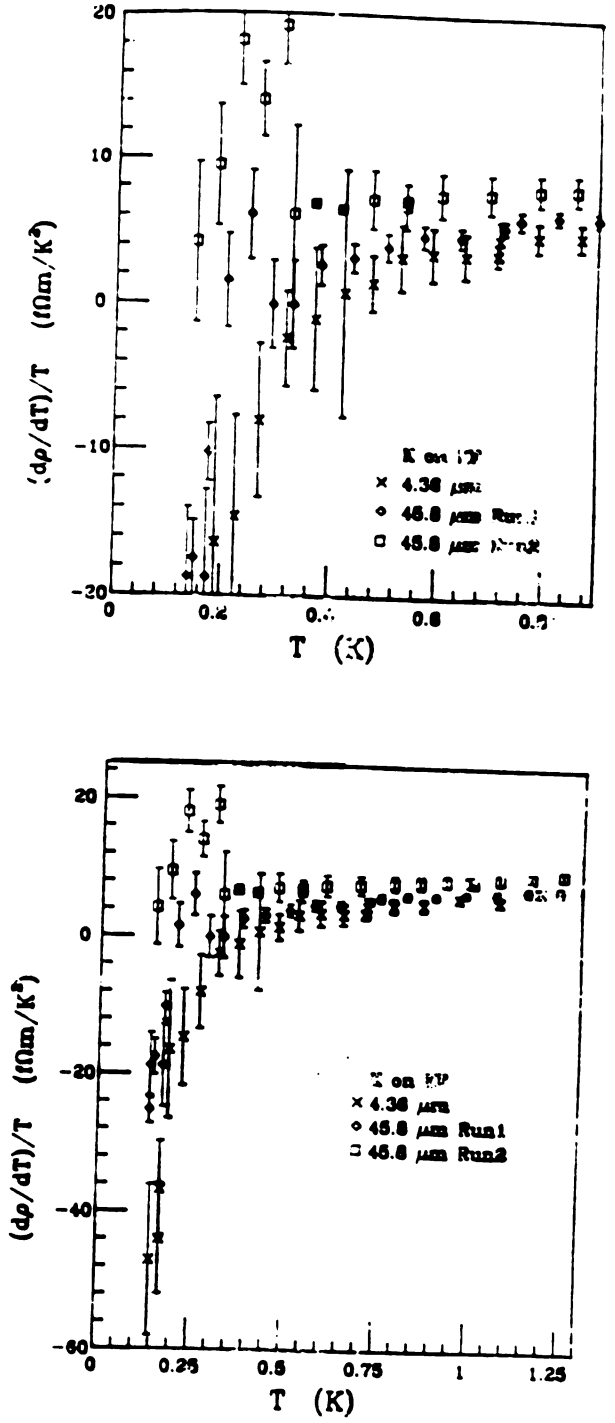

Fig. 3.8.1 $(d\rho/dT)/T$ vs. T for K on KF substrate. There is a small peak at T=0.2 K for the 45.8 μm sample.

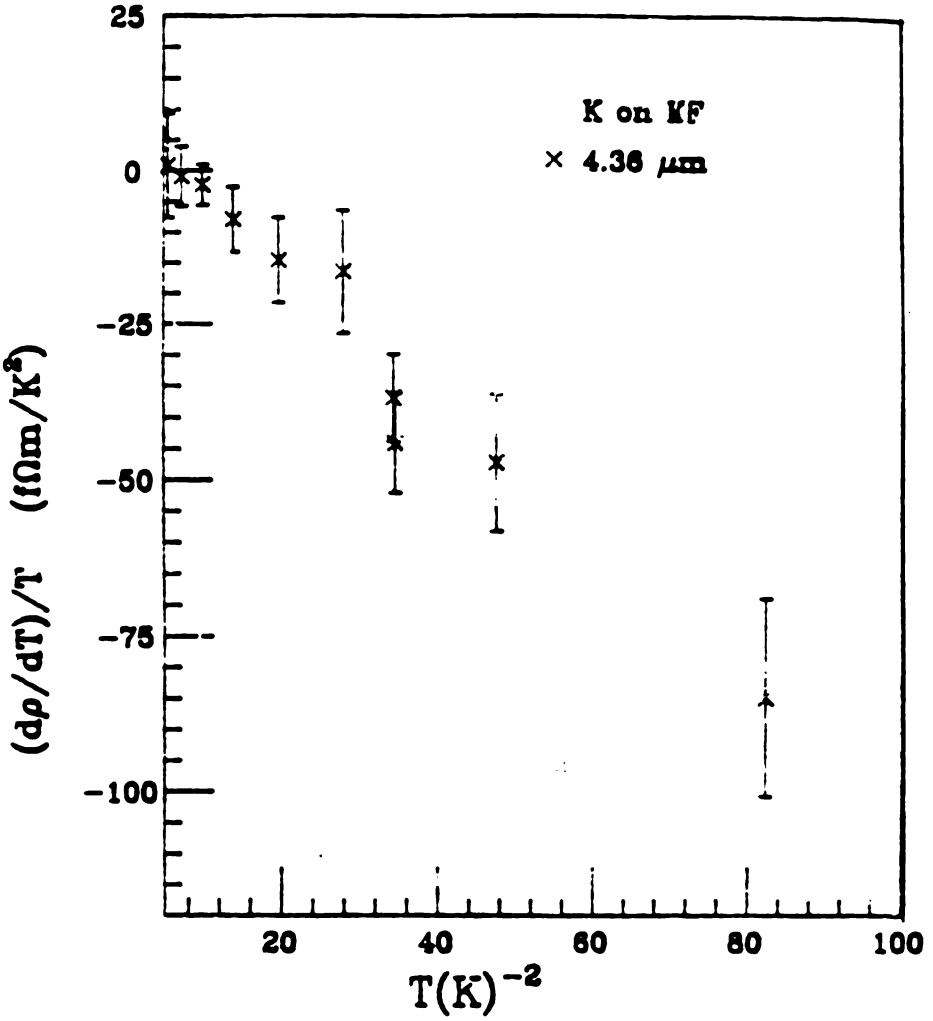

Fig. 3.8.2 $(d\rho/dT)/T$ vs. T^{-2} to obtain the coefficient of Kondo-like term from the slope.

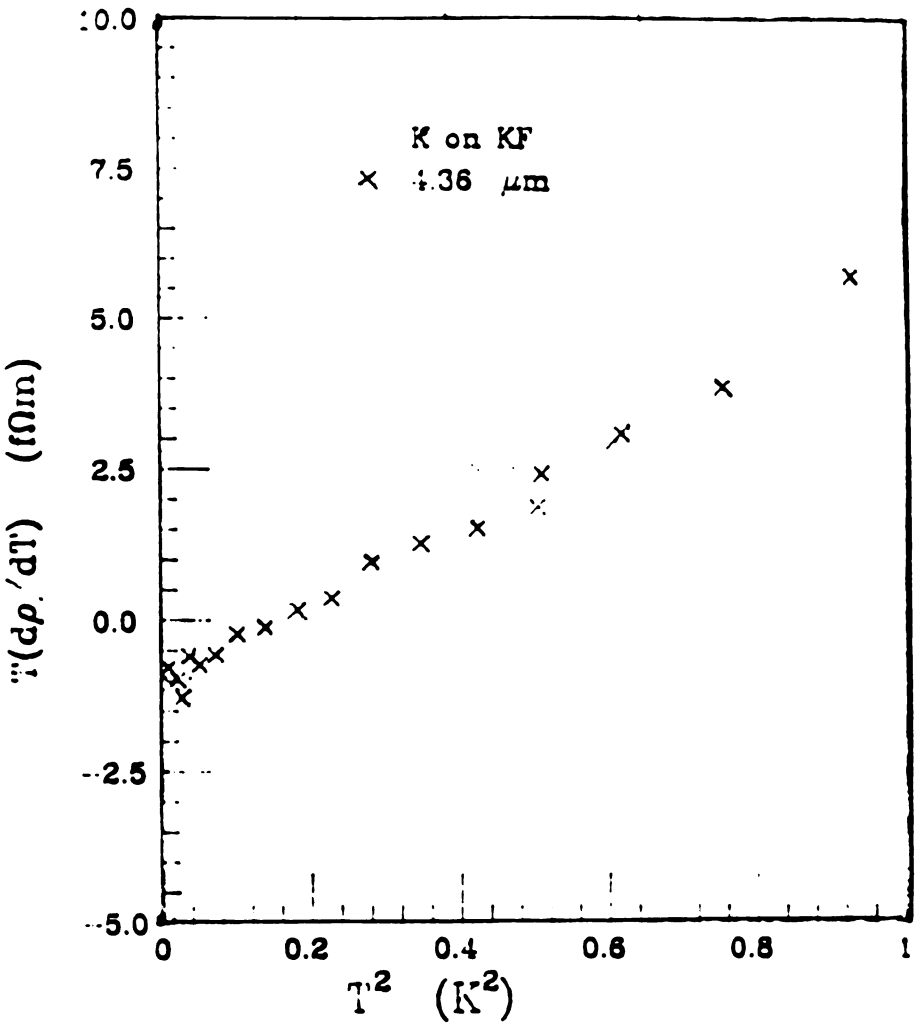

Fig. 3.8.3 T(dρ/dT) vs. T^2 to obtain coefficient 2A from the slope.

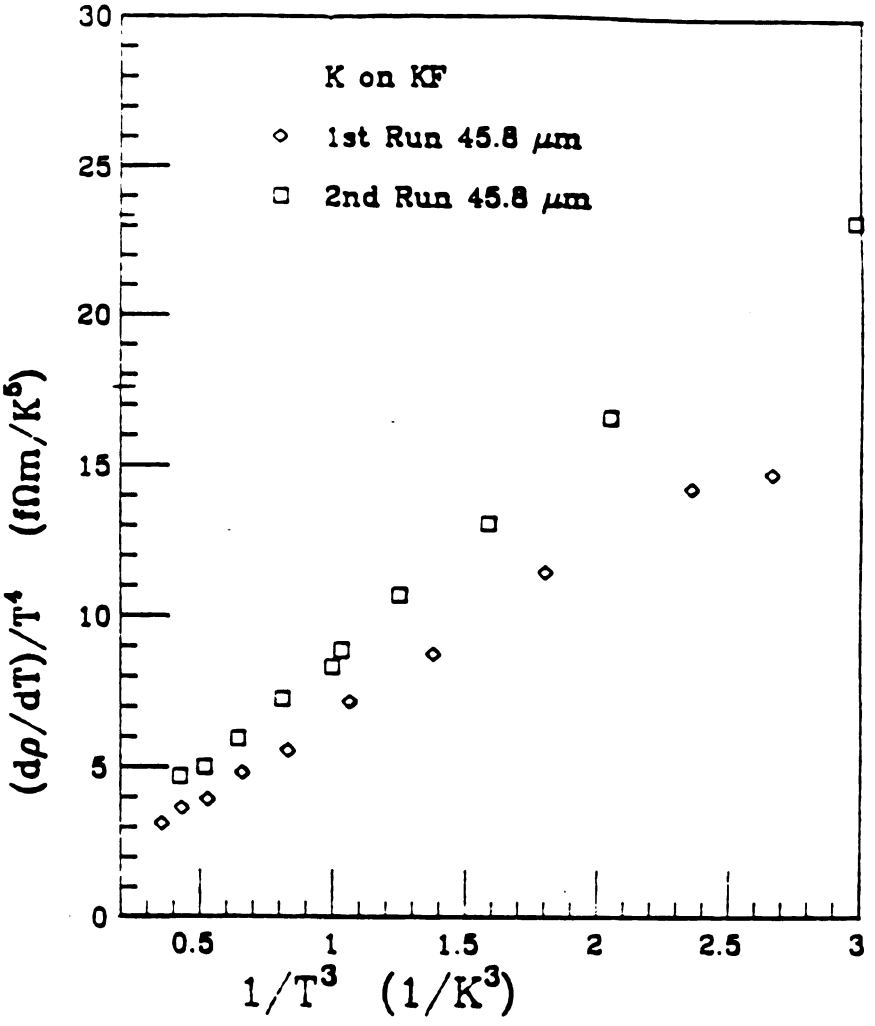

Fig. 3.8.4 Two runs on the 45.8μm thick film on KF substrate. The sample in the second run is seriously eroded. The 2A is obtained from the slope.

Table 5 Values of A and B for el-el scattering and Kondo-like terms, where LT stands for the data obtained in lower temperature region (0.1 to 1 K) and HT for higher temperature region.(1 to 4.2 K)

t(μm)	days at RT	RRR	ρ_0(nΩ-cm)	A(fΩ-m/K^2)		B(fΩ-m)	Substrates
				LT	HT		
2.69	0.5	203	35.4	10.3	9	6.5	Glass
5.03	0.5	725	9.9	7.6	7.8	3.8	Glass
5.33(#1)	0.5	365	19.6	7.5	5.9	1.2	Glass
5.33(#2)	7.5	413	17.4	10.9	15	1.1	Glass
5.33(#3)	20	432	16.6	10.9	15	1.0	Glass
10	0.5	930	7.73	6.6	4.3	5.5	Glass
76.2	0.5	1139	6.31	2.8	2.9	--	Glass
2.57	3	423	17.0	6.8	8.4	0.4	Si
4.98	0.5	407	17.6	8.8	8.5	1.5	Si
8.1(#1)	0.5	1329	5.39	4.9	4.7	0.5	Si
8.1(#2)	7.5	1024	6.99	5.5	6.5	---	Si
8.1(#3)	20	842	8.54	5.0	3.3	---	Si
10	0.5	981	7.29	4.2	4.2	0.3	Si
20	0.5	2280	3.14	3.4	3.3	0.4	Si
46.6(#1)	0.5	1908	3.77	3.0	2.9	0.2	Si
46.6(#2)	11.5	1963	3.66	4.8	4.5	---	Si
4.36	0.5	419	17.2	3.2	3.5	1.2	KF
45.8(#1)	0.5	1688	4.26	2.8	2.3	0.8	KF
45.8(#2)	19	1722	4.18	3.7	3.7	0.7	KF

3.9 Discussion of Results for T=0.1 to 1.3 K

In all three kinds of substrates there exists a logarithmic term, which is weakest for the Si substrates, and strongest for the microslide glass substrates. We now consider the question of the origin of this logarithmic behavior.

As pointed out in chapter 1 localization theory (KW and Anderson) has predicted that for very impure metals, there is a correction to the conductivity, which may be written as[18]

$$\sigma = \sigma_B - \Delta\sigma_L \qquad (3.9.1)$$

where σ_B is the bulk conductivity and $\Delta\sigma_L$ is due to the localization effect and depends on the shortest inelastic scattering time τ_{in}. For a two dimensional system the theoretical prediction for $\Delta\sigma_L$ is

$$\Delta\sigma_L(T,H=0) = \alpha\ln(\frac{\tau_{in}}{\tau}) \qquad (3.9.2)$$

where α is a positive constant and τ is the scattering time due to the disorder in metal. At very low temperature τ_{in}^{-1} is dominated by the electron-electron scattering which is proportional to T^2. If one put this relation into the equation 3.9.2, the correction term becomes

$$\Delta\sigma_L(T,H=0) = -2\alpha\ln(T\tau) \qquad (3.9.3)$$

and the corresponding correction to the resistivity becomes

$$\begin{aligned}\rho &= 1/(\sigma_B - \Delta\sigma_L) \\ &= \frac{1}{\sigma_B}(1 + \frac{\Delta\sigma_L}{\sigma_B}) \\ &= \rho_B + \rho_B^2(-2\alpha\ln(T\tau)) \qquad (3.9.4)\end{aligned}$$

The equation 3.9.4 gives a negative logarithmic term of the form seen in the experiment, but the derivation of this formula requires a very impure sample having $k_F l < 10$, where l is mean free path of the electrons. k_F of potassium is 0.75 $Å^{-1}$ and localization effects thus requires that $l < 13.4$ Å. But in our experiment the bulk potassium we used has a RRR of 2000, which corresponds to an l_B of about 60 μm at liquid helium

temperature. Furthermore the thinnest sample used in our experiment is about 3 μm, so that the condition for localization to be effective is not satisfied. It is therefore very difficult to see how localization theory can be applied in our experimental results.

As pointed out in chapter 1 a negative logarithmic term is a property of a "two level system" model, which assumes that in a disordered system there are internal degrees of freedom resulting from atoms being free to tunnel between two different positions of local equilibrium. Such double potential wells are only considered to exist in a disordered system and will vanish on crystallization. This "double well" tunneling results in a resistivity given by

$$\rho_{TLS}(T) \propto -\ln[k_B^2(T^2 + T_K^2)/D^2] \qquad (3.9.5)$$

where T_K is a characteristic temperature and D is the electron band width. It is very doubtful this theory is ever applicable in our case, because the potassium sample we used is of high purity, very well annealed crystalline sample, and the condition of two different positions of local equilibrium could never be satisfied.

The "Kondo" effect, as pointed out in chapter 1, also gives rise to a negative logarithmic term if there are magnetic impurities in a non-magnetic host. The interaction between the conduction electrons and the magnetic ions results in a term

$$\rho_{Kondo} = -B\ln(T/T_K) \qquad (3.9.6)$$

where B is a positive constant and T_K is a characteristic temperature associated with the "Kondo" effect. It has been shown experimentally that ppm concentration of magnetic impurities is often enough to show the effect. In our experiments the high purity potassium used is nonmagnetic, and the logarithmic behavior has never been observed for bare bulk potassium. The microslides glass substrate on which we observed the largest logarithmic behavior in our K films measurements

are known to contain large amount of magnetic impurities. On the other hand, the K films on clean nonmagnetic Si substrates showed comparatively little logarithmic behavior. Z. Z. Yu[45] et al. have done measurements on bulk potassium enclosed in polyethlene, Figure 3.9.1 illustrates some of their typical results. In their experiments both G and $d\rho(T)/dT$ measurements have shown large dependences on magnetic field, which is a very important confirmation that this is indeed a "Kondo" effect. The similarity of their data and our data in both the magnitude and effective region (or characteristic temperature T_K) is evident in figure 3.9.1. This is further evidence that the logarithmic behavior results from the "Kondo" effect. From all the above arguments we think that the "Kondo" effect is the best possible explanation for the logarithmic behavior of $\rho(T)$.

In figure 3.9.2 we plot the coefficient B of the Kondo effect against the inverse of thickness. From this figure we see that the coefficient B is very large for K films on microslide glass substrates and generally tends to increase as the thickness decreases. For the K films on Si substrates B tends to be constant except one point at t=5 μm. The same could be said for K films on KF substrates but its value is generally larger than films on Si substrates. If one assumes that the magnetic impurities come from the substrates, then there are two ways for the magnetic impurities to be effective. First magnetic impurities migrate into the K films from the substrate and interact with the conduction electrons. Second magnetic impurities stay on the surface of the substrate and only interact with the conduction electrons when there is surface scattering. We observed in figure 3.9.2 that repeated measurements on the same sample give little difference in the coefficient B for both the glass and KF substrates. This suggests that migration of magnetic impurities is not very important. And the B

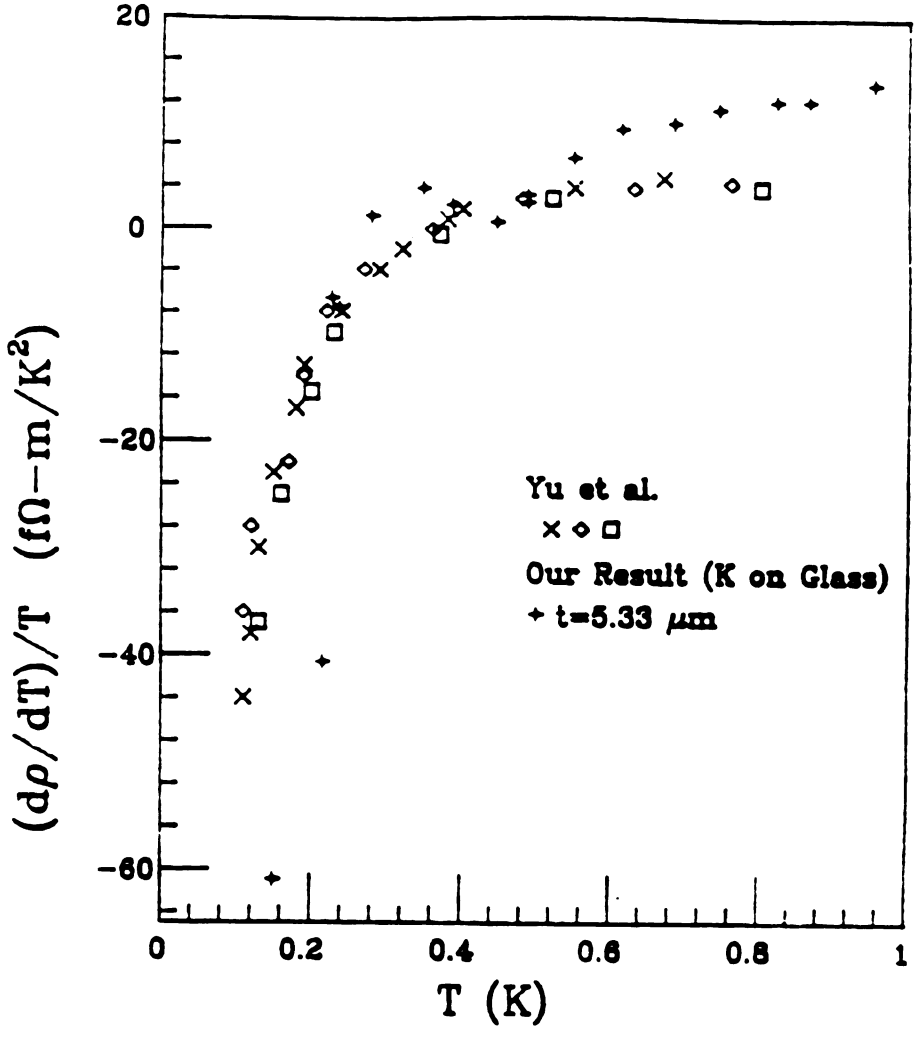

Fig. 3.9.1 Comparison of our result with these of Yu. et al.[45]

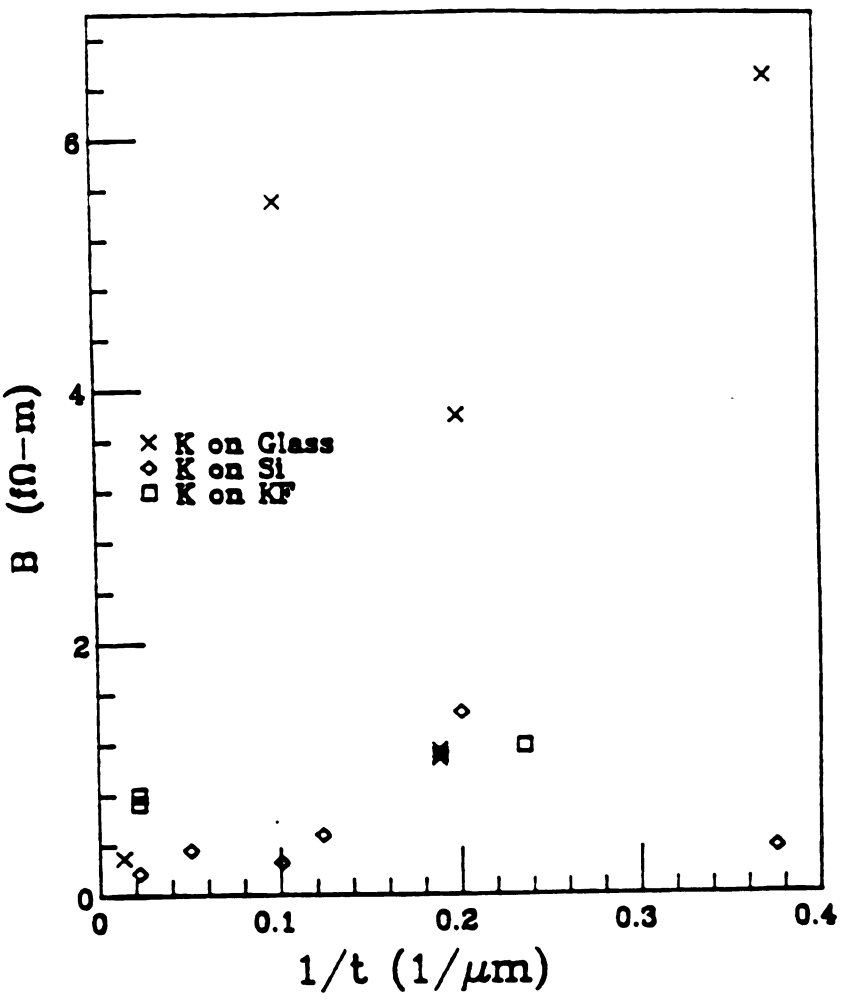

Fig. 3.9.2 The coefficient B of Kondo-like term vs. the inverse of film thickness.

values for glass substrates do vary widely with the K film thickness, but for the KF and Si substrates there is little dependence of B on film thickness. Since the mean free path of the electrons is larger than the the film thickness, one expects that there should be no dependence of B on the thickness. Perhaps the glass results are random depending on the local magnetic impurity where the film was deposited. All this suggests that only the boundary scattering of magnetic impurities is important. To further investigate the "Kondo" like effects, we specifically made a sample on Si substrates with a deposition of 4 Å Mn on the top of a K film of thickness is 3.6 μM, but unfortunately due to very large scatter in the very low temperature data. No conclusion could be drawn from this experiment.

In figure 3.9.3 we plot the coefficient A of the T^2 term obtained from very low temperature data. Generally there is no substantial difference between coefficients obtained in high (1.3 to 4.2 K) and low (0.1 to 1.3 K, for which the value of A is more reliable) temperature data. From the fig. 3.9.3 we can see that A is almost independent of thickness for KF substrates but tends to increase as the film thickness is decreasing for films on glass and Si substrates.

But things are more complicated when we compare the results of repeated measurements on four samples listed in table 6 with the experimental conditions. From this table we see that except for the 8.1 μm thick sample on Si substrates, the samples all show RRR increasing with time, or ρ_0 decreasing with time, even when their room temperature resistance goes up! One is especially puzzled by the fact that before the second run on the 46.6 μm thick sample, we left the sample in the belljar in a pressure of 10 torr pure oxygen gas for about 3 hours, with no visible effects on the sample. Then we put some air (containing water vapor) into the belljar. In a few seconds the surface of the

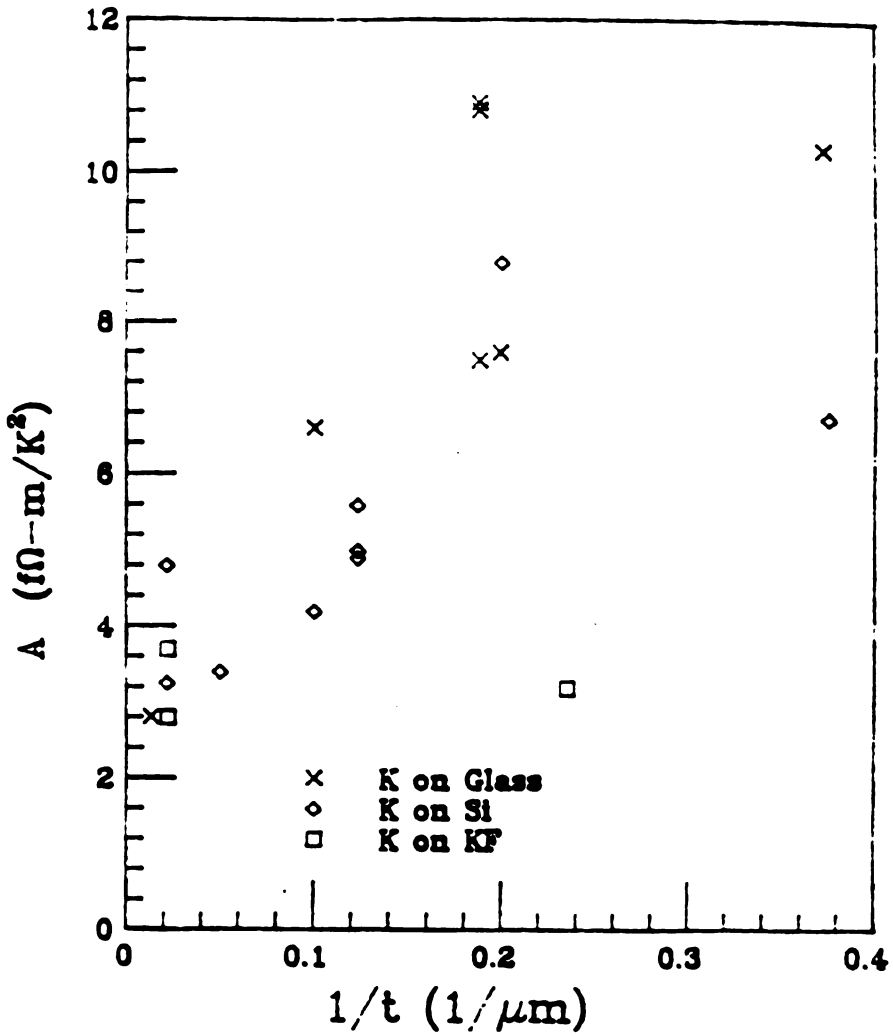

Fig. 3.9.3 A vs. the inverse of the film thickness.

Table 6 List of values of A for the repeatetive experiment

t(μm)	days at RT	RRR	ρ_0(nΩ-cm)	A(fΩ-m/K^2)	Substrates
5.33(#1)	0.5	365	19.6	7.5	Glass
5.33(#2)	7.5	413	17.4	10.9	Glass
5.33(#3)	20	432	16.6	10.9	Glass
8.1(#1)	0.5	1329	5.39	4.9	Si
8.1(#2)	7.5	1024	6.99	5.5	Si
8.1(#3)	20	842	8.54	5.0	Si
46.6(#1)	0.5	1908	3.77	2.9	Si
46.6(#2)	11.5	1963	3.66	4.8	Si
45.8(#1)	0.5	1688	4.26	2.8	KF
45.8(#2)	19	1722	4.18	3.7	KF

sample quickly became very white due to chemical reaction of potassium with water vapor, and its room temperature resistance increased by 14%. However its RRR still increased, and its A value increased from 3.25 fΩ-m/K^2 to 4.8 fΩ-m/K^2. For the 8.1 μm thick sample on Si substrates, A increased a little in the second run and then went back to the value for first run in the third run. At the same time its RRR value decreased with time. From these experiments one concludes that whenever the RRR increases with time, the value of A tends to increase too, but this is not without exception, and the reason why the film behaves like this in not clear.

Instead of thermal evaporation of K onto a substrate, we also used mechanical means to make thin films. First a thin wire was made from pure bulk potassium (RRR=8000). Then the thin potassium wire was sandwiched between two plastic sheets and this ensemble in turn was sandwiched between two smooth Al blocks and transferred into the press device as shown in figure 3.9.6. The K film was made by applying pressure. We used two kinds of plastic sheets in our experiments, Teflon and polyethlene. It has been shown that when K touches Teflon, it becomes black but its transport properties are not altered. On the other hand K in contact with polyethlene remains shiny but exhibits a "Kondo" effect in its transport properties (see ref. 45 by Z. Z. Yu). In figure 3.9.4 we plot results of the measurements according to equation 3.6.8. We did two runs separated by about 15 days for K between Teflon. From this figure we see that the behavior of the film shows little difference from bulk potassium and the T^2 law is well observed in the temperature region we measured, but the value of A for the two runs is quite different. The A value of the second run has decreased by 34% from 3.8 fΩ-m to 2.5 fΩ-m while its RRR value has actually increased by 10%. This is in contrast with what we see in the thermally evaporated

films. Also in the same figure the "Kondo" effect is clearly shown for the K film between the two polyethlene plastic sheets. The thickness of this sample is about 51 μM, which is comparable to the very thick samples on glass, Si and KF substrates made by thermal evaporation. In figure 3.9.5 we have made plots similar to that for the K films on microslide glass substrates and analyzed them using equations 3.6.8 and 3.6.9. The data do indeed show the behavior expected from these equations. From these two figures we obtained the value of A of 2.9 fΩ-m/K^2 and B of 0.30 fΩ-m. The similar behavior between this sample and films on glass substrates by thermal evaporation is further evidence that the "Kondo" effect plays a very important role in $\rho(T)$ of the latter. Notice that the purity (RRR≈8000) of bulk potassium from which the above samples was made is much higher than the ones (RRR≈2000) used for thermal evaporation, but one still could not observe the deviations from the T^2 law seen in the thin K wires experiments.

Here our experiments in thin K films raise two questions; first, why is the behavior of films so much different from that of thin wires in the temperature range of 0.1 to 1.3 K? With the thickness of the films one to two order of magnitude smaller than the diameters of thin wires, one might have anticipated to see an accentuation of the thin wire results; second how can we explain the variation of A with different thicknesses of the samples, and on different substrates?

In chapter 1 we discussed the different models proposed for the deviation of T^2 law observed in thin wires. The localization model proposed by Farrel et al.[18] predicts that deviation to T^2 law only occurs in 1D case. It gives one explanation of why one does not see the deviation from a T^2 law in thin films. The normal electron-phonon surface scattering model proposed by Kaveh and Wiser[20] gives a negative

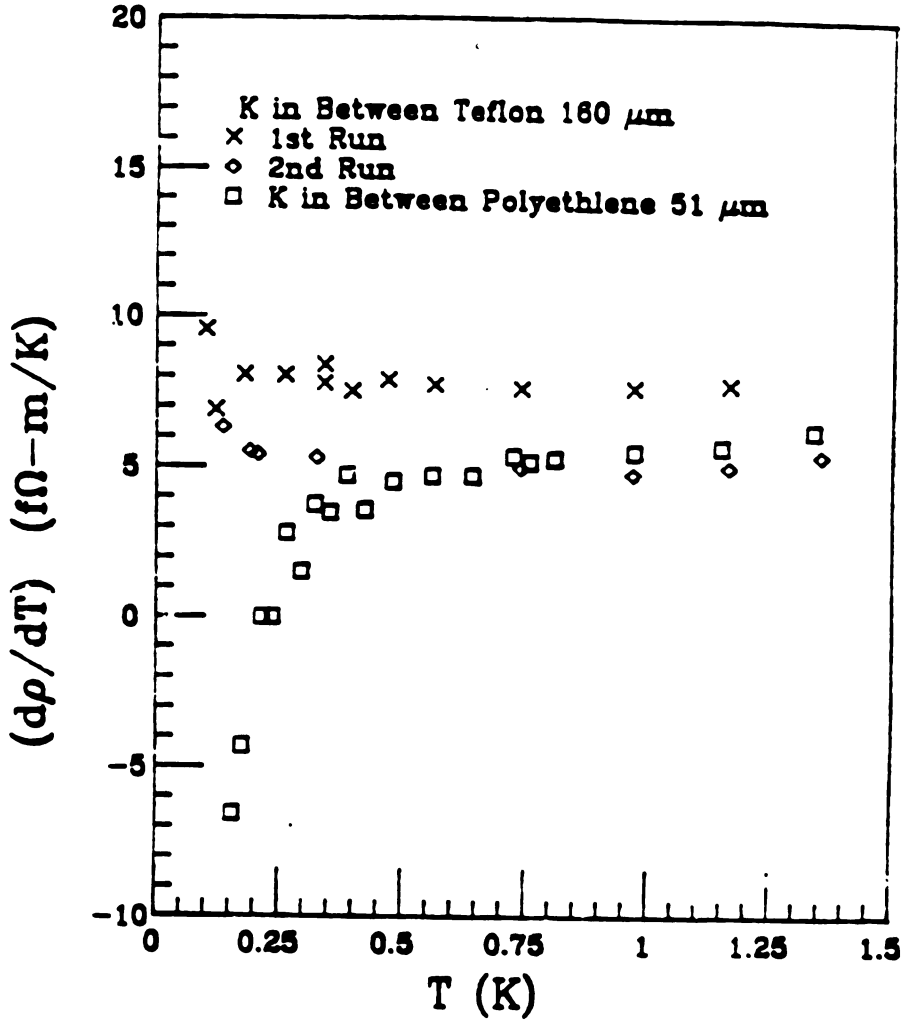

Fig. 3.9.4 Three runs for K the film enclosed in plastic sheets. The residual resistivities for K between Teflon are, ρ_0(#1)=2.229 nΩ-cm ρ_0(#2)=1.907 nΩ-cm. The residual resistivity for K between polyethlene is ρ_0=4.722 nΩ-cm.

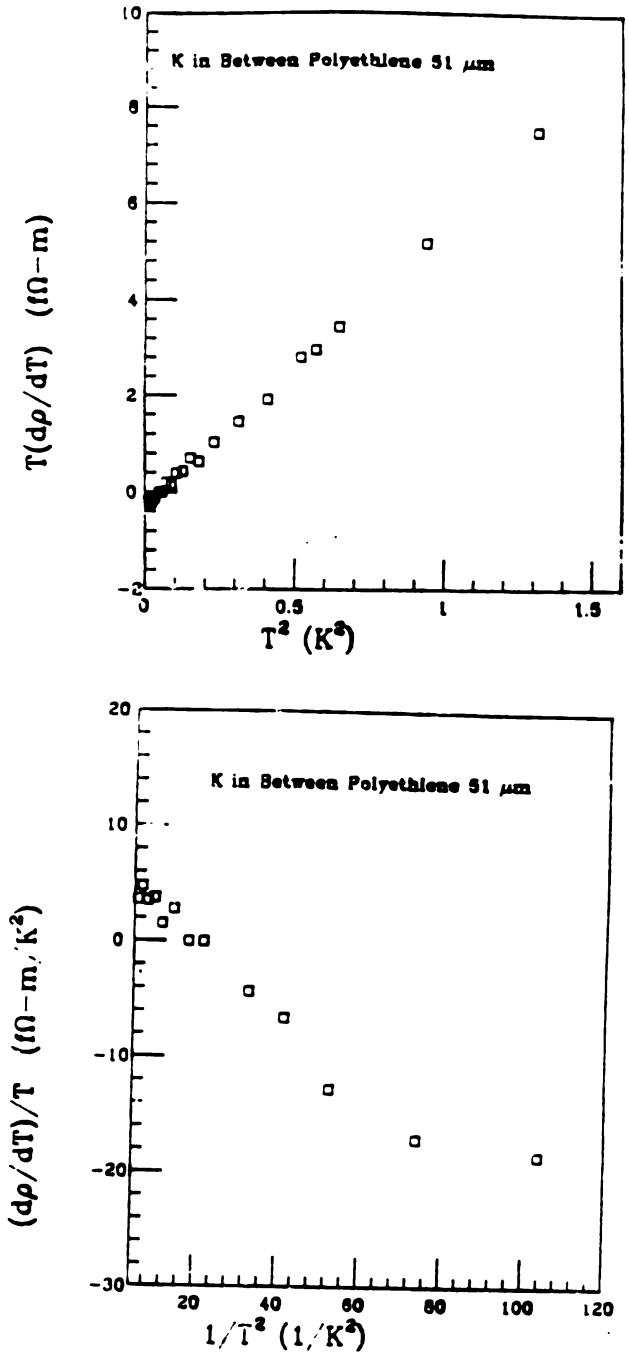

Fig. 3.9.5 The linear relation showed in the above figures indicates $(d\rho/dT)=2AT-B/T$ is well observed for K between polyethlene sheets.

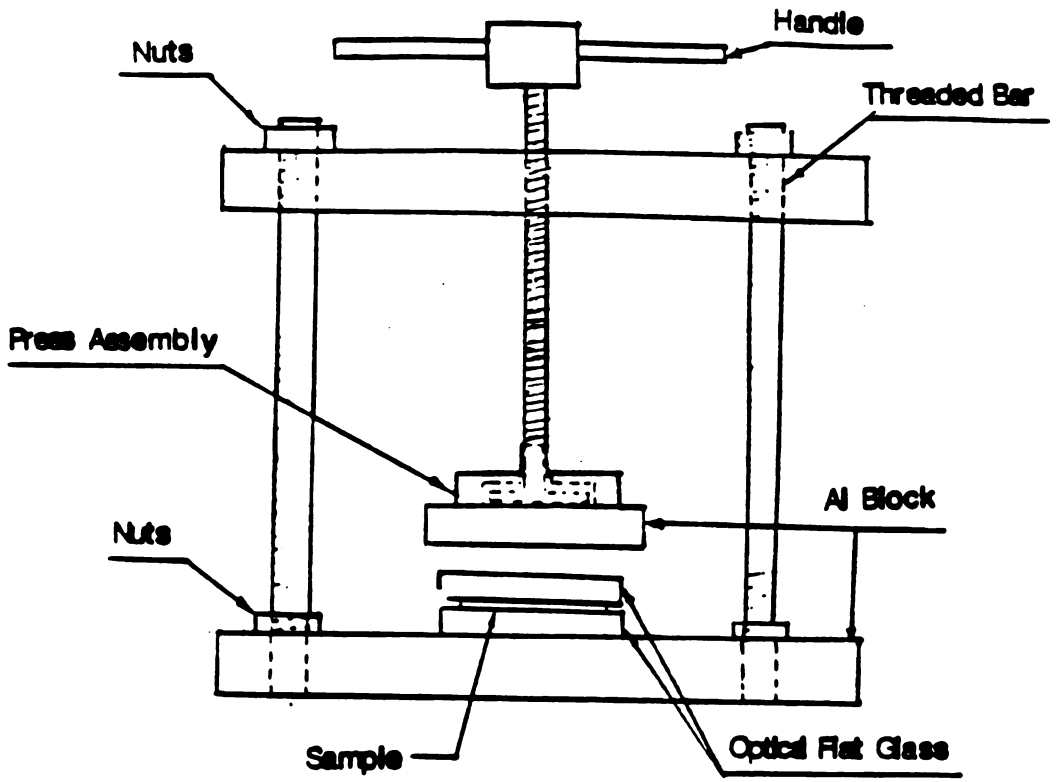

Fig 3.9.6 By rotating the handle, the press assembly will exert pressure on the Optical Flat Glass to make a K film from a K thin wire.

resistivity with T^5 temperature dependence. Because of suppression of the phonon drag effect in thin films the results suggest that a very large positive T^5 term due to the normal electron-phonon scattering exists. This in turn cancels the effect of the negative resistance proposed by KW' model, and hence the deviation from T^2 law can not be observed. But without detailed numerical calculation, we can not determine if this is indeed the case.

In chapter 1 we discussed the effect of surface scattering on temperature dependent part of the resistivity. The classic Fuch theory predicts

$$d\rho/dT = (\rho_{film}/\rho_{bulk})(d\rho_{Bulk}/dT)(1/\ln(\ln\kappa)) \quad (3.9.7)$$

where $\kappa = t/\lambda$, t is film thickness and λ is the mean free path for bulk sample. In table 7 we list the results of calculations for K films on Si substrates using eq. 3.9.7. We can see from the table that the values given by eq. 3.9.7 is too small to explain the results. Similar results obtained for glass and KF substrates are not listed.

Kaveh and Wiser[36] proposed an anisotropic model to explain the variation of A for bulk K. They derived the following result.

$$A = A^{iso}\left[1+ \frac{7}{(1+\rho_{imp}/\rho_{dis})^2}\right] \quad (3.9.10)$$

Here ρ_{imp} is the residual resistivity from isotropic electron-impurity scattering and ρ_{dis} from any anisotropic scattering, such as dislocations, and $\rho_{dis}=\rho_{total}-\rho_{imp}$. If we assume $A^{iso} = 2.2$ ($f\Omega$-m/K^2) and RRR=2000 for bulk K, we can calculate the value of A. The result for K films on Si substrates is listed in table 7. We can see the values derived from eq. 3.9.10 is too large. One possible reason is that eq. 3.9.10 is not applicable to the surface scattering, so that we can not use eq. 3.9.10 in the case of thin film. We reach the same conclusions for glass and KF substrates.

In fig. 3.9.6 we also plotted the residual resistivity vs. 1/t(μm), noteice that the solid line is the calculation of Fuch's theory assuming the specular coefficient p=0 (Which resulted largest possible value of residual resistivity), and the dash line is the result of assuming p=0.5. From the figure we obtained the two results, first the residual resistivities of K films with (100) planes parallel to surface, which were deposited on KF crystal arenot much different from the residual resistivity of K film with (110) planes parallel to suface, which were deposited on glass and Si substrates. Second the Fuch's model can be applied to the thickness dependence of the residual resistivity of K films.

Table 7 Size effect on values of A using classic Fuch's theory and Kaveh and Wiser's Model. Note the Fuch's formular used here is only applicable to cases of film thickness much less than the mean free path. We assume the RRR=2000 for the bulk K when we us the KW's model to do calculatin.

t(μm)	ρ_0(nΩ-cm)	A(fΩ-m/K^2)		
		Experimental	Fuch	KW
2.57	17.0	6.8	3.3	11.8
4.98	17.6	8.8	4.2	12.0
8.1(#1)	5.39	4.9	1.6	3.9
10	7.29	4.2	2.4	6.2
20	3.14	3.4	1.7	---
46.6(#1)	3.77	3.0	---	2.2

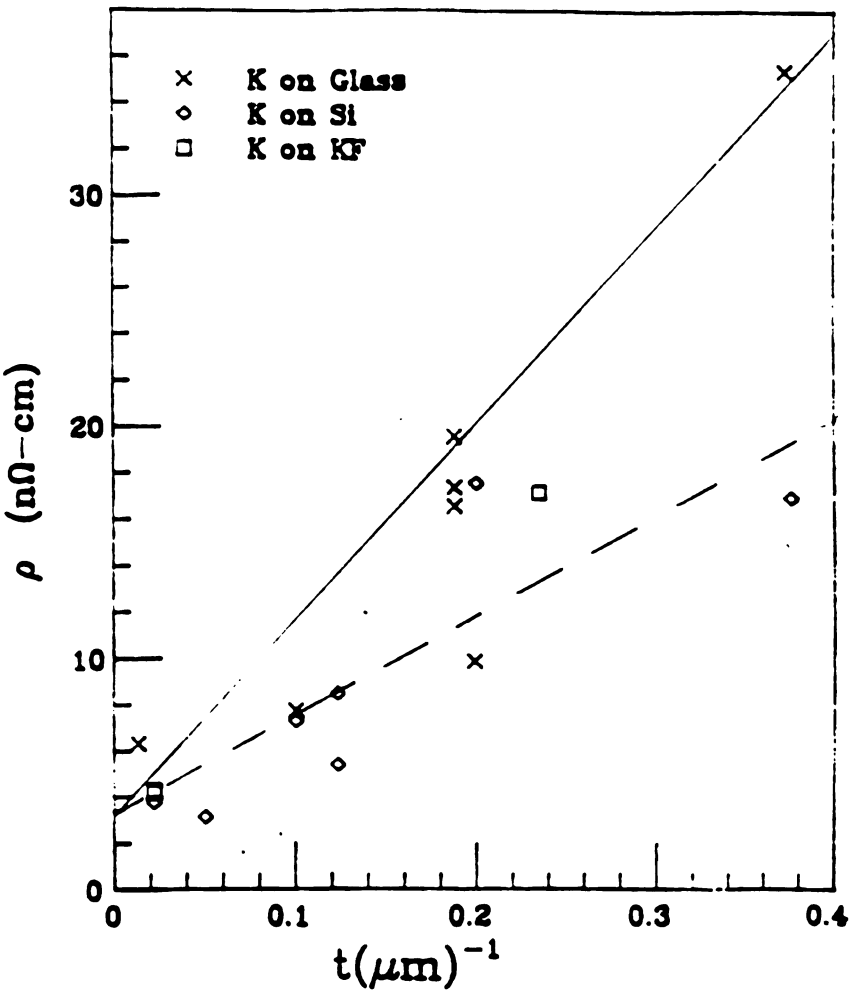

Fig. 3.9.7 The thickness dependence of the residual resistivity. The calculation of Fuch's model is presented with solid line(p=0) and dash line(p=0.5).

Chapter 4 Summary and Conclusions

The unique properties of potassium metal makes it an ideal system to test our fundamental knowledge of solid state physics. We have performed high precision resistivity measurements of thin K films on various substrates, including microslide glass, single crystal Si and single crystal KF cleaved along (100) plane. The thin film samples were mounted in adilution refrigerator equipped with a rf SQUID and a high precision current comparator. The measurements were done over the temperature range of 0.1 K to 4.2 K.

The K film samples were made inside a glass belljar under a vacuum of $\approx 1 \cdot 10^{-6}$ torr. Once the K film was made it was transferred into sample can inside an Ar filled glove-box. A sheet of copper coated with K was inserted into the sample can where it acted as an absorbant of contamination gas, so that the film surface kept shiny for days at room temperature. The K film structures were determined by x-ray diffraction. The K films on microslides glass and Si substrates have their surfaces parallel to (110) planes, and K films on substrates of single KF crystal cleaved along (100) planes have their surface parallel to (100).

We found that there were no unusually large residual resistivity for K films on single KF crystal cleaved along (100) planes, which contradicts the prediction of charge density wave theory proposed by Overhauser. And none of our experiment data for K film resistivity for KF, Si and glass substrates showed $T^{3/2}$ temperature dependence, which is also predicted by charge density wave theory.

We found that there is a Kondo-like effect in K thin films on all glass, Si, and KF substrates. This effect for films on glass substrates is very strong. It is only effective in the lowest temperature region (usually 0.5 K or below). We believe that it is a contribution from electron scattering by magnetic impurities on the surface of the substrates.

We found that the temperature dependent part of the resistivity $\rho(T)$ for thin films of K on all substrates is larger than the values for the bulk K.

$\rho(T)$ for the thinnest film on single KF crystal with (100) planes parallel to the surface is much smaller than the values obtained from K films of similar thickness on glass and Si substrates.

In our K films on all three kinds of substrates, (even though the thickness of our thinnest K film sample is two orders of magnitude smaller than the diameter of the thinnest wire) we did not observe non monotonic increase of $d\rho/dT$ with T, which is seen in thin K wires.

To further analyse the resistivity of thin K films for all the temperature regions measured, we assume that the resistivity results from electron-surface scattering and the same mechanisms that operate in bulk K, namely electron-electron scattering, electron-phonon scattering, and electron-magnetic impurities scattering if magnetic impurities exist. The Fuchs and Sambles theory of surface scattering indicates that the form of temperature dependent part of the resistivity should be the same for bulk K, we therefore assume that the temperature dependent part of the resistivity for thin films can be written as

$$\rho(T) = \rho_{el\text{-}el}(T) + \rho^{N}_{el\text{-}ph}(T) + \rho^{U}_{el\text{-}ph}(T) + \rho_{Kondo}(T)$$

$$= AT^2 + CT^5 + DT\exp(-\theta/T) - B\ln(T/T_K) \quad (4.1)$$

where $\rho_{el\text{-}el}(T)$ is the contribution from electron-electron scattering, $\rho^{N}_{el\text{-}ph}(T)$ from normal electron-phonon scattering, $\rho^{U}_{el\text{-}ph}(T)$ from umklapp electron-phonon scattering, and $\rho_{Kondo}(T)$ from the electron scattered by magnetic impurities, ρ_{Kondo} and $\rho_{el\text{-}el}$ are only effective below 1 K and $\rho^{U}_{el\text{-}ph}$ and $\rho^{N}_{el\text{-}ph}$ terms are dominant above 1 K.

For the temperature range of 0.1 K to 1 K the resistivity of thin K films on glass, Si and KF substrates can be written as following

$$\rho(T) = AT^2 - B\ln(T/T_K) \qquad (4.2)$$

the origin of the second term, which is only effective in the lowest temperature region (usually 0.5 K or below), is not totally clear to us. We believe the logarithmic term is the contribution from electron scattering by magnetic impurities on the surface of the substrates, and we called it a Kondo-like term. The values of coefficient B are nearly zero for K films on Si substrates, and very small and nearly constant for K films on KF substrates. But B varies widely for K films on glass substrates. This may be due to the random distributions of magnetic local moments on the surface where the films were deposited.

The values for the coefficient A are crudely inversely proportional to the inverse of film thickness for glass and Si substrates. However our experimental data indicates that it varies little with respect to film thickness on single crystal KF cleaved along (110) planes. The variation of values of A on Si and glass substrates can not be explained by either the classical Fuch's theory or the anisotropic model proposed by Kaveh and Wiser. And it is not clear why there is little variation for thin films on KF substrates. The severe erosion of the surface by air for the 46.6 μm film on Si substrate produced a change of A and C,

but no unusual form of temperature dependence. This is not the case for thin wires[45,51].

For a high purity bulk K sample there is no measurable resistivity contribution from normal electron-phonon scattering due to the phonon drag effect, since the phonon gas is not in a equilibrium state at low temperature. According to theoretical calculation $\rho^{U}_{el\text{-}ph}$ is also reduced by ≈40% by phonon drag. Because θ is determined from phonon dispersion curves and the thinnest film in our experiment contains several thousands monolayers, we assume that the θ in the $\rho^{U}_{el\text{-}ph}$ term is same for both thin films and bulk potassium. We did a least square fit to our experiment by using eq. 4.1, and found that the coefficient D varies little but has a tendency to decrease with decreasing K film thickness. Assuming that surface scattering of phonons would tend to equilibrate the latter, this contradicts the theoretical prediction of Kaveh and Wiser and others[26,27]. For our graphical analysis we chose to ignore the small variation in D and used the same value for the thin films as for the high purity bulk K. We obtained the corresponding value of coefficient C. A can be determined from lower temperature (0.1 K to 1 K) experimental data without complication from electron-phonon scattering.

For the thin K films on Si and glass substrates, there is considerable evidence for the suppression of phonon drag effect, and the consequent emergence of a T^5 term with a coefficient C that is crudely inversely proportional to the film thickness. For the very thin films on Si and glass substrates the C values are 2 to 3 times larger than the value predicted by theory with an equilibrium phonon gas. For the K films on single KF crystal cleaved along (100) planes, the result

indicates that there is very little thickness dependence for C, and its values are smaller than the value predicted by theory for the T^5 component.

On the basis of the data it appears that A and C are significantly more thickness dependent for K on Si and glass substrates. This suggests that the surface structure of the K on KF is significantly more perfect for these films resulting in specular reflection of phonons with a reduced equilibrating tendency. So far there is no theoretical calculation of how or whether the surface scattering suppresses the phonon drag affect, and why the umklapp electron-phonon scattering should not be effected by the surface scattering in contrast to the behavior of normal electron-phonon scattering.

The one experiment in which we admitted pure oxygen to a K film strongly suggests that oxygen by itself has a minimal corrosive effect. The effect of humid air on the other hand was immediate and obvious.

A lot of further experimental research needs to be done on thin K films. We need to measure more K film samples of different thickness on KF substrates to confirm the thickness dependence of the coefficients of the T^2 term A, the Kondo-like term B and the T^5 term C. To clarify the origin of this Kondo-like term we need to measure $\rho(T)$ of the K film samples inside a magnetic field, and to measure the K films covered with an atomic layer of magnetic elements such as iron, or cobalt. We also need to make even thinner K films at low temperatures, such as liquid N_2 temperature, to further test the suppression of the phonon drag effect.

LIST OF REFERENCES

List of References

1. A. Smith, J. Janak and R. Adler.
   Electronic Conductions in Solid (McGraw Hill Inc., 1967).

2. Drude, Annalen der Physik 1, 566 3, 369 (1900).

3. N.W. Aschcroft, N.D. Mermin, Solid State Physics, (Holt, Rinehart and Winston Inc., NY 1976).

4. R. Peierls, Ann. Phys. 12, 154, (1932).

5. J. Ziman, Electrons and Phonons. (Oxford Press, 1960).

6. M. Kaveh and N. Wiser, Phys. Rev. B, 9, 4042 and 4053 (1974).

7. L.D. Landau and I. Pomeranchuk, Phys. Z. (1936) and Sowjun,10,649 (1937).

8. W. G. Baber, Proc. R. Soc A 158, 383 (1937).

9. G. F. Giuliani and J.J. Quinn, Phys. Rev. B, 26 4421 (1982).

10. K. Fuchs, Proc. Camb. Phil. Soc, 34, 100 (1938).

11. I. Holwech and J. Jeppesen, Phil. Mag. 15, 1217 (1967).

12. J. Van Zytveld and J. Bass, Phy. Rew. 177, 1072 (1969).

13. S.B. Soffer, J. Appl. Phys. 38, 1710 (1967).

14. D.C. Larson, Physics of Thin Films, 6, 81 (1971).

15. J.R. Sambles and T.W. Preist, J. of Phys. F, 12, 1971 (1982).

16. R.N. Gurzhi, Sov. Phys--JETP, 17, 521 (1963).

17. M. Knudsen, Ann. Phys., LP 228 (4), 75 (1909).

18. M. Farrel, M. Bishop, N. Kumar and W. Lawrence, Phys. Rev. Lett, 55, 626 (1985).

19. P.W. Anderson, Phys. Rev. B, 23, 4828 (1981).

20. M. Kaveh and N. Wiser, J. Phys. F, 15, L195 (1985).

21. J. Kondo, Prog. Theo. Phys., 32,37 (1964).

22. H. Suhl, Magnetism, Vol. V. (Academic Press, New York, 1973).

23. R.W. Cochrane and O. Strom-Olsen, Phys. Rev. B, 29, 1088 (1984).

24. I. Stone, Phys. Rev. 6, 1 (1898).

25. J.J. Thomson, Proc. Cambridge Phil. Soc., 36, 3947 (1901).

26. M. Kaveh and N. Wiser, Phys. Lett., 53A, 407 (1975).

27. C.R. Leavens and M. Laubitz, J. Phys. F, 5, 1519 (1975).

28. R. Taylor, C.R. Leavens, M.S. Duesberg and M.J.Laubitz, J. de Physique Coll. Suppl., 39, c6,1058 (1978).

29. M. Danino, M. Kaveh and N. Wiser, J. Phys. F, 11, L197-11 (1981).

30. D. Gugan, J. Phys. F, 12, L173 (1982).

31. H. van Kempen, J.H.J.M. Ribot and P. Wyder, J. of Phys. F,11, 597 (1981).

32. H. Engquist, Phys. Rev. B, 25, 2175, (1981).

33. M. Danino, M. Kaveh and N. Wiser, J. Phys. F, 13, 1665 (1983).

34. Z.Z. Yu, J.M. Haerle, J.W. Zwart, J. Bass, W.P. Pratt Jr., and P.A. Schroeder, Phys. Rev. Lett., 52, 368 (1984).

35. R. van Vucht, H. van Kempen and P. Wyder, Rept. Prog. Phys. (GB), 48, 853 (1985).

36. M. Kaveh and N.Wiser, Adv. in Phys., 33, 257 (1984).

37. A.W. Overhauser, Phys. Rev. Lett., 53, 64 (1984).

38. W. Gurney and D. Gugan, Phil. Mag. 24, 857 (1971).

39. J.W. Ekin and B.W. Maxfield, Phys. Rev. B, 4, 4215 (1971).

40. H. van Kempen, J. Lass, J. Ribot, and P. Wyder, Phys. Rev. Lett., 37, 1574 (1976).

41. J.A. Rowland, C. Duvvury and S. B. Woods, Phys. Rev. Lett, 40, 1201 (1978).

42. M. Bishop and A.W. Overhauser, Phys. Rev. Lett 42, 1776 (1979).

43. B. Levy, M. Sinvani and A. J. Greenfield, Phys. Rev. Lett., 43, 1822 (1979).

44. C.W. Lee, M.L. Haerle, V. Heinen, J. Bass, W. P. Pratt Jr., J.A. Rowlands and P.A. Schroeder, Phys. Rev. B, 25, 1411 (1982)

45. Z.Z. Yu, Ph.D. Thesis, MSU, 1987.

46. M.L. Haerle, W.P. Pratt Jr., and P.A. Schroeder, J. Phys. F, 13, L243 (1983).

47. R.J. van Vucht, G. van de Walle, H. van Kempen and P. Wyder, J. Phys. F, 12, L217 (1982).

48. M. Haerle, W.P. Pratt, Jr. and P.A. Schroeder, J. Low Temp. Phys. 62, 397 (1986).

49. R. Taylor, Sol. State Comm. 28, 167 (1978).

50. Z.Z. Yu, M. Haerle, J. Zwart, J. Bass, W.P. Pratt Jr., and P.A. Schroeder, Phys. Rev. Lett,. 52, 368 (1984).

51. J. Zhao, Ph.D. Thesis, MSU, 1988.

52. D. Movshovitz and N. Wiser, J. Phys. F, 17, 985 (1987).

53. M. Kaveh and N. Wiser, J. Phys. 10, L37 (1980).

54. D.L. Edmunds, W.P. Pratt, Jr. and J.A. Rowlands, Rev. Sci. Inst. 51, 15 1980.

55. C.W. Lee, M.L. Haerle, V. Heinen, J. Bass, W.P. Pratt, Jr., and P.A. Schroeder, Phys. Rev. B25, 1411 (1982).

56. J.L. Imes, G.L. Neiheisel and W.P. Pratt, Jr., J. Low Temp. 21, 1 (1975).

57. G.L. Neiheisel and W.P. Pratt, Jr., J. Low Temp. Phys. 28, 317 (1977).

58. M. Kaveh and N. Wiser, J. Phys. 10, L3 (1980).

59. H. Mayer, H. Rechlinger, P. Schmider: Thin Solid Films, 43, 215, (1977).

60. A.W. Overhauser, Adv. in Phys. 27 , 343 (1978).

61. Kittel, Solid State Physics

62. A. Wilson, Elements of X-ray crystallography. (Addison-Wesley Publishing Company 1970).

63. G-A. Boutry and H. Dormont, Phillips Technical Review, 30, 226 (1969).

64. D.L. Edmunds, W.P. Pratt, Jr., and J.A. Rowlands, Rev. Sci. Inst., 51, 1516 (1980).

65. M. Khoshnevisan, W.P. Pratt, Jr., P.A. Schroeder, S. Steenwyk and C. Uher, J. Phys. F, 1, 1 (1979).

66. W.P. Pratt, Jr., C.W. Lee, M.L. Haerle, V. Heinen, J. Bass, J.A. Rowlands, and P.A. Schroeder, Physica 108 B, 863 (1981).